MicroRNA-146a:

A Potential Therapeutic Target in Multiple Sclerosis

by

© Andrew Michael Graham Snelgrove, B.Eng.

A thesis submitted to the School of Graduate Studies

in partial fulfillment of the requirements for the

degree of

Master of Science in Medicine (Neurosciences)

Division of BioMedical Sciences, Faculty of Medicine

Memorial University of Newfoundland

May 2018

St. John's, Newfoundland and Labrador

Abstract

Multiple sclerosis (MS) is a neuroinflammatory disease characterized by demyelinated neurons in the central nervous system. Decreased levels of the anti-inflammatory microRNA-146a have previously been observed in macrophages/microglia in MS patients compared to controls. Therapeutically elevating microRNA-146a expression in MS may produce a conducive environment for remyelination. Inflammatory cytokines were assessed from both primary mouse and human macrophages and microglia, and THP-1 macrophages that were transfected with a microRNA-146a mimic and polarized towards a pro-inflammatory phenotype. Inflammatory cytokines and MS-relevant targets were measured following activation; neuro- and oligodendrogenesis were also assessed *in vitro* while the effect of microRNA-146a on myelin phagocytosis was also examined. MicroRNA-146a may decrease pro-inflammatory TNF but may have little to no effect on IL-6; RhoA may decrease in both mouse and human macrophages. MicroRNA-146a increased myelin phagocytosis of unstimulated primary mouse microglia. Finally, *in vitro* experiments suggest that supernatants collected from LPS-stimulated murine macrophages transfected with a microRNA-146a mimic do not affect neurogenesis or oligodendrogenesis. It is suggested that increasing microRNA-146a may promote an anti-inflammatory environment beneficial for promoting remyelination in MS.

Keywords: multiple sclerosis; microRNA-146a; macrophage; microglia; remyelination; neurogenesis; oligodendrogenesis.

Acknowledgements

I would like to thank my supervisor, Dr. Craig Moore, for accepting my application as his Master's student, and for his guidance, patience, and expertise throughout my Master's program. I would also like to thank my committee members, Dr. Jacqueline Vanderluit and Dr. Michael Grant, for their time, advice, and support throughout my program. In addition, I would like to thank my lab members Tangyne Berry (Lab Assistant) and Brad Williams (Research Assistant), my colleagues Dylan Galloway, Sasha Power, and Stephanie Blandford, and our past undergraduate students Megan Parker, Ryan Hughes, Dylan Upshall, and Joshua Lehr, for their camaraderie and help. I would also like to thank all lab members in the Department of Biomedical Sciences, Faculty of Medicine at Memorial University, for their camaraderie and support. I would also like to thank my mom, dad, Aunt Cherry, and my siblings Jessica, Gregory, Cherry, Joanna, and Matthew, for their support and understanding with my many long and late hours. I would like to thank Memorial University of Newfoundland for their financial support through the Graduate Studentship, and the Multiple Sclerosis Society of Canada, the Canada Research Chair, and the Research and Development Corporation of Newfoundland and Labrador for their financial support. I would like to thank all of the human donors of our monocyte-derived macrophages and all of the human adult brain and microglia donors for choosing to participate in our research. Finally, I would like to sincerely thank our human fetal donors and their families for choosing to take part in our research. I hope

that the information uncovered from this research is a helpful step forward in finding an effective therapy and cure for multiple sclerosis.

Table of Contents

Abstract……. ..... **ii**

Acknowledgements ..... **iii**

List of Figures…… ..... **ix**

List of Abbreviations and Symbols ..... **xi**

List of Appendices ..... **xiv**

Chapter 1 - Introduction **1**

1.1 Overview of Multiple Sclerosis **1**

1.2 Immunopathology and Recovery in Multiple Sclerosis **4**

1.2.1 Remyelination and the M1 to M2 Shift in Macrophages/Microglia in MS 11

1.2.2 Neurogenesis, Neuron Recovery, and M1 to M2 Polarization 14

1.2.3 Treatment for MS 14

1.3 MicroRNAs in Disease and MS **15**

1.4 MicroRNA-146a **19**

1.4.1 MicroRNA-146a in MS 21

1.5 Thesis Hypothesis and Objectives **22**

Chapter 2 - Methods and Materials **28**

2.1 Isolation and Culture of Animal Cells **28**

2.1.1 Isolation of Primary Mouse Bone Marrow-Derived Macrophages 28

2.1.2 Isolation of Primary Mouse Microglia 31

2.2 Isolation and Culture of Human Cells **35**

2.2.1 Culture of THP-1 Macrophages 35

2.2.2 Isolation of Primary Human Monocyte-Derived Macrophages 35

2.2.3 Isolation of Primary Human Fetal and Adult Microglia 37

2.3 MicroRNA Transfection, LPS Stimulation, and Collection of Supernatant **38**

2.4 Flow Cytometry **39**

2.5 RNA Isolation, Preamplification Polymerase Chain Reaction, and Quantitative Polymerase Chain Reaction 40
2.6 Western Blotting 41
2.7 Enzyme-Linked Immunosorbent Assay 46
2.8 Microscopy of Mouse and Human Myeloid Cells 47
2.9 Analysis of Indirect Effect of miR-146a Transfected Cells on Neurosphere Development 47
2.9.1 Mouse Neurosphere Culture 47
2.9.2 Immunocytochemistry of Mouse Neurospheres 50
2.9.2.1 Immunocytochemistry of Mouse Neurospheres for Neurons 50
2.9.2.2 Immunocytochemistry of Mouse Neurospheres for OPCs 51
2.9.3 Image Analysis 51
2.10 Myelin Phagocytosis Assay 57
2.11 Statistical Analysis 58
Chapter 3 - Results 59
3.1 Proof of MicroRNA Transfection 59
3.1.1 MiR-146a mimic can be successfully transfected into primary mouse BMDMs and primary mouse microglia using Lipofectamine RNAiMAX 59
3.1.2 MicroRNAs can be successfully transfected into human THP-1 macrophages using Lipofectamine RNAiMAX 61
3.2 Assessing Inflammatory Response of Primary Mouse Myeloid Cells Transfected with a MiR-146a Mimic 63
3.2.1 ELISAs 63
3.2.1.1 TNF production decreases in LPS-stimulated primary mouse BMDMs transfected with a miR-146a mimic 63
3.2.1.2 IL-6 production decreases in LPS-stimulated primary mouse microglia transfected with a miR-146a mimic 65
3.2.2 Western Blots 65

3.2.2.1 iNOS expression may increase upon LPS stimulation, but may not change in LPS-stimulated primary mouse BMDMs transfected with a miR-146a mimic 65
3.2.2.2 RhoA expression may decrease in LPS-stimulated primary mouse BMDMs transfected with a miR-146a mimic 67

3.3 Assessing Inflammatory Response of Human Myeloid Cells Transfected with a MiR-146a Mimic 67

3.3.1 ELISAs 67
3.3.1.1 TNF and IL-6 production may decrease in LPS-stimulated THP-1 macrophages transfected with a miR-146a mimic 67
3.3.1.2 TNF production decreases in LPS-stimulated primary human MDMs transfected with a miR-146a mimic 69
3.3.1.3 TNF production may decrease in LPS-stimulated primary human fetal microglia transfected with a miR-146a mimic 69
3.3.1.4 TNF production may decrease in LPS-stimulated primary human adult microglia transfected with a miR-146a mimic 69
3.3.2 Western Blots 71
3.3.2.1 iNOS expression may not change in LPS-stimulated primary human MDMs transfected with miR-146a mimic 71
3.3.2.2 RhoA expression may decrease in LPS-stimulated primary human MDMs transfected with a miR-146a mimic 71
3.3.2.3 iNOS expression may not change in LPS-stimulated primary human fetal microglia transfected with a miR-146a mimic .. 73
3.3.2.4 RhoA expression may not change in LPS-stimulated primary human fetal microglia transfected with miR-146a mimic 73

3.4 Assessing Indirect Effect of Primary Mouse BMDMs Transfected with miR-146a Mimic and LPS Stimulation on Neural Stem Cell Development 75

3.4.1 Supernatants derived from LPS-stimulated murine BMDMs transfected with a miR-146a mimic did not affect neurogenesis *in vitro* 75
3.4.2 Supernatants derived from LPS-stimulated murine BMDMs transfected with a miR-146a mimic did not affect oligodendrogenesis *in vitro* 79
3.5 MiR-146a Increases Phagocytosis of Myelin by Unstimulated Primary Mouse Microglia 83
Chapter 4 - Discussion 85
Chapter 5 - Future Directions 107
Chapter 6 - Conclusion 111
Bibliography…… 112

List of Figures

Figure 1: Biogenesis of MicroRNAs 17
Figure 2: Overall hypothesis of the potential role of miR-146a in acute and chronic inflammation in multiple sclerosis 25
Figure 3: Examples of mouse and human cells successfully cultured *in vitro* 30
Figure 4: Separation of primary mouse astrocytes from mouse microglia using the modified mild trypsinization method 34
Figure 5: Primary mouse neurosphere development *in vitro* 49
Figure 6: Overview of image analysis for mouse neurospheres 54
Figure 7: Mouse neurosphere processed using Fiji to count neurons 55
Figure 8: Mouse neurosphere processed using Fiji to count OPCs 56
Figure 9: Transfection of miR-146a mimic into primary mouse BMDMs and microglia using Lipofectamine RNAiMAX 60
Figure 10: MicroRNA mimics can be successfully transfected into THP-1 macrophages using Lipofectamine RNAiMAX 62
Figure 11: MiR-146a significantly decreases TNF in primary mouse BMDMs and IL-6 in primary mouse microglia after 6 hours under M1-polarizing conditions 64
Figure 13: MiR-146a may decrease TNF and IL-6 production by THP-1 macrophages after 6 hours under M1-polarizing conditions 68
Figure 14: MiR-146a may decrease TNF, but not IL-6, in primary human monocyte-derived macrophages, fetal microglia, and adult microglia, after 6 hours under M1-polarizing conditions 70
Figure 15: MiR-146a may decrease RhoA, but not iNOS, in primary human MDMs after 6 hours under M1-polarizing conditions 72
Figure 16: MiR-146a may not alter iNOS or RhoA expression in primary human fetal microglia after 6 hours under M1-polarizing conditions 74

Figure 17: Neurogenesis analysis from primary mouse neurospheres cultured with supernatant from miR-146a-transfected primary mouse BMDMs with M1-polarizing conditions 76
Figure 18: Mouse neurospheres cultured in media from LPS-stimulated mouse BMDMs transfected with miR-146a mimic had no effect on neuron differentiation 78
Figure 19: Oligodendrogenesis analysis from primary mouse neurospheres cultured with supernatant from miR-146a-transfected primary mouse BMDMs with M1-polarizing conditions 80
Figure 20: Mouse neurospheres cultured in media from LPS-stimulated mouse BMDMs transfected with miR-146a mimic had no effect on OPC differentiation 82
Figure 21: Myelin phagocytosis increases in miR-146a-transfected primary mouse microglia 84
Figure 22: Proposed scheme of signalling pathways between miR-146a, TNF, and RhoA in either primary mouse BMDMs or human MDMs after 6 hours of LPS stimulation 103

List of Abbreviations and Symbols

Ago2: Argonaute-2
BBB: Blood-Brain Barrier
BCA: Bicinchoninic Acid
BMDM: Bone Marrow-Derived Macrophage(s)
BSA: Bovine Serum Albumin
CD#: Cluster of Differentiation/Designation or Classification Determinant (Number)
CIS: Clinically Isolated Syndrome
CNS: Central Nervous System
CSF: Cerebrospinal Fluid
CXCL8: C-X-C Motif Chemokine Ligand 8
CXCL9: C-X-C Motif Chemokine Ligand 9
CXCL10: C-X-C Motif Chemokine Ligand 10
CXCL11: C-X-C Motif Chemokine Ligand 11
CXCL13: C-X-C Motif Chemokine Ligand 13
DAPI: 4',6-Diamidino-2-Phenylindole, Dihydrochloride
DGCR8: DiGeorge critical region 8
DMEM: Dulbecco's Modified Eagle's Medium
DS: Dissection Solution
EAE: Experimental Autoimmune Encephalomyelitis
EBV: Epstein-Barr Virus
ECL: Enhanced Chemiluminescence
EDSS: Expanded Disability Status Scale
EDTA: Ethylenediaminetetraacetic Acid
EGF: Epidermal Growth Factor
ELISA: Enzyme-Linked Immunosorbent Assay
eNOS: Endothelial Nitric Oxide Synthase (also known as NOS3)
Exportin-5-Ran-GTP: Exportin-5-Ran-Guanosine Triphosphatase
FACS Buffer: Fluorescence-Activated Cell Sorting Buffer
FBS: Fetal Bovine Serum (Heat-Inactivated)
FGF-2: Basic Fibroblast Growth Factor 2
GDP: Guanosine Diphosphate
GTP: Guanosine Triphosphate
GTPase: Guanosine Triphosphatase
HAM: Human Adult Microglia
HEPES: 4-(2-Hydroxyethyl)piperazine-1-ethanesulfonic acid
HFM: Human Fetal Microglia
HI: Heat-Inactivated
HKLM: Heat-Killed *Listeria monocytogenes*
HLA: Human Leukocyte Antigen
Iba1: Ionized Calcium-Binding Adapter Molecule 1

IFNγ: Interferon-γ
IgG: Immunoglobulin G
IL-1β: Interleukin-1 β
IL-4: Interleukin-4
IL-6: Interleukin-6
IL-10: Interleukin-10
IL-12: Interleukin-12
iNOS: Inducible Nitric Oxide Synthase (also known as NOS2)
IRAK1: Interleukin-1 Receptor-Associated Kinase 1
IRAK2: Interleukin-1 Receptor-Associated Kinase 2
JAK/STAT: Janus Kinase/Signal Transducers and Activators of Transcription
LPS: Lipopolysaccharide
M. bovis BCG: *Mycobacterium bovis* bacillus Calmette-Guérin
MBP: Myelin Basic Protein
M-CSF: Macrophage Colony Stimulating Factor
MDM(s): Monocyte-Derived Macrophage(s)
MHC: Major Histocompatibility Complex
MiR- or miR- or microRNA: Micro Ribonucleic Acid
MRI: Magnetic Resonance Imaging
mRNA: Messenger Ribonucleic Acid
MS: Multiple Sclerosis
MyD88: Myeloid Differentiation Primary Response 88
NADPH: Nicotinamide Adenine Dinucleotide Phosphate
NC: Negative Control
NF-κB: Nuclear Factor Kappa-Light-Chain-Enhancer of Activated B Cells
NG2: Neural/Glial Antigen 2
NGS: Normal Goat Serum
nNOS: Neuronal Nitric Oxide Synthase (also known as NOS1)
NO: Nitric Oxide
NOS1: Nitric Oxide Synthase 1 (also known as nNOS)
NOS2: Nitric Oxide Synthase 2 (also known as iNOS)
NOS3: Nitric Oxide Synthase 3 (also known as eNOS)
No/T: No Treatment
ns: Not Statistically Significant
NSC(s): Neural Stem Cell(s)
OPC(s): Oligodendrocyte Precursor or Progenitor Cell(s)
P#: Postnatal Day #
PBMC(s): Peripheral Blood Mononuclear Cell(s)
PBS: Phosphate-Buffered Saline
PBST: Phosphate-Buffered Saline with Triton X (0.3%)
PCR: Polymerase Chain Reaction
PFA: Paraformaldehyde
PMA: Phorbol 12-Myristate 13-Acetate
PPMS: Primary Progressive Multiple Sclerosis
P/S: Penicillin/Streptomycin

pre-microRNA: Precursor Micro Ribonucleic Acid
pri-miRNA: Primary Micro Ribonucleic Acid
RhoA: Ras homolog A
RIPA Buffer: Radioimmunoprecipitation Assay Buffer
RISC: Ribonucleic Acid-Induced Silencing Complex
RNA(s): Ribonucleic Acid(s)
ROCK: Rho-Associated Protein Kinase
ROS: Reactive Oxygen Species
RPMI: Roswell Park Memorial Institute
RRMS: Relapsing-Remitting Multiple Sclerosis
RT-qPCR: Quantitative Reverse Transcription Polymerase Chain Reaction (Assay)
SDS: Sodium Dodecyl Sulphate (Buffer)
SPMS: Secondary Progressive Multiple Sclerosis
STAT1: Signal Transducer and Activator of Transcription 1
SVZ: Subventricular ZoneTGFβ: Transforming Growth Factor β
TLR2: Toll-Like Receptor 2
TLR4: Toll-Like Receptor 4
TMEV: Theiler's Murine Encephalomyelitis Virus
TNF: Tumour Necrosis Factor (Alpha)
TRAF6: Tumour Necrosis Factor Receptor-Associated Factor 6
TRBP: Transactivation Response Ribonucleic Acid-Binding Protein
-mer suffix (MicroRNA context): Number of bases (e.g. 6-8mer)

List of Appendices

APPENDIX A: Densitometry Procedure……160

APPENDIX B: Neurosphere Image Processing Program for Fiji Software…….164

Chapter 1 - Introduction

1.1 Overview of Multiple Sclerosis

Multiple sclerosis (MS) is a neuroinflammatory disease characterized by demyelinated neurons in the brain and/or spinal cord. This disease affects twice as many females as males (Multiple Sclerosis International Federation 2013b), and the average age of onset of MS worldwide is 30 years (Multiple Sclerosis International Federation 2013b). According to the latest *Atlas of MS 2013* report database by the MS International Federation, Canada has the highest MS prevalence in the world, with 291 people developing MS per 100,000 people (Multiple Sclerosis International Federation 2013a).

Central to MS pathology is the destruction of myelin sheaths that normally ensheath the axons of neurons. Myelination increases the rate, the energy efficiency, and the refractory period of electrical signals along a neuronal axon (Blank and Prinz 2014). If myelin sheaths are damaged, electrical signals along these demyelinated neurons are diminished (Smith et al. 1979), which can clinically manifest into patients developing highly heterogeneous neurological and physical symptoms. These symptoms can include syndromes associated with the brainstem, muscle weakness and/or paralysis, spasticity, fatigue, sensory and cognitive impairment, depression, sensitivity to heat, headache, myelitis, and optic neuritis (Gelfand 2014).

MS is clinically diagnosed using the revised 2010 McDonald Criteria (Polman et al. 2011). These criteria utilize two clinical biomarkers to support an

MS diagnosis: examining magnetic resonance imaging (MRI) scans that are T2-weighted with or without gadolinium-enhancement, and measuring immunoglobulin G (IgG) synthesis in the cerebrospinal fluid (CSF) by calculating the IgG index and/or observing oligoclonal bands (Polman et al. 2011). MRI scans are used to identify lesions, while gadolinium is used to provide evidence of blood-brain barrier (BBB) breakdown (Housley et al. 2015). Relapse onset and severity can be predicted based on the size and number of lesions found on MRI scans (Housley et al. 2015). The IgG index (the ratio of IgG/albumin in CSF to IgG/albumin in serum (Perkin et al. 1983)) or presence of oligoclonal bands indicates potentially pathological intrathecal IgG synthesis (Bonnan 2015; Fortini et al. 2003). Apart from MRIs and examining CSF IgGs, other potential MS biomarkers being examined for their diagnostic validity include myelin-reactive T cells, genetic biomarkers, messenger ribonucleic acids (mRNAs), and micro ribonucleic acids (microRNAs or miRNAs) (Housley et al. 2015).

MS may manifest itself in a variety of forms upon initial investigation, and can progress in distinct patterns. Clinicians have classified three general MS disease courses (or phenotypes) that can develop: relapsing-remitting MS (RRMS), secondary progressive MS (SPMS), and primary progressive MS (PPMS) (Lublin and Reingold 1996; Lublin et al. 2014). First, RRMS may begin as a clinically isolated syndrome (CIS), which is defined as the initial clinical presentation of a characteristic inflammatory demyelinating disease but requires meeting dissemination in time criteria to suggest an MS diagnosis (Lublin et al. 2014; Miller et al. 2005). If the CIS becomes active and meets MS diagnostic

criteria, the CIS transitions into RRMS (Lublin et al. 2014). RRMS consists of pronounced acute attacks with full or partial recovery and no apparent disease progression between attacks (Lublin and Reingold 1996; Lublin et al. 2014). Approximately 85% of patients are first diagnosed with RRMS (Multiple Sclerosis International Federation 2013b). Second, SPMS patients have a disease course initially defined as RRMS, but it transitions into disease progression with or without plateaus, minor relapses, and/or minor remissions (Lublin and Reingold 1996). It is suggested that approximately 58% to 80% of patients with RRMS transition into SPMS (2012; Scalfari et al. 2014; Tremlett et al. 2008). Third, PPMS patients have disease progression from the onset of symptoms, with or without plateaus and/or minor improvements in disability (Lublin and Reingold 1996). It is estimated that approximately 10% (Koch et al. 2009) of patients with MS have PPMS. To measure the extent of clinical disability in all forms of MS, the Kurtzke Expanded Disability Status Scale (EDSS) (Kurtzke 1983) is used. This scale ranges from 0.0 to 10.0, where neurological and physical disability increases as the score increases, ending at death with a score of 10.0 (Kurtzke 1983).

Epidemiological and genome-wide association studies have identified several factors that increase the risk of developing MS. There is evidence that the human leukocyte antigen (HLA) *HLA-DRB1*15:01* allele is positively associated with MS susceptibility in European populations (Hollenbach and Oksenberg 2015). Viral infection by Epstein-Barr virus (EBV) is also associated with an increased MS risk (Levin et al. 2010). Furthermore, there is evidence to suggest

that CD4+ T cells may cross-react between myelin and EBV antigens (Lunemann et al. 2008; Wucherpfennig and Strominger 1995). Non-infectious environmental risk factors can include smoking (Hedström et al. 2009) and low levels of vitamin D (Munger et al. 2006). Smokers have an increased risk of developing MS, but nicotine was ruled out as a possible risk factor (Hedström et al. 2009). High levels of vitamin D in blood serum is also associated with a reduced risk of MS (Munger et al. 2006). Besides factors influencing MS in general, factors influencing MS phenotype have also been identified. In one study, more females than males tend to be in the SPMS population (Tremlett et al. 2009), and exposure to EBV may possibly increase risk of developing RRMS over PPMS (McKay et al. 2015). Besides relapsing disease, there are also factors that can influence progressive disease. For example, the male gender and the onset of motor symptoms was associated with a faster time from disease onset to SPMS (Koch et al. 2010). In contrast, regarding disease progression in PPMS, the onset of sensory symptoms was associated with a delayed clinical progression to an EDSS score of 6.0 (Koch et al. 2009).

1.2 Immunopathology and Recovery in Multiple Sclerosis

MS is considered to be an immune-mediated disease, where T and B cells of the body coordinate the destruction of the body's own myelin sheath by directing phagocytic cells, including microglia and blood-derived macrophages. White matter (Kutzelnigg et al. 2005) and grey matter (Damasceno et al. 2014; Kidd et al. 1999; Peterson et al. 2001) can be damaged. How the demyelinating

attack may begin is still unclear. One general idea is the “inside-out, outside-in hypothesis”, where the cause of demyelination is found either inside the CNS or outside of the CNS (Stys et al. 2012). The “inside-out” portion of the hypothesis suggests that a threat is detected within the CNS, causing CNS immune cells to signal to other immune cells outside of the CNS to cross the BBB and take part in demyelination. In contrast, the “outside-in” portion of the hypothesis suggests that reactive immune cells cross the BBB into the CNS and initiate demyelination. Regardless of how demyelination might have etiologically originated, common features are found in all MS patients, including inflammation, demyelination, and in certain cases, remyelination and CNS repair. In each of these stages, microglia, macrophages, and their immunological phenotype, have an important role to play.

In the normal CNS environment, oligodendrocytes produce, wrap, and maintain myelin found along the axons of neurons. Two classes of distinct myeloid cells, blood-derived macrophages and CNS-resident microglia, survey the environment for either threats or damage. Both cells express similar cell markers, making it difficult to distinguish between them pathologically and/or immunohistochemically. In this quiescent environment with no perceived threats or damage, microglia and blood-derived macrophages are in a “resting” immunological phenotype. Although not strictly “resting”, these myeloid cells constantly survey their environment. Microglia exhibit a ramified phenotype with extended processes to monitor signals from their environment for any change in homeostasis, and to respond quickly (Nimmerjahn et al. 2005). Blood-derived

macrophages originate as circulating monocytes in the blood, and can move into other tissues, such as the brain or spinal cord, during inflammatory episodes (Serbina et al. 2008; Shi and Pamer 2011).

During inflammatory conditions, macrophages and microglia receive certain stimuli that alter their phenotype and function. In the literature, a proposed classification of the various phenotypes of macrophages and microglia is the M0/M1/M2 classification (Fairweather and Cihakova 2009; Franco and Fernández-Suárez 2015; Mantovani et al. 2004; Martinez et al. 2009; Martinez et al. 2008; Michell-Robinson et al. 2015), Although this is a helpful and simplified classification of phenotypes, activation states of macrophage and microglia likely exist in a spectrum or combination of phenotypes *in vivo*. M0 is considered to be a “resting” phenotype and they are non-activated/non-polarized (Chistiakov et al. 2018; Michell-Robinson et al. 2015) . M1 polarization, also known as “classical” activation, arises when either macrophages or microglia are cultured with lipopolysaccharide (LPS) and/or interferon-γ (IFNγ). This phenotype is considered to be pro-inflammatory. M1-polarized macrophages or microglia characteristically release pro-inflammatory cytokines/chemokines (*e.g.* tumour necrosis factor (TNF), interleukin-12 (IL-12), CXCL8-11, CXCL13) and reactive oxygen species (ROS) (Fairweather and Cihakova 2009; Mantovani et al. 2004) and limit growth factor and nutrient availability to cells infected with pathogens (Fairweather and Cihakova 2009). In contrast, M2 polarization, also known as “alternative” activation, is considered to be an “anti-inflammatory” phenotype and is characterized by their involvement with the elimination of parasites, promoting

angiogenesis, and cell/tissue regeneration (reviewed in (Franco and Fernández-Suárez 2015)). M2 cells can be further classified into M2a, M2b, M2c, (and M2d for macrophages) as described in the literature (Franco and Fernández-Suárez 2015; Michell-Robinson et al. 2015), and can be polarized *in vitro* in the presence of interleukin-4 (IL-4), interleukin-10 (IL-10), IL-13, or transforming growth factor β (TGF β) (Franco and Fernández-Suárez 2015; Michell-Robinson et al. 2015).

In MS, during immune surveillance, the CNS-targeted immune response becomes triggered and involves a complex pathophysiology. The following are common characteristics found in MS pathology, and it is important to note that these may occur simultaneously and not strictly in this order of events. First, the BBB shows signs of leakage in MRI studies (Cramer et al. 2014; McFarland et al. 1992). Second, T cells, B cells, and monocytes/macrophages cross the BBB into the CNS (Larochelle et al. 2011), whereby monocytes become activated and differentiate into macrophages (Brück et al. 1995). Third, there is evidence of either loss, death, or damage to oligodendrocytes, oligodendrocyte progenitor or precursor cells (OPCs), and neurons, as well as demyelination (Kuhlmann et al. 2002; Lucchinetti et al. 1999; Trapp et al. 1998).

Macrophages and microglia participate in the demyelination process by destroying myelin, acting as antigen presenting cells to naïve T and B cells, cause oxidative damage to tissue, and release pro-inflammatory cytokines. Evidence for these behaviours during MS pathology are supported in the following studies. Increased numbers of activated macrophages/microglia appear

in lesions (Brück et al. 1995; Ferguson et al. 1997) and near axons (Trapp et al. 1998). Although four distinct patterns of MS lesions may develop, all include evidence of microglia/macrophage participation (Lucchinetti et al. 2000). Furthermore, it has been suggested that microglia may initiate demyelination in humans (Gay et al. 1997), and there is evidence of macrophages ingesting myelin in early and active MS lesions (Newcombe et al. 1994; van Horssen et al. 2008). Moreover, *in vitro*, rat and human microglia are capable of ingesting myelin fragments (Chastain et al. 2011; Smith 1993; Williams et al. 1994). In active demyelinating MS lesions, both microglia and blood-derived macrophages express major histocompatibility complex (MHC) class II antigens (Bö et al. 1994b; Boyle and McGeer 1990; Cuzner et al. 1988; Hayes et al. 1988), suggesting that they may be involved in antigen presentation to T cells during demyelination. In MS, there is also evidence to suggest that microglia and blood-derived macrophages may contribute to tissue damage by releasing reactive oxygen species. For example, there is evidence to suggest that in initial MS lesions, activated microglia and macrophages may be a source of ROS, which could contribute to oxidative injury (Fischer et al. 2012). In another example, nitrotyrosine, a biochemical marker for peroxynitrite (Cross et al. 1998) (a chemical generated by nitric oxide reacting with superoxide, capable of damaging cells and tissue (Cross et al. 1998)), is found in human MS brains (Bagasra et al. 1995; Cross et al. 1998; Hooper et al. 1997) and there is evidence to suggest it may have originated from macrophages/microglia expressing inducible nitric oxide synthase (iNOS) (Bagasra et al. 1995; Hooper et al. 1997). An increase in

myeloperoxidase (an enzyme that catalyzes the production of the highly cytotoxic hypochlorous acid (Gray et al. 2008b; Minohara et al. 2006; Spickett et al. 2000)) by macrophages/microglia is evident in white matter (Gray et al. 2008b) and cerebral cortex (Gray et al. 2008a) in MS, and is associated with demyelination. Oxidative damage within human neurons, oligodendrocytes, and myelin is evident in MS (Fischer et al. 2013; Haider et al. 2011). In addition to oxidative damage, there is also parallel pro-inflammatory cytokine modulation, including increased TNF and interleukin-6 (IL-6) cytokine/mRNA expression (Cannella and Raine 1995; Maimone et al. 1997; Schönrock et al. 2000; Selmaj et al. 1991; Woodroofe and Cuzner 1993). Several studies have identified macrophages/microglia as a source of TNF and IL-6 within active lesions (Cannella and Raine 1995; Selmaj et al. 1991; Woodroofe and Cuzner 1993). This production and release of reactive oxygen species, effective antigen-presentation capacity, and pro-inflammatory cytokine production by macrophages/microglia during demyelination in MS, are all characteristics of the pro-inflammatory M1 phenotype (Durafourt et al. 2012; Franco and Fernández-Suárez 2015; Sica et al. 2015).

Following active demyelinating episodes, neurons may degrade due to glutamate excitotoxicity (Pitt et al. 2000), axonal transection (Trapp et al. 1998), Wallerian degeneration (Dziedzic et al. 2010), or due to ion imbalances such as sodium or calcium imbalances (Smith 2007). Remyelinating a damaged myelin sheath will occur if the damage is worth expending an appropriate amount of energy versus allowing the neuron/axon itself to degrade. Remyelination is the

production of myelin sheaths by newly differentiated oligodendrocytes; these new sheaths form “shadow” plaques (as evidenced through MRI). Remyelination is important for recovery because it improves both electrical conduction and communication (Smith et al. 1979; Smith et al. 1981), saves demyelinated neurons from deterioration (Irvine and Blakemore 2008), and recovers motor deficits (Jeffery and Blakemore 1997; Murray et al. 2001). In humans, there is evidence that the degree of spontaneous remyelination can be considerable in MS patients (Barkhof et al. 2003; Goldschmidt et al. 2009; Patani et al. 2007; Patrikios et al. 2006), however, the extent of remyelination diminishes with disease progression (Goldschmidt et al. 2009).

The remyelination of axons is a simple solution in theory, but it is challenging to implement, as it requires three general conditions (Chandran et al. 2008; Franklin and ffrench-Constant 2008). First, following the demyelinating episode, the environment must be cleared of both axonal and myelin fragments/debris. Second, remyelination requires an influx and/or presence of oligodendrocyte progenitor cells (OPCs). Finally, OPCs recruited and existing within the demyelinated area need to successfully differentiate into myelin-producing oligodendrocytes that eventually remyelinate neurons. Failing to achieve any of these conditions will result in remyelination failure.

The key to meeting these criteria for remyelination may be encouraging the transition of pro-inflammatory “M1” myeloid cells towards an anti-inflammatory “M2” phenotype that encourages repair. Indeed, there is evidence that this transition tends to occur during remyelination. In an *in vivo* lysolecithin

demyelination model in mice, a transition from a M1 to a M2 phenotype in microglia and macrophages is observed at the beginning of remyelination (Miron et al. 2013). In MS cases, most macrophages/microglia expressed M1 markers in active demyelinating MS lesions, and a portion of those macrophages/microglia also expressed M2 markers, and so those cells expressing both M1 and M2 markers were considered to be in an intermediate activation state (Vogel et al. 2013); in a later study, there was evidence of microglia exhibiting an intermediate activation state by expressing markers for both M1 and M2 in preactive and remyelinating lesions (Peferoen et al. 2015), This may suggest a majority of cells are “M1-like” during active demyelination, while in remyelination, more cells shift toward an “M2-like” state, expressing both markers for M1 and M2. To further explain how the transition from an M1 to M2 phenotype in myeloid cells is important for remyelination, evidence for each of the remyelination challenges will be briefly discussed, along with evidence that the M1 to M2 transition could help address that challenge (Chandran et al. 2008; Franklin and ffrench-Constant 2008).

1.2.1 Remyelination and the M1 to M2 Shift in Macrophages/Microglia in MS

To begin, the first requirement for remyelination is that the CNS environment must be cleared of both axonal and myelin debris/fragments (Chandran et al. 2008; Franklin and ffrench-Constant 2008). *In vivo*, myelin fragments impair remyelination (Kotter et al. 2006) and prevents the differentiation of OPCs if they are not removed (Kotter et al. 2006; Robinson and

Miller 1999). Cells that are capable of removing this debris include microglia/macrophages, and they can achieve this by phagocytosing the debris. Evidence for this includes the observation of microglia phagocytosing cellular and myelin debris in a mouse cuprizone demyelination model (Olah et al. 2012), and the observation that remyelination becomes impaired if the phagocytic ability of macrophages/microglia becomes impaired (Lampron et al. 2015; Natrajan et al. 2015). A transition from an M1 to an M2 phenotype in microglia/macrophage polarization could encourage the phagocytosis of myelin/cellular debris, as M2-polarized microglia/macrophages are more phagocytic compared to their M1 counterparts (Durafourt et al. 2012), and therefore could remove more debris than M1-polarized myeloid cells.

Second, remyelination require an influx and/or presence of OPCs near the demyelinated area (Chandran et al. 2008; Franklin and ffrench-Constant 2008). Evidence for this comes from the fact that post-mitotic oligodendroytes do not contribute to remyelination in rats (Keirstead and Blakemore 1997). Instead, in rodents, neural stem cells (NSCs) and/or OPCs travel to demyelinated lesions and contribute to remyelination (Di Bello et al. 1999; Xing et al. 2014). Furthermore, in mice, the number of OPCs from SVZ progenitors increase near demyelinated lesions in surrounding white matter (Nait-Oumesmar et al. 1999; Picard-Riera et al. 2002). A similar observation was also seen in MS, when OPC numbers increase in the human SVZ in response to demyelination (Nait-Oumesmar et al. 2007). The transition from M1 myeloid cells to an M2 phenotype could encourage successful OPC recruitment. In a study by Choi et al. (Choi et

al. 2017) supernatants from M2-polarized BV-2 microglia encouraged neural stem/progenitor cell proliferation in the SVZ in *ex vivo* cultures. Although there is some evidence to suggest that M1 macrophages may encourage more movement of stem cells in the injured CNS in mice than M2 macrophages (Zhang et al. 2015), I argue that these cells would need to eventually polarize towards an M2 phenotype, as there is evidence that M2 cells encourage OPC differentiation (Butovsky et al. 2006; Choi et al. 2017; Miron et al. 2013; Moore et al. 2015; Zhang et al. 2015), the third requirement for remyelination.

Third, remyelination requires the successful differentiation of OPCs into myelinating oligodendrocytes (Chandran et al. 2008; Franklin and ffrench-Constant 2008). In MS, there is evidence that OPCs are successfully recruited to lesions but fail to differentiate into myelinating oligodendrocytes (Kuhlmann et al. 2008; Wolswijk 1998). A transition from M1 to M2 polarized microglia/macrophages could help address this problem. In rodent models, studies found that M2-polarized microglia or macrophages significantly increased oligodendrogenesis from stem/progenitor cells compared to controls than M1-polarized cells *in vitro* (Butovsky et al. 2006; Choi et al. 2017; Miron et al. 2013; Zhang et al. 2015). In addition, depleting M2-polarized macrophages/microglia in a demyelinated lesion hindered OPC differentiation and delayed remyelination *in vivo*, while depleting M1-polarized macrophages/microglia did not hinder remyelination (Miron et al. 2013). Supernatants from human M1 blood-derived macrophages and microglia were cytotoxic to human A2B5+ neural progenitors and reduced galactocerebroside and O4+ oligodendrocyte lineage cells *in vitro*,

while supernatant from human M2 polarized cells had little to no effect (Moore et al. 2015). Therefore, the data suggests that M1-polarized cells may hinder oligodendrogenesis, while M2 cells may maintain or promote oligodendrogenesis.

1.2.2 Neurogenesis, Neuron Recovery, and M1 to M2 Polarization

Not only is remyelination helpful in MS, but neurogenesis can also play a part in recovery. Indeed, there is evidence that neurogenesis is possible in chronic white matter lesions of MS (Chang et al. 2008). Similar to remyelination, there is evidence that the transition from M1 to M2 polarization in microglia/macrophages is beneficial for neurogenesis and neuron recovery. For example, in mice, the presence of M1-polarized microglia inhibited the survival of mouse neurons (Kobayashi et al. 2015). In addition, the presence of supernatants from M1-polarized microglia/macrophages was associated with reduced neurogenesis from mouse neural stem cells compared to M2 polarized cells (Butovsky et al. 2006; Choi et al. 2017; Zhang et al. 2015). Furthermore, neurites *in vitro* can regrow more efficiently following the removal of axonal debris (Tanaka et al. 2009), and so it is possible that M2 myeloid cells, which are more phagocytic than their M1 counterparts (Durafourt et al. 2012), could encourage efficient debris clearance and lead to neurite regrowth.

1.2.3 Treatment for MS

To encourage remyelination and recovery in MS, the development of novel treatments is paramount. Current treatments include rehabilitation and modulating/suppressing the immune response through medication (Miller 2012);

however, there is evidence to suggest that the applicability of immunomodulatory/immunosuppressive drugs to chronic and progressive forms of MS is limited (Larochelle et al. 2016), which is most likely due to a significant neurodegenerative component at this stage of disease. Developing new drugs for MS is complicated by the fact that there is a low clinical trial success rate when translating results from rodent experiments (Baker and Amor 2015). Stem cell therapy is also being investigated to treat MS (Meamar et al. 2016), although they do not address all three conditions necessary for remyelination. Theoretically, an optimal treatment would need to focus on addressing all conditions necessary for remyelination. Encouraging myeloid cells to transition from M1 to M2 phenotype may serve as a clinically relevant and viable approach, which could be achieved using microRNAs.

1.3 MicroRNAs in Disease and MS

MicroRNAs (or miRNAs) are small, non-coding ribonucleic acids (RNAs) that are approximately 18-22 nucleotides in length (Rodriguez et al. 2004). First discovered in 1993 (Lee et al. 1993), microRNAs are believed to regulate many biological processes. It is estimated that greater than 60% of human genes are conserved microRNA targets (Friedman et al. 2009), and as of February 2015, there are approximately 2,800 human microRNAs described in public repositories (Londin et al. 2015). In addition, microRNAs are highly conserved across species, highlighting their important regulatory functions (Bartel 2004; Lagos-Quintana et al. 2001; Lau et al. 2001; Lee and Ambros 2001). It is believed that if a microRNA

is expressed, it inhibits the production of its target protein by targeting its mRNA, which decreases the amount of protein available for its downstream functions (Guo et al. 2010).

In the linear canonical microRNA processing pathway, beginning in the nucleus of the cell, the gene or intron of mammalian microRNAs are first transcribed by RNA polymerase II or III to produce the primary-microRNA (pri-miRNA), the microRNA transcript. The pri-miRNA is further cut by the Drosha-DiGeorge critical region 8 (Drosha-DGCR8) microprocessor complex into the precursor microRNA (pre-miRNA), a hairpin structure which moves outside of the nucleus into the cytoplasm by the transporter Exportin-5-Ran-guanosine triphosphate (Exportin-5-Ran-GTP). The transactivation response ribonucleic acid-binding protein (TRBP) with the Dicer enzyme further cuts the “loop” end of the pre-miRNA, creating the -3p and -5p mature microRNAs. The Argonaute-2 (Ago2) protein then binds to the mature microRNA, creating the ribonucleic acid-induced silencing complex (RISC). The RISC with the mature microRNA then binds to target mRNAs, which can induce either translational repression, cleavage, or deadenylation (Bartel 2004; Winter et al. 2009). Figure 1 summarizes this process.

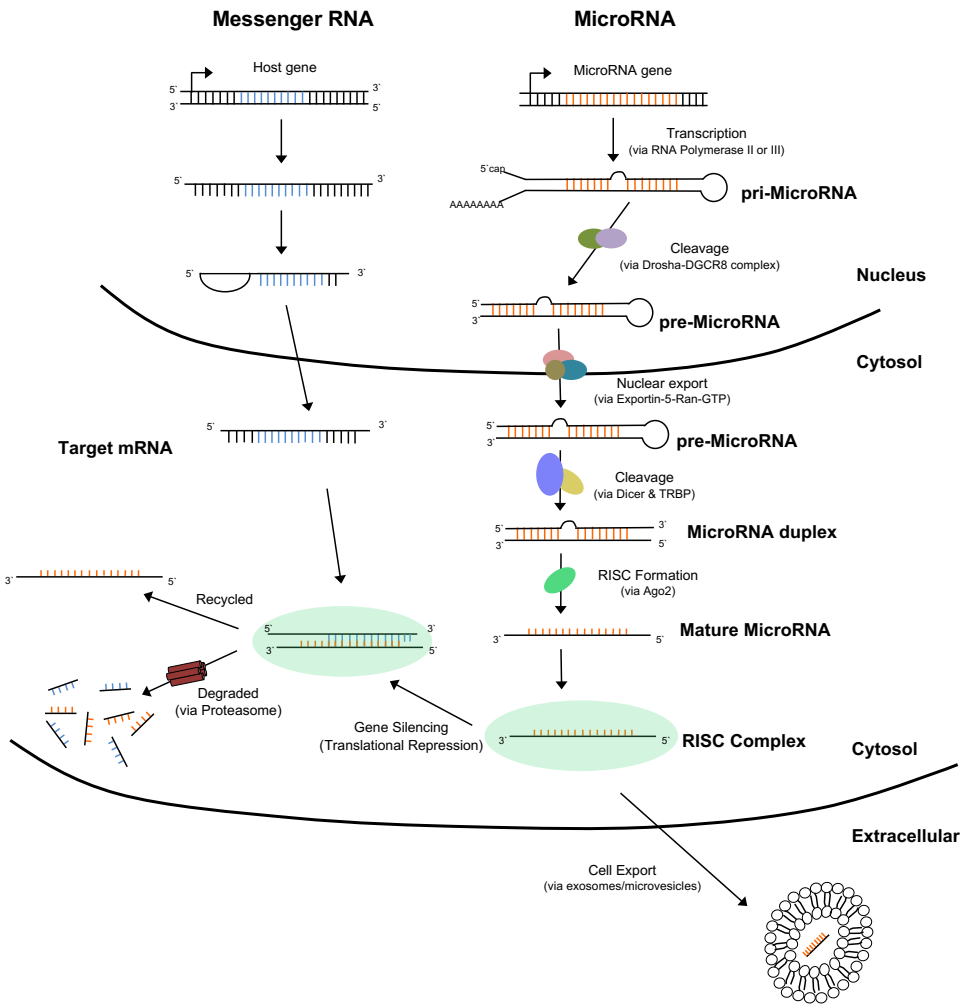

Figure 1: Biogenesis of MicroRNAs

MicroRNAs are initially transcribed by RNA polymerase II or III, generating primary microRNAs (pri-miRNA) with hairpin structures. Pri-miRNAs are further processed by the Drosha-DGCR8 microprocessor complex to produce pre-microRNAs. Pre-microRNAs are exported from the nucleus into the cytosol by Exportin-5-Ran-GTP. In the cytosol, pre-miRNAs are cleaved by the ribonucleases Dicer and transactivation response RNA-binding protein (TRBP), and form mature microRNAs that are recruited to the RNA-induced silencing complex (RISC) where they come in contact with their target mRNAs and the Argonaute-2 (Ago2) protein. Mature microRNAs bind target mRNAs via a short seed sequence (6-8mer) that is located at their 5` end. The binding of the miRNA to its targeted mRNA results in either degradation of the mRNA transcript or it is recycled back into the cytoplasm. Alternatively, miRNAs can be actively released into the extracellular space (via microvesicles & exosomes) and be transported to neighbouring cells (Bartel 2004; Winter et al. 2009; Zampetaki et al. 2012).

Since their discovery, dysregulated microRNA expression has been suggested to contribute to disease development. Whether found in abnormally high or low concentrations, dysregulated microRNAs could also serve as diagnostic biomarkers for disease. Their potential as biomarkers arises from the fact that circulating microRNAs are relatively stable and resistant to RNAse degradation, potentially due to being encapsulated in microvesicles or non-vesicle associated microRNA-protein/lipoprotein complexes (Zampetaki et al. 2012). MicroRNAs have been identified as potential biomarkers in many cancers, including prostate (Mitchell et al. 2008), ovarian (Häusler et al. 2010), breast (Schrauder et al. 2012), and lung (Patnaik et al. 2012). MicroRNAs may also serve as potential biomarkers in immune-mediated diseases such as rheumatoid arthritis (Pauley et al. 2008) and MS (Gandhi 2015). Not only can dysregulated microRNAs potentially be used to diagnose disease, they may also be amenable to therapeutic manipulation, which has led to the field of microRNA therapeutics. Notably, in different animal cancer models, Garo and Murugaiyan (Garo and Murugaiyan 2016) highlight several papers outlining microRNA target-specific technology that have shown potential in curing disease with few or no side-effects (Babar et al. 2012; Chen et al. 2010; Huang et al. 2013; Wu et al. 2013). MicroRNA therapeutics are therefore an exciting and relatively new field of biomedical research that could be instrumental in curing disease.

1.4 MicroRNA-146a

MiR-146a is a member of the miR-146 family, of which there are two types: miR-146a and miR-146b. MiR-146a is found on human chromosome 5 within the non-coding RNA host gene MIR3142HG (chromosome 5q33.3) (Paterson and Kriegel 2017). To date, miR-146a is known to play a role in innate immunity, inflammation, and cancer (Paterson and Kriegel 2017); however, it may also have a role in adaptive immunity (Lu et al. 2010). In humans, besides MS (Lescher et al. 2012), miR-146a is associated with other diseases, including rheumatoid arthritis (Nakasa et al. 2008; Nakasa et al. 2011), prion disease (Saba et al. 2012), and sepsis (Zhou et al. 2015). MiR-146a is also associated with cancer development, including breast (Bhaumik et al. 2008), thyroid (He et al. 2005), and pancreatic (Li et al. 2010) cancer.

In general, miR-146a is considered to have anti-inflammatory properties when expressed (Paterson and Kriegel 2017). There is evidence that miR-146a expression depends on NF-kB expression, and acts as a negative feedback regulator of NF-kB signalling by targeting pro-inflammatory genes, including tumour necrosis factor receptor-associated factor 6 (TRAF6) and interleukin-1 receptor-associated kinase (IRAK1) (Taganov et al. 2006). Components derived from either bacteria (*e.g*. LPS) (Nahid et al. 2009) or viruses (Cameron et al. 2008; Motsch et al. 2007; Tang et al. 2009) can induce miR-146a expression, and miR-146a has been associated with endotoxin tolerance (Doxaki et al. 2015; Nahid et al. 2009; Nahid et al. 2015). Furthermore, there is also evidence that

miR-146a is required for regulatory T cells to restrict IFNγ-mediated pathogenic Type 1 T helper responses by targeting signal transducer and activator of transcription 1 (STAT1) in regulatory T cells (Lu et al. 2010). MiR-146a knockout mice have a hyperresponsive immune response, where knockout mice produced more pro-inflammatory cytokines in blood serum compared to wild-type after LPS injection, and BMDMs from knockout mice produced more pro-inflammatory cytokines compared to wild type after exposure to LPS (Boldin et al. 2011). Furthermore, miR-146a-null mice experienced massive myeloproliferation, and aged mice experienced features suggestive of autoimmune disease and tumours as they aged with multi-organ inflammation compared to controls (Boldin et al. 2011). This strongly suggested the role of miR-146a in preventing autoimmunity and tumour/myeloid cell development (Boldin et al. 2011).

MiR-146a expression may also be altered with age. In a study by Jiang et al. (Jiang et al. 2012), miR-146a levels in peritoneal macrophages from untreated aged mice were elevated compared to younger mice. However, the peritoneal macrophages from aged mice could not increase miR-146a levels as high as levels from peritoneal macrophages from younger mice when mice were injected with LPS, or when the peritoneal macrophages were exposed to pro-inflammatory cytokines in culture (such as TNF or IL-6) (Jiang et al. 2012). Furthermore, elevated levels of miR-146a were found in mouse microglia when they were cultured *in vitro* for long periods of time compared to cells that were not cultured as long (Caldeira et al. 2014).

Although a majority of the literature describes miR-146a as anti-inflammatory, there have been some studies that suggest otherwise, particularly in the context of Alzheimer's disease. In a study by Cui et al. (Cui et al. 2010), miR-146a appeared to be associated with the downregulation of IRAK1 and upregulation of interleukin-1 receptor-associated kinase 2 (IRAK2) induced NF-κB, which maintained a prolonged inflammatory response in human astroglial cells. There is also evidence that a repressor of brain inflammation, complimentary factor H, is a target of miR-146a (Lukiw et al. 2008). However, the evidence provided by Taganov et al. (Taganov et al. 2006) and Boldin et al. (Boldin et al. 2011) in animal knockout studies, provides more direct evidence that miR-146a works as a negative regulator of inflammation and halting myeloid development. Therefore, both studies offer more compelling evidence that miR-146a, when expressed, is anti-inflammatory.

1.4.1 MicroRNA-146a in MS

MiR-146a is elevated in peripheral blood mononuclear cells (PBMCs) and CD14+ monocytes in the blood of RRMS patients compared to controls (Moore et al. 2013; Waschbisch et al. 2011). In progressive forms of MS, including both SPMS and PPMS, there is evidence that miR-146a levels are similar to controls (Fenoglio et al. 2011). In cerebrospinal fluid (CSF), Quintana et al. measured a downregulation of miR-146a levels in RRMS patients compared to other neurological disease controls (Quintana et al. 2017). Besides examining miR-146a in blood and CSF, miR-146a alterations have also been examined in MS

brain tissue. There is evidence showing that miR-146a levels increased in active MS lesions and in the microvessels of MS-active lesions (Junker et al. 2009; Wu et al. 2015). This increase in miR-146a in human active lesions is also consistent with increased miR-146a levels found in active lesions in mouse and marmoset models of MS (Lescher et al. 2012).

Recently, Moore et al. (Moore et al. 2013) measured miR-146a expression in CD68+ macrophages/microglia from the brain parenchyma of non-inflamed control tissue and in inflamed untreated MS lesions using laser-capture microdissection. There was a suggested decrease in miR-146a fold change expression in laser-captured CD68+ macrophages/microglia in the untreated MS brains compared to controls, although the sample size was small (n = 3 for control and n = 4 for MS patient) and the difference was not statistically significant at the time of publication (p = 0.264, unpaired t-test). This suggested decrease was not consistent with previous reports of increased miR-146a in active MS lesions (Junker et al. 2009; Wu et al. 2015), PBMCs (Fenoglio et al. 2011; Waschbisch et al. 2011) and CD14+ monocytes from the blood in RRMS MS patients (Moore et al. 2013). Therefore, this potential inconsistency of miR-146a levels in macrophages/microglia in the context of MS warranted further investigation.

1.5 Thesis Hypothesis and Objectives

Based on the recent finding by Moore et al. (Moore et al. 2013) in CD68+ macrophages/microglia in the brains of untreated MS patients, and the current

understanding of miR-146a and remyelination in MS, the following general hypothesis was proposed. During acute inflammation, myeloid cells are initially polarized toward an M1 pro-inflammatory phenotype and take part in demyelination in MS. As mentioned before, miR-146a is generally considered to be anti-inflammatory and functions as a negative regulator of inflammation (Boldin et al. 2011; Taganov et al. 2006). While M1 myeloid cells take part in demyelination, at the same time miR-146a levels naturally increase in these cells over time. As miR-146a increases over time, these pro-inflammatory M1 myeloid cells become less M1-like, and polarize towards an anti-inflammatory M2 phenotype over time. As a result, the anti-inflammatory M2 myeloid cells take part in addressing the three criteria required for remyelination. This leads to repair and an eventual resolution of inflammation and disease activity. Having served its purpose as a negative regulator of inflammation, miR-146a naturally decreases in the M2 myeloid cells to homeostatic levels.

Chronic CNS inflammation and an insufficient miR-146a expression within myeloid cells may promote disease activity. This theory is supported by the potential decrease of miR-146a in myeloid cells in untreated MS patients (Moore et al. 2013), and by the attenuation of miR-146a expression to pro-inflammatory stimuli in older mice compared to younger mice (Jiang et al. 2012). As a consequence, the M1 phenotype found in active demyelination in MS will dominate without hindrance by miR-146a. As a result, the M2 phenotype does not develop, leading to a failure to remyelinate, and thus the inflammation and disease activity does not resolve. Correspondingly, there is evidence that the

more chronic the MS disease, the less remyelination tends to occur (Goldschmidt et al. 2009). Finally, although speculative, one could postulate that decreased miR-146a in RRMS myeloid cells may signal the beginning of progressive disease towards SPMS, where higher levels of PBMC miR-146a were found in RRMS patients compared to controls, while PBMC miR-146a in SPMS and PPMS was similar to controls (Fenoglio et al. 2011). Based on this information, therapeutically elevating miR-146a expression in myeloid cells in chronic RRMS, SPMS, or PPMS patients may promote and maintain the tissue-repairing M2-like phenotype in myeloid cells, which is associated with remyelination and recovery. A visual outline of this overall hypothesis is described in Figure 2.

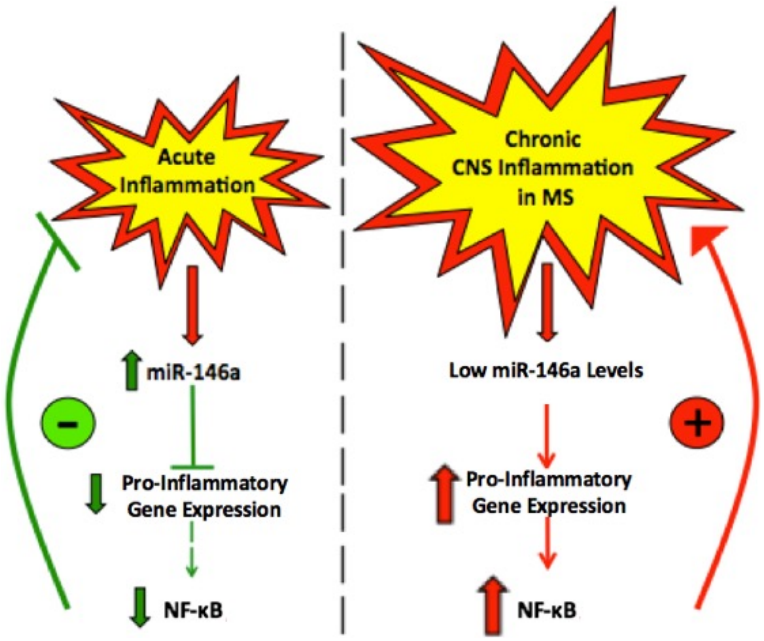

Figure 2: Overall hypothesis of the potential role of miR-146a in acute and chronic inflammation in multiple sclerosis

A well-known function of miR-146a is its negative regulation of the pro-inflammatory NF-κB pathway by inhibiting pro-inflammatory gene expression, such as IRAK1 and TRAF6 (Taganov et al. 2006). Based on a potentially lower miR-146a expression in primary human CD68+ macrophages/microglia in patients with untreated MS compared to controls (Moore et al. 2013), no significant rise in miR-146a compared to controls in PBMCs in patients with progressive forms of MS (Fenoglio et al. 2011), and a potentially attenuated miR-146a response to pro-inflammatory stimuli in macrophages due to age (Jiang et al. 2012), the following hypothesis is proposed. During acute inflammation, miR-146a levels naturally increase over time. The rise of miR-146a inhibits the expression of pro-inflammatory genes that are already highly expressed during the initial stages of inflammation. As a result, pro-inflammatory gene pathways (such as the NF-κB pathway), are inhibited, leading to a reduction and eventual resolution of inflammation. This could be described as being similar to a negative feedback loop. However, during chronic central nervous system inflammation, miR-146a levels may decrease over time. Since the availability of miR-146a is insufficient to bind to the higher amounts of mRNA of pro-inflammatory genes present, the mRNA of these genes continue to be translated, and inflammation continues without a resolution. This could be described as being similar to a positive feedback loop. To resolve chronic inflammation, therapeutically increasing and maintaining a sufficiently high expression of miR-146a may help to overcome the functional deficiencies of miR-146a in macrophages/microglia by inhibiting pro-inflammatory gene translation.

From this overall hypothesis, I formulated a more detailed hypothesis and generated aims to facilitate an investigation. I hypothesize that miR-146a upregulation in myeloid cells can shift a pro-inflammatory (M1) phenotype towards an anti-inflammatory (M2) phenotype, which will promote differentiation of neural stem cells to OPCs and neurons. The four aims of the study will use synthetically-made miR-146a mimic, as it is a cost-effective way to test the effect of endogenous miR-146a, compared to isolating enough miR-146a from living tissues for experimentation. The four aims include:

Aim #1: Provide evidence that microRNAs can be transfected into primary mouse and human macrophages/microglia and human THP-1 macrophages.

To achieve Aim #1, each cell type will be treated in either of two ways. Cells will be transfected with a synthetic miR-146a mimic and miR-146a will be measured using the quantitative reverse transcription polymerase chain reaction (RT-qPCR) assay, or cells will be transfected with a fluorescently labelled microRNA, and the amount of microRNA transfected will be measured using flow cytometry.

Aim #2: Analyze supernantants for production of pro-inflammatory cytokines from pro-inflammatory activated (M1) myeloid cells transfected with miR-146a mimics.

To achieve Aim #2, each cell type will be cultured *in vitro* and transfected with miR-146a mimic. Subsequently, cells will be polarized towards an M1 phenotype using LPS, similar to the phenotype seen in active demyelination.

Supernantants derived from these cells will be analyzed for pro-inflammatory cytokine production relevant to MS.

Aim #3: Validate miR-146a gene targets, inducible nitric oxide synthase (iNOS) and Ras homolog A (RhoA).

To achieve Aim #3, predicted targets of miR-146a, iNOS and RhoA, will be examined on all cell types. iNOS and RhoA are both predicted targets of miR-146a and are also associated with MS pathology. Cells will be transfected with miR-146a mimic, then stimulated with LPS, as mentioned previously. Following stimulation, cells will be collected and western blots will be used to examine iNOS and RhoA production in cells.

Aim #4: Determine if miR-146a can indirectly influence OPC differentiation and neuron development in mice.

Finally, to determine if miR-146a can influence neurogenesis and oligodendrogenesis from neural stem cells, mouse bone marrow-derived macrophages (BMDMs) will first be treated with miR-146a mimic and stimulated with LPS. Next, supernatant from these cells will be cultured with mouse neurospheres. The total number of cells, neurons, OPCs, neurosphere area, the percentage of total cells that are either neurons or OPCs, and the density of neurons or OPCs, will be analyzed and normalized per neurosphere.

Chapter 2 - Methods and Materials

2.1 Isolation and Culture of Animal Cells

2.1.1 Isolation of Primary Mouse Bone Marrow-Derived Macrophages

Primary BMDMs were isolated from wild-type C57BL/6 mice (Charles River) using a modified protocol by Ying et al. (Ying et al. 2013). Briefly, wild-type C57BL/6 mice from 6 weeks of age or older were euthanized by CO_2. The body and fur were disinfected with 70% ethanol, and the hind limbs were removed. The muscle was carefully cut away from the bone, and the femur and tibia bones were separated. Separate petri dishes were used for each individual mouse preparation; instruments were sterilized between each dissection. For each femur and tibia, both ends were cut, and the marrow was ejected from the bone using a sterile 21 - 21 ½ gauge needle and 3mL of sterile phosphate-buffered saline (PBS, pH 7.4, 10mM PO_4, 2.7mM KCl, 137mM NaCl, 1.76mM KH_2PO_4). The marrow was then either triturated using the needle 4-6 times and passed through either a 40uL or 70uL strainer, or ground in the strainers, to remove larger tissue and bone fragments. This ensured a preparation that was dissociated into single cells. Dishes, needles and strainers were rinsed with an additional 2mL of PBS and passed through the strainer to yield the maximal cell number. A 0.8% sterile ammonium chloride red blood cell lysis solution (pH 7.2-7.6) (University of Washington 2017) was added to 3 times the volume of the BMDM preparation to remove red blood cells, and this mixture was left on ice for 10 minutes. Then, the mixture was spun at 500 x g for 5 minutes at 4°C. The supernatant was

aspirated, and a BMDM growth media consisting of Dulbecco's Modified Eagle Medium (DMEM) (Cat. #: 12100-046, Gibco, Life Technologies), 10% heat inactivated fetal bovine serum (HI FBS) (Cat. # 35-015-CV, USA Sourced, Corning, USA) or heat inactivated NuSerum IV (Cat. # 355500, Corning, USA), 100 U/mL of penicillin and 100 g/mL of streptomycin (1x P/S) (Cat. # 15140122, Gibco, Life Technologies or Cat. #: P4333, Sigma-Aldrich) and 2mM of L-alanyl-L-glutamine dipeptide (1X GlutaMAX) (Cat. # 35050-061, GlutaMAX, Gibco, Life Technologies) with 10ng/mL of recombinant human Macrophage Colony-Stimulating Factor (M-CSF) (Cat. # 300-25, PeproTech) was added. Cells were counted, additional BMDM growth media was added to the cells to make the cell concentration 2 x 10^6 cells/mL, and cells were plated into 12- (2 x 10^6 cells/well) or 6-well (6 x 10^6 cells/well) tissue culture treated wells, marking Day 0. Cultures were grown at 37^{o}C in 5% CO_2. On Day 3, a half media change was performed using fresh media as described above. On Day 7-8, the cells were washed once with PBS prior to use. A typical picture of mouse BMDMs can be found in Figure 3.

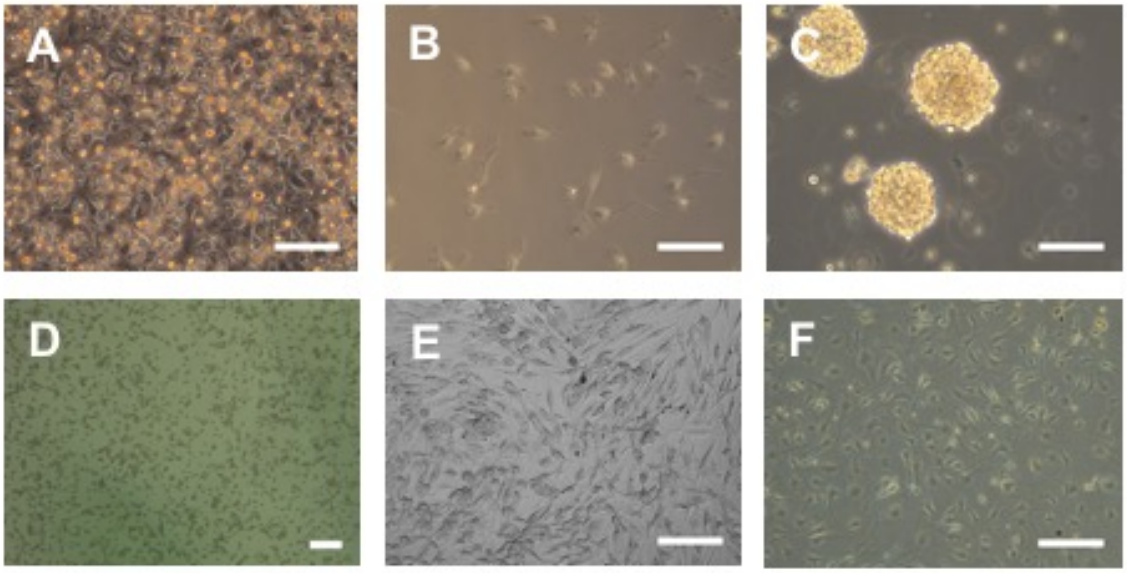

Figure 3: Examples of mouse and human cells successfully cultured *in vitro*

(A) Primary mouse BMDMs. (B) Primary mouse microglia. (C) Primary mouse neurospheres. (D) Human THP-1 monocyte-derived macrophages. (E) Primary human fetal microglia. (F) Primary human adult microglia. Scale bar = 100μm.

2.1.2 Isolation of Primary Mouse Microglia

Primary mouse microglia were isolated from a mouse mixed glial culture by mild trypsinization using a protocol by Saura et al. (Saura et al. 2003) with modification. Dissection solution (DS) consisted of Hank's Balanced Salt Solution (Cat. # H8264, Sigma Life Science), 2mM of HEPES solution (Cat. # H0887, Sigma Life Science), and P/S. A portion of DS was pre-warmed into a 37°C water bath. A trypsin inhibitor solution consisting of 20% heat-inactivated (HI) FBS in DS was prepared, and placed in the 37°C water bath. Finally, astrocyte media consisting of DMEM, 10% HI FBS or HI NuSerum IV, P/S and GlutaMAX was prepared, and a portion was pre-warmed in the 37°C water bath. Throughout the whole procedure, separate instruments and solutions were used for each experimental group of cortices.

Briefly, wild-type postnatal day 1 – postnatal day 6 (P1-P6) C57BL/6 mouse pups were euthanized by decapitation and the brain was removed and placed into a sterile dish containing DS. The cortices were isolated and transferred into another clean sterile dish with DS. The meninges containing blood vessels were removed, and cortices were placed into another final clean sterile dish with DS. The cortices were then divided into smaller pieces using sterile forceps and washed with fresh DS. Then, per 6 mouse cortices, a solution containing 0.8% trypsin (Cat. # 15090-046,ThermoFisher Scientific) in DS with 0.05mg/mL of DNase I (Cat. #11 284 932 001, Roche) was added. The cortices were then incubated at 37°C on a rotating Nutator for 17 minutes. Cortices were

washed once with pre-warmed DS. Next, pre-warmed trypsin inhibitor was added and the cortices were incubated on a rotating Nutator at 37°C for another 10 minutes to inhibit any remaining trypsin. Cortices were then washed with pre-warmed astrocyte media, and then resuspended in 6mL of pre-warmed astrocyte media. Cortices were then triturated into a single cell suspension. The single cell suspension was then spun at 270 x g for 5 minutes at room temperature, supernantant was aspirated, and cells were resuspended in mixed glial culture media and plated in tissue-culture treated flasks. Mixed glial cultures were incubated at 37°C in 5% CO_2. Media was replaced 1-2 days later, and every 4-16 days after the initial media change as necessary. To collect mouse astrocyte conditioned media, media was collected from mixed culture during media changes, spun at 751 x g for 20 minutes, and the clean supernatant was collected and stored at either 4°C (for use within 7 days) or -80°C (for long-term storage). Once astrocytes were at least confluent for 3-5 days or more, the flasks were washed once with either PBS or serum-free defined media for 1 minute to remove residual serum. Trypsin-EDTA (Cat. # 15400-054, ThermoFisher Scientific) was diluted to 0.25% with PBS, and was added to serum free defined media at a ratio of 1:3. This was the “mild trypsin” solution. The mild trypsin solution was then added to the mixed glial culture for 20-30 minutes in the incubator at 37°C until the astrocyte layer peeled off. If necessary, the original flask was washed once with PBS to remove any residual astrocytes that

detached. A figure of the separation of mouse astrocytes and microglia is found in Figure 4.

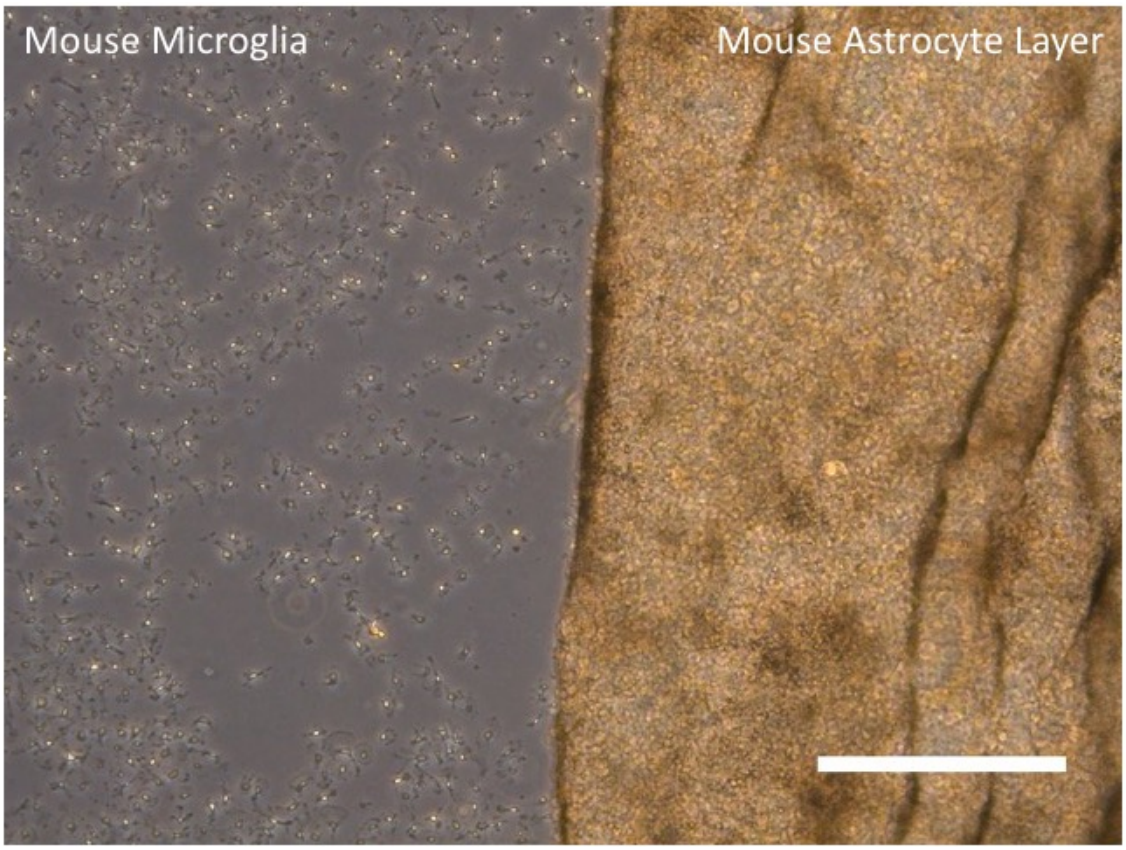

Figure 4: Separation of primary mouse astrocytes from mouse microglia using the modified mild trypsinization method

To separate mouse microglia from mouse astrocytes in a mixed culture, the mild trypsinization method (Saura et al. 2003) with modification was used. Using this method, a highly confluent astrocyte layer (right) separates from the bottom of the flask, leaving a relatively pure population of mouse microglia still adhered to the flask (left). The microglia are then collected and replated. Scale bar = 500μm.

Diluted 0.25% trypsin-EDTA in PBS was then added to the microglia for 5-15 minutes in the incubator, with an additional 2mM of EDTA if needed to recover a higher yield of microglia. Cells were vigorously pipetted and collected. Cells were centrifuged at 270 x g for 10 minutes at 4^{o}C. Mouse microglia were then resuspended in mouse astrocyte-conditioned media, counted, resuspended at 1 x 10^5 cells/mL, and plated into either 24-well (5 x 10^4 cells/well) or 12-well (1 x 10^5 cells/well), or 6-well (3 x 10^5 cells/well) tissue culture treated plates in mouse astrocyte-conditioned media for 24 hours prior to experimentation.

2.2 Isolation and Culture of Human Cells

2.2.1 Culture of THP-1 Macrophages

THP-1 monocytes (Cat. # TIB-202^{TM}, ATCC®) of passage <15 were cultured in complete Roswell Park Memorial Institute (RPMI) 1640 media (Cat. #R8758, Sigma-Aldrich) containing 10% HI FBS, P/S and GlutaMAX at 37^{o}C in 5% CO_2. Monocytes were plated at 5 x 10^5 cells/mL in a 24-well plate (2.5 x 10^5 cells/well) with complete media with 20ng/mL of phorbol 12-myristate 13-acetate (PMA) (Cat. # P8139, Sigma) for 24 hours for cells to adhere and differentiate into macrophages. After 24 hours cells were washed once with fresh complete media.

2.2.2 Isolation of Primary Human Monocyte-Derived Macrophages

Human monocyte-derived macrophages (MDMs) were isolated using a protocol as described in Moore et al. (Moore et al. 2013). All studies using human samples followed Canadian Institutes of Health Research guidelines and were

approved by the institutional review board at McGill University and Memorial University of Newfoundland (Health Research Ethics Authority). Briefly, peripheral blood was collected from healthy donors with informed consent. A Ficoll density gradient was used to isolate peripheral blood mononuclear cells (PBMCs) from whole blood. Briefly, blood from one individual was collected into a BD Vacutainer® vial, and 2 vials were poured into a 50mL centrifuge tube. Vials were rinsed with PBS and contents were added to the tube to collect as many cells as possible. The centrifuge tube was topped up to 35mL using PBS. A 60mL syringe with a spinal needle containing 15mL of Ficoll-Hypaque solution (Cat. # 17-1440-03, GE Healthcare) was slowly added to the bottom of the 50mL centrifuge tube. The centrifuge tube was spun at 609 x g for 30 minutes without the brake. When the centrifuge came to a complete stop, the plasma (top layer) was removed, and the middle white buffy layer (PBMCs) were pipetted and placed into another 50mL tube. PBMCs were washed once by topping up the tube to 50mL with PBS, inverting the tube to mix, and centrifuging the tube at 423 x g for 15 minutes with the brake. The supernatant was poured off, and the tube was scratched against a grated surface to resuspend the pellet. The pellet (or 2 pellets combined from the same individual if another tube was being processed at the same time) were placed into one 50mL centrifuge tube, and the volume was brought up to 50mL using PBS. The tube was spun at 270 x g for 10 minutes. Supernatant was poured off and the tube was scratched against a grated surface to resuspend the pellet. All PBMC pellets from the individual were pooled into one 50mL centrifuge tube. To further isolate CD14+ cells from the PBMC population,

anti-CD14 immunomagnetic microbeads (Miltenyi Biotec, Auburn, CA) were used following the manufacturer's instructions, resulting in a CD14+ monocyte population of 95-98% purity.

CD14+ monocytes were subsequently plated at a density of 5×10^5 cells/mL in RPMI 1640 media containing 10% HI FBS, P/S and GlutaMAX at 37°C in 5% CO_2 in 12-well (5×10^5 cells/well) and 6-well (1.5×10^6 cells/well) tissue-culture treated plates. MDMs were obtained by culturing the monocytes with M-CSF (25ng/mL) over 5 days.

2.2.3 Isolation of Primary Human Fetal and Adult Microglia

Human fetal and adult microglia were isolated in a similar manner as outlined in Moore et al. (Moore et al. 2013). All studies using human samples followed Canadian Institutes of Health Research guidelines, and were approved by the institutional review board at McGill University and Memorial University of Newfoundland (Health Research Ethics Authority).

Briefly, human fetal CNS tissue was obtained from either consenting donors (Health Sciences Centre – General Hospital, St. John's, NL), from Novogenix Laboratories (Torrance, CA, USA), or from a human fetal tissue repository (Albert Einstein College of Medicine, Bronx, USA). Brain tissue from the temporal lobe of patients undergoing surgery for non-tumour-related intractable epilepsy was used to isolate human adult microglia. Brain tissue within the suspected focal area was not used. Human fetal and adult microglia cells were isolated and cultured as described previously (Durafourt et al. 2013; Moore

et al. 2013). Once fetal and adult microglia were isolated, they were plated at 1 x 10^5 cells/mL in 12-well (1 x 10^5 cells/well) and 6-well (3 x 10^5 cells/well) tissue culture treated plates.

2.3 MicroRNA Transfection, LPS Stimulation, and Collection of Supernatant

For transfection of negative control and miR-146a microRNAs into all cell types, Lipofectamine® RNAiMAX Transfection Reagent (Cat. # 13778-100, Invitrogen, Life Technologies) was used according to the manufacturer's instructions. For mouse cells and THP-1 macrophages, mirVana™ miRNA mimic Negative Control #1 (Cat. # 4464058, Ambion) and hsa-miR-146a-5p mirVana™ miRNA mimic (Cat. # 4464066, mature miRNA sequence: UGAGAACUGAAUUCCAUGGGUU, Ambion) were used for transfection. For human MDMs, human fetal microglia, and human adult microglia, miR-146a mimic (Cat. #: C-300630-03-0002, hsa-miR-146a-5p, associated mature miRNA: UGAGAACUGAAUUCCAUGGGUU, Dharmacon) and negative control (Cat. #: CN-001000-01-05, Based on cel-miR-67, mature sequence: UCACAACCUCCUAGAAAGAGUAGA, Dharmacon) were used for transfection. Lipofectamine was diluted 1:100 in serum-free DMEM, P/S and GlutaMAX (considered as the vehicle mixture). Then, miRNA controls and mimics were added to the corresponding vehicle mixture and left to equilibrate for 20-30 minutes at room temperature. Before transfection, mouse BMDMs and human microglia and MDMs were washed once with PBS. Human THP-1 macrophages were washed once with complete media before transfection.

Primary mouse microglia were transfected for 24 hours. Primary mouse bone-marrow-derived macrophages were transfected for 48 hours. THP-1 macrophages and primary human monocyte-derived macrophages were transfected for 72 hours. Primary human microglia were transfected for 72 hours. Previous optimization experiments for transfection of microRNAs in primary human MDMs and microglia were conducted by Moore et al. using this procedure (Moore et al. 2013).

Following transfection of human MDMs and microglia, cells were washed once with PBS. THP-1 macrophages were washed once with complete media after transfection. Next, either complete media or complete media containing lipopolysaccharide (100ng/mL, Cat. # L 5024, serotype O127:B8, Sigma) was added to the appropriate wells for 6 hours. Following transfection for mouse BMDMs and microglia, no PBS wash was conducted to avoid losing cells. Instead, the original transfection media was removed and replaced with either complete media for the “No Treatment” experimental group or complete media containing lipopolysaccharide to the other experimental groups for 6 hours.

After 6 hours, the supernatant was collected on ice. Clean supernatant was obtained by centrifuging at 500-700 x g for 10 minutes at 4^{o}C to separate cellular debris, and the clean supernatant was stored at -80^{o}C.

2.4 Flow Cytometry

To evaluate microRNA transfection efficiency using Lipofectamine RNAiMAX in THP-1 macrophages, THP-1 macrophages were developed as

described above in a 24-well plate, plated at 5 x 10^5 cells/mL (2.5 x 10^5 cells/well). THP-1 macrophages were divided into two groups: untreated cells, and cells transfected with 30nM of Cy3-labelled microRNA (Cy3™ Dye-Labelled Anti-miR™ Negative Control #1, Cat. #: AM17011, Invitrogen, ThermoFisher Scientific) using Lipofectamine RNAiMAX as described above. Cells were transfected for 48 hours. After 48 hours of transfection, cells were scraped in PBS, spun for 5 minutes at 270 x g, washed 1x in fluorescence-activated cell sorting (FACS) buffer (1% Bovine Serum Albumin (BSA) (Cat. # A9647-100G, Sigma) in PBS) and resuspended in FACS buffer. Data was acquired using a FACSCalibur flow cytometer (BD Biosciences), and analyzed using FlowJo software V.10.0.8 (FlowJo, LLC, Ashland, Oregon, USA).

2.5 RNA Isolation, Preamplification Polymerase Chain Reaction, and Quantitative Polymerase Chain Reaction

At the end of each experiment, cells were washed with PBS and TRIzol® Reagent (Cat. # 15596018, Ambion by Life Technologies) or QIAzol® Lysis Reagent (Cat. # 79306, QIAGEN) was added directly to wells. RNA was extracted according to the manufacturer's protocol. RNA concentration was determined on a Nanodrop 1000 Spectrophotometer (Thermo Scientific). Reverse transcription was performed using the TaqMan® MicroRNA Reverse Transcription Kit (Cat. # 4366597 and Cat. # 4366596, Applied Biosystems) according to the manufacturer's protocol. Polymerase chain reaction (PCR) was conducted with the Taqman® Universal PCR Master Mix (Cat. # 4304437, Applied Biosystems) (Hold at 95°C for 10min, and then 40 cycles of 95°C for 15

seconds to 60°C for 1min). Probes and primers used were hsa-miR-146a-5p (Cat. # 4427975, Taqman™ MicroRNA Assays, ThermoFisher Scientific), RNU48 (Cat. # 4427975, Taqman™ MicroRNA Control Assays, ThermoFisher), and SNO202 (Cat. # 4427975, Taqman™ MicroRNA Control Assays, ThermoFisher Scientific or Cat. # CCU001S**,** ThermoFisher Scientific). RT-qPCR was read on an Applied Biosystems® ViiA 7 Real-Time PCR System and analysis was conducted on QuantStudio™ Software by Applied Biosystems. Minus reverse transcriptase and no-template cDNA controls were included. Fold changes were calculated using the $2^{-\Delta\Delta CT}$ method (Livak and Schmittgen 2001; Schmittgen and Livak 2008).

2.6 Western Blotting

At the end of the experiment, cells were placed on ice. Supernatant was removed, then either sodium dodecyl sulphate (SDS) sample buffer (10% w/v glycerol, 5% v/v β-mercaptoethanol, 2.3% w/v SDS, 0.0625M Tris pH 6.8, 0.1-0.2% bromophenol blue, overall pH 6.8) or standard radioimmunoprecipitation assay (RIPA) buffer (10mM Tris-Cl (pH 8.0), 1mM EDTA, 1% Triton X-100, 0.1% sodium deoxycholate, 0.1% SDS, 140mM NaCl) with 1mM Na_3VO_4 and BD Baculogold protease inhibitors (BD Biosciences) were added to each well. The wells was scraped, and the contents were collected into a 1.5mL eppendorf tube, vortexed, and placed into -80^{o}C for later use. Protein concentration was determined by using the Total Protein Kit, Micro Lowry, Peterson's Modification (Cat. # TP0300-1KT, Sigma Aldrich), measuring readings using Genesys 10uv

Scanning (Thermo Scientific) or by using the Pierce™ Bicinchoninic Acid (BCA) Protein Assay Kit (Cat. # 23227, Thermo), measuring readings using the Cytation™ 5 Cell Imaging Multi-Mode Reader (BioTek).

All western blots were developed in the following procedure. Briefly, equivalent amounts of protein were loaded into wells of a gel, along with prestained markers (PageRule Prestained Protein Ladder, Cat. # 26616, Thermo Scientific or MagicMark XP Western Protein Standard, Cat. # LC5602, ThermoFisher Scientific). The gel was run at 180V until the bands and ladder passed through the gel, and then the proteins were transferred to a polyvinylidene difluoride membrane (PVDF). The membrane was blocked in 5% milk/phosphate-buffered saline with Triton X (0.3%) (PBST) for 1 hour at room temperature on a shaker. Primary antibodies in 5% milk/PBST with 0.02% NaN_3 were added to the membrane and shaken overnight at 4°C. Afterwards, the membrane was washed three times for 5 minutes each in PBST, and the appropriate IgG antibody conjugated to the horseradish peroxidase enzyme (IgG-HRP) in 5% milk/PBST was added to the membrane and shaken for 1 hour at room temperature. Afterwards, the membrane was washed three times for 5 minutes each in PBST. Detection was achieved using the Pierce Enhanced Chemiluminescence (ECL) Western Blotting Substrate (Cat. #: 32106, Thermo Scientific), and blots were exposed to x-ray film and developed. Densitometry was conducted as a form of semi-quantification using ImageJ (version 1.51w), (Schindelin et al. 2015; Schneider et al. 2012), and the densitometry procedure is outlined in Appendix A, based on information and tutorials from the *ImageJ User*

Guide – IJ 1.46r (Ferreira and Rasband 2012), Luke Miller (Miller 2010), and Tim Starr (Starr 2013) with modification.

If the blot needed to be stripped to test for actin, the following was performed. Briefly, the blot was washed three times for five minutes each in PBST. Stripping buffer that was made in the lab (0.0625M Tris, pH 7.2, 2% SDS, 0.007% β-Mercaptoethanol in deionized water) was added to cover the blot, and incubated at 60°C in a water bath for 30 minutes. The membrane was then washed three times for 5 minutes each in PBST, and reblocked in 5% milk/PBST for 1 hour at room temperature on a shaker or overnight on a shaker at 4°C. Then, the membrane was reprobed for actin using the procedure mentioned above.

The western blot examining iNOS in mouse BMDMs had 40ug of protein for each sample, and the samples were run on a gradient gel (Cat. # NW04122BOX, Bolt™ 4-12% Bis-Tris Plus Gels, Invitrogen). The primary antibody that was used was anti-iNOS (2ug/mL (1:26), Cat. # ab15323, rabbit polyclonal antibody, Abcam), and the secondary antibody that was used was goat anti-rabbit IgG-HRP (1:2000, Cat. # sc-2004, Santa Cruz). The blot was then stripped and probed for actin as described above. For testing actin, the primary antibody that was used was anti-actin (1:1000, Cat. # A4700, mouse monoclonal antibody, Sigma), and the secondary antibody that was used was goat anti-mouse IgG-HRP (1:2000, Cat. # sc-2005, Santa Cruz Biotechnology).

The western blot examining RhoA in mouse BMDMs had 40ug of protein for each sample, and the samples were run on a gradient gel (Cat. # NW04122BOX, Bolt™ 4-12% Bis-Tris Plus Gels, Invitrogen). The primary antibody that was used was anti-RhoA (26C4) (1:200, Cat. # sc-418, mouse monoclonal antibody, Santa Cruz Biotechnology), and the secondary antibody that was used was goat anti-mouse IgG-HRP (1:2000, Cat. # sc-2005, Santa Cruz Biotechnology). The blot was then stripped and probed for actin as described above. For testing actin, the primary antibody that was used was anti-actin (1:1000, Cat. # A4700, mouse monoclonal antibody, Sigma), then the secondary antibody that was used was goat anti-mouse IgG-HRP (1:2000, Cat. # sc-2005, Santa Cruz Biotechnology).

The western blot examining human MDM iNOS had 10ug of protein for each sample, and the samples were run on a 10% 1mm acrylamide gel made in the lab. For efficient probing without the need to strip the blot, the blot was cut into two, dividing the protein of interest from the actin loading control. Each portion was processed separately. For the iNOS portion, the primary antibody that was used was anti-iNOS (1:500, Cat. # NB300-605SS, rabbit polyclonal antibody, Novus Biologicals), and the secondary antibody that was used was goat anti-rabbit IgG-HRP (1:2000, Cat. # sc-2004, Santa Cruz). For the actin portion, the primary antibody that was used was anti-actin (1:1000, Cat. # A4700, mouse monoclonal antibody, Sigma), and the secondary antibody that was used was goat anti-mouse IgG-HRP (1:2000, Cat. # sc-2005, Santa Cruz Biotechnology).

The western blot examining human MDM RhoA had 10ug of protein in each sample, and the samples were run on a 10% 1mm acrylamide gel made in the lab. For efficient probing without the need to strip the blot, the blot was cut into two, dividing the protein of interest from the actin loading control. Each portion was processed separately. For the RhoA portion, the primary antibody that was used was anti-RhoA (26C4) (1:200, Cat. # sc-418, mouse monoclonal antibody, Santa Cruz Biotechnology), and the secondary antibody that was used was goat anti-mouse IgG-HRP (1:2000, Cat. # sc-2005, Santa Cruz Biotechnology). For the actin portion, the primary antibody that was used was anti-actin (1:1000, Cat. # A4700, mouse monoclonal antibody, Sigma), and the secondary antibody that was used was goat anti-mouse IgG-HRP (1:2000, Cat. # sc-2005, Santa Cruz Biotechnology).

The western blot examining human Microglia iNOS had 20ug of protein in each sample, and the samples were run on a 10% 1mm acrylamide gel made in the lab. For efficient probing without the need to strip the blot, the blot was cut into two, dividing the protein of interest from the actin loading control. Each portion was processed separately. For the iNOS portion, the primary antibody that was used was anti-iNOS (1:500, Cat. # NB300-605SS, rabbit polyclonal antibody, Novus Biologicals), and the secondary antibody that was used was goat anti-rabbit IgG-HRP (1:2000, Cat. # sc-2004, Santa Cruz Biotechnology). For the actin portion, the primary antibody that was used was anti-actin (1:1000, Cat. # A4700, mouse monoclonal antibody, Sigma), and the secondary antibody

that was used was goat anti-mouse IgG-HRP (1:2000, Cat. # sc-2005, Santa Cruz Biotechnology).

The western blot examining human microglia RhoA had 10ug of protein in each sample, and the samples were run on a 10% 1mm acrylamide gel made in the lab. For efficient probing without the need to strip the blot, the blot was cut into two, dividing the protein of interest from the actin loading control. Each portion was processed separately. For the RhoA portion, the primary antibody that was used was anti-RhoA (26C4) (1:200, Cat. # sc-418, mouse monoclonal antibody, Santa Cruz Biotechnology), and the secondary antibody that was used was goat anti-mouse IgG-HRP (1:2000, Cat. # sc-2005, Santa Cruz Biotechnology). For the actin portion, the primary antibody that was used was anti-actin (1:1000, Cat. # A4700, mouse monoclonal antibody, Sigma), and the secondary antibody that was used was goat anti-mouse IgG-HRP (1:2000, Cat. # sc-2005, Santa Cruz Biotechnology).

Ponceau S solution (Cat. # P7170-1L, Sigma) was used to further identify relative actin concentrations on blots, following the manufacturer's instructions.

2.7 Enzyme-Linked Immunosorbent Assay

Human tumour necrosis factor (TNF) (Cat. # 555212) and interleukin-6 (IL-6) (Cat. # 555220), and mouse TNF (Mono/Mono) (Cat. # 555268) and IL-6 (Cat. # 555240) OptEIA enzyme-linked immunosorbent assay (ELISA) kits were used from BD Biosciences, and performed according to the manufacturer's

instructions. Absorbance readings were obtained using a Cytation^{TM} 5 Cell Imaging Multi-Mode Reader by BioTek.

2.8 Microscopy of Mouse and Human Myeloid Cells

Pictures of living cell cultures were taken on an Inverted Microscope for Cell and Tissue Culture Leica DMi1 (Leica Microsystems CMS GmbH).

2.9 Analysis of Indirect Effect of miR-146a Transfected Cells on Neurosphere Development

2.9.1 Mouse Neurosphere Culture

Mouse neurospheres were isolated from wild-type C57BL/6 pups using a modified protocol from Moore et al. (Moore et al. 2011). Briefly, 24-48 hours after plating the mixed glial cultures from P1-P7 pups using the same procedure as described above, the media from the culture was removed and fresh media was added to the adhered cells. The media that was removed was centrifuged at 270 x g for 10 minutes at room temperature. If needed, a 40uL strainer was used to avoid any clumping of cells. The supernatant was aspirated, and the pellet was resuspended in an equivalent amount of PBS or more to remove traces of serum and centrifuged for an additional 10 minutes. The PBS was aspirated off of the pellet, and the pellet was resuspended in mouse neurosphere growth media. For neurospheres used to count neurons, this media consisted of serum-free DMEM/Nutrient Mixture F-12 Ham (Cat. # D8437, Gibco, Life Technologies) with P/S and GlutaMAX, 20ng/mL of human recombinant basic fibroblast growth factor 2 (FGF-2) (Cat. # F0291, Sigma-Aldrich), 10ng/mL of mouse epidermal growth

factor (EGF) (Cat. # E4127, Sigma), 1x B27 supplement without vitamin A (Cat. # 12587, Life Technologies). For neurospheres used to count OPCs, media was the same as above, with the addition of 2ng/mL of filter-sterilized heparin (Cat. # H3149-10KU, Sigma-Aldrich). All neurospheres were then cultured in 6-well non-tissue culture treated plates.

As neurospheres grew in suspension in the 6-well non-tissue culture treated plates, they were lightly triturated as necessary to avoid clumping until a majority of spheres had grown to approximately 500μm to 1000μm in diameter (7 days). An image of a growing neurosphere can be found in Figure 3. After 7 days, neurospheres were collected, divided into tubes equalling the number of experimental groups, spun at 200 x g for 4 mins at 4°C, the supernatant was removed, and neurospheres were mixed with serum-containing supernantant from conditioned mouse BMDMs. For neurospheres used to count OPCs, 1x N1 supplement (Cat. # N6530-5ML, Sigma-Aldrich) was mixed with the BMDM supernatant.

For neurospheres used to count neurons, neurospheres adhered and differentiated in 24 well plates with sterile laminin-coated coverslips. For neurospheres used to count OPCs, neurospheres adhered and differentiated in the wells of a Nunc™ Lab-Tek™ Chamber Slide System permanox slide (Cat. # 177445, Thermo-Fisher Scientific). In the presence of serum contained in the supernatant, all neurospheres adhered to the bottom of the well and differentiated for a maximum of 7 days. A typical example of neurosphere development is seen in Figure 5.

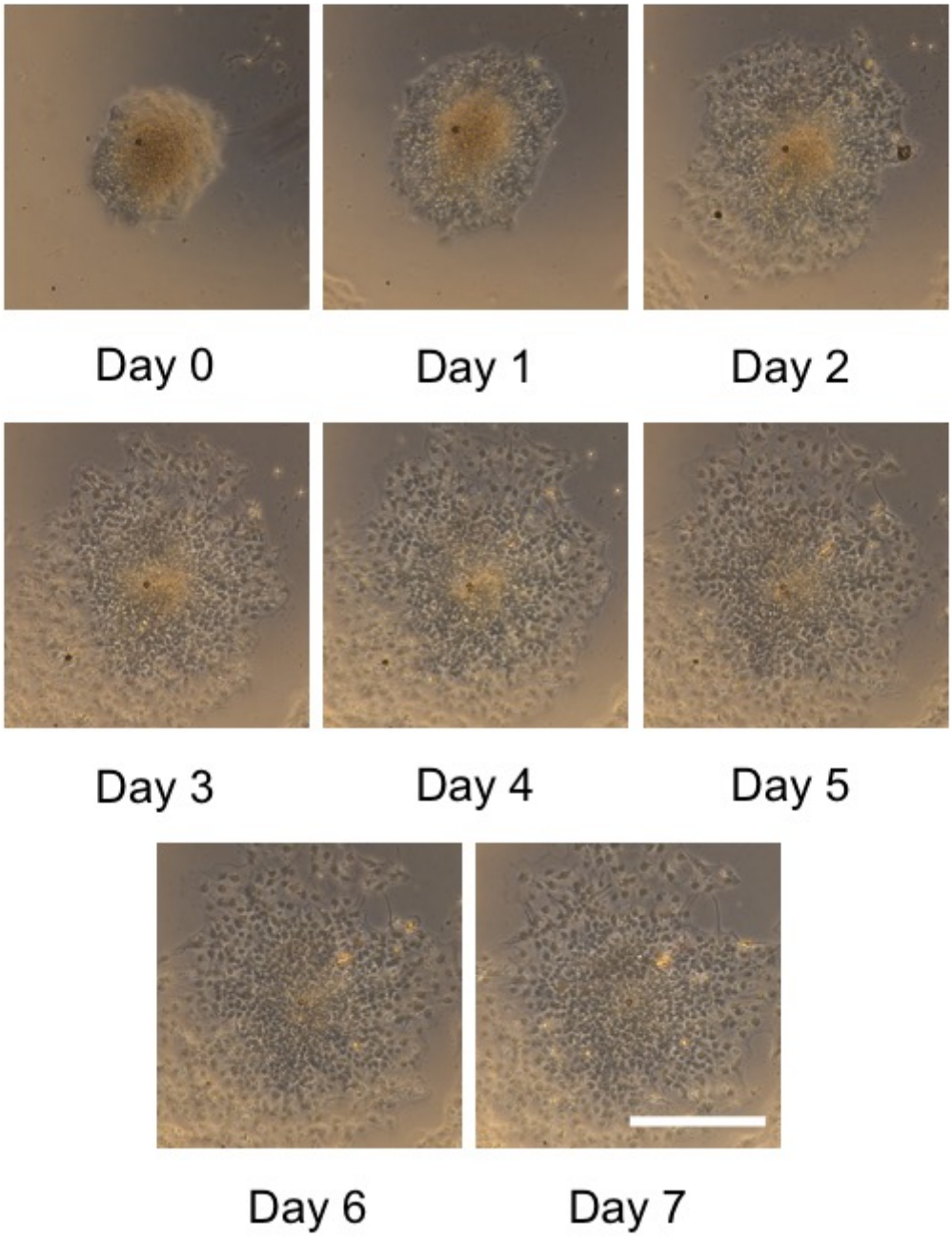

Figure 5: Primary mouse neurosphere development *in vitro*

Murine-derived neurospheres were grown to approximately 500-1000μm in diameter (7 days). At this stage, neurospheres were cultured in the presence of supernatants derived from mouse BMDMs and their associated experimental conditions. At this stage, in the presence of FBS, the neurospheres immediately adhered to the wells and differentiated into astrocytes, neurons, and OPCs for a maximum of 7 days. Scale bar = 500μm.

2.9.2 Immunocytochemistry of Mouse Neurospheres

Once neurospheres differentiated after 7 days, the cells were washed once with PBS, fixed with 4% paraformaldehyde (PFA) for 5 minutes at room temperature, and washed twice with PBS before storage in PBS at 4^{o}C until staining.

2.9.2.1 Immunocytochemistry of Mouse Neurospheres for Neurons

For mouse neurospheres used to count for neurons, cells were permeabilized and blocked using PBST with 10% normal goat serum (NGS) for 0.5 hours at room temperature. Then, anti-βIII-Tubulin (1:500, Cat. #801201, Mouse IgG2a, BioLegend) with 1% NGS in PBST was added and left overnight at 4°C. Then, cells were washed 3x with PBS, 5 minutes each, and secondary antibody (1:1000, Cat. # A11005, Alexa Fluor® 594 goat anti-mouse IgG, Life Technologies) was added with 1% NGS in PBS for blocking for one hour at room temperature. Cells were washed 3x with PBS, 5 minutes each, and DAPI (1:1000 in PBS, Cat. #: D1306, Invitrogen, ThermoFisher Scientific) was used to stain nuclei for 5 minutes, and then cells were washed for 15 minutes in PBS, then washed 3x in PBS for five minutes each. Laminin-coated discs were then mounted onto slides with fluoromount gel (Cat. #: 0100-1, Fluoromount-G®, SouthernBiotech) and stored at 4°C.

2.9.2.2 Immunocytochemistry of Mouse Neurospheres for OPCs

For mouse neurospheres used to count for OPCs, cells were permeabilized and blocked using PBST with 10% NGS and 2% horse serum (blocking solution) for 0.5 hours at room temperature. Then, neural/glial antigen 2 (NG2) primary antibody (1:500 in blocking solution, Cat. # AB5320, rabbit polyclonal antibody EMD Millipore) was incubated with slides for 1 hour at room temperature. Cells were washed twice with PBS, then incubated with 10% NGS, 2% horse serum, and PBS with secondary antibody (1:1000, Alexa Fluor® 594 goat anti-rabbit IgG Cat. # A11012, Life Technologies) for 1 hour at room temperature. Then, cells were washed once with PBS and DAPI (1:1000, Cat. #: D1306, Invitrogen, ThermoFisher Scientific) for 2 minutes, washed briefly with PBS alone, coverslipped using flouromount-G, then stored at 4°C. Immunocytochemistry for mouse OPCs was conducted by Dylan Galloway.

2.9.3 Image Analysis

For neurospheres used to count neurons, images were taken on a Carl Zeiss inverted microscope Axio Observer.Z1 (Zeiss) and used the accompanying Zen 2 (blue edition) software (Zeiss). For neurospheres used to count OPCs, images were taken on the Cytation^{TM} 5 Cell Imaging Multi-Mode Reader (BioTek) and used the accompanying Gen5 software (BioTek). All images were captured by a blinded observer. Similar microscopy settings were maintained across all images. Three representative neurospheres were taken for each experimental group. For ease in distinguishing neurospheres for either neuron or OPC

counting, βIII-tubulin+ cells in this thesis are coloured red, while NG2+ cells in this thesis are coloured green (colors edited from channel .tif file using Fiji).

The images for neurospheres were analyzed using Fiji (Version 2.0.0-rc-49/1.51a) for Mac (Schindelin et al. 2012; Schindelin et al. 2015; Schneider et al. 2012). The specific settings used in the macro (or program), written in the "IJ1 Macro" language, can be found in the program code in Appendix B. Briefly, the DAPI and βIII-Tubulin or NG2 channels of the neurosphere image are saved as separate .tif files. These files are then blinded to the researcher for counting. First, the DAPI and βIII-Tubulin/NG2 images are manually adjusted in Fiji to clearly see nuclei and the perimeter of the neurosphere. Next, using the Fiji selection tool, selections of the center (using the adjusted nuclei image) and perimeter of the neurosphere (using the adjusted neuron image) are saved. Next, using a written macro for Fiji, all original channel images are automatically adjusted for brightness and contrast. The DAPI image is processed further. Background noise is subtracted, a set threshold on nuclei size is set, the white nuclei are turned black on a white background, and the nuclei are automatically divided up into individual particles by the "Convert To Mask" and "Watershed" programs in Fiji. Next, the center of the neurosphere and the outside of the neurosphere are eliminated by automatically overlaying the center and perimeter .roi files, leaving a ring of nuclei. The nuclei in this ring are then counted and tallied using the "Analyze Particles" program in Fiji. The outlines of each nuclei that the program counts are saved for later. Finally, channel images with automatically adjusted brightness and contrast are merged: nuclei and neurons

or OPCs. For each merged image, one more is made with the overlay of the counted nuclei by the macro. After the images are made, the number of βIII-tubulin+ or NG2+ cells from the cells with circled nuclei, and the total area of the neurosphere, is counted and measured by a blinded researcher. Figure 6 outlines this entire procedure. Figure 7 and Figure 8 outline the final neurosphere pictures created by the program for neurons and OPCs, respectively.

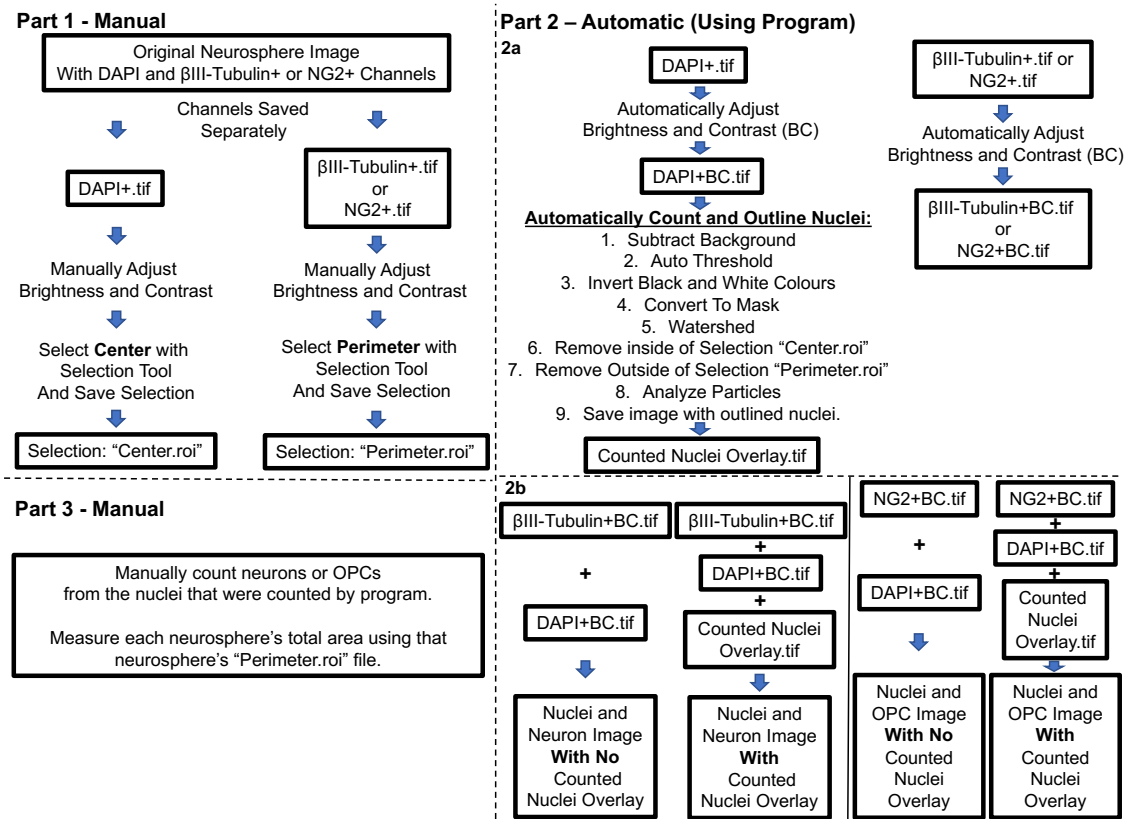

Figure 6: Overview of image analysis for mouse neurospheres

A detailed explanation of the image processing of mouse neurospheres is found in the Materials and Methods section. (Part 1) Channel images of each neurosphere were saved separately. Using Fiji, each channel image was manually adjusted for BC to see structures clearly, and outlines and centers of the neurosphere were created manually and saved. (Part 2a) Using the program, the original channel images were automatically adjusted for BC. The nuclei (DAPI) image was processed further to automatically count the number of nuclei, and create a separate image outlining which nuclei were counted. (Part 2b) For each neurosphere, all channel images are merged together and two final images are created: one with, and one without, the outlines of nuclei counted by the program. (Part 3) With the two final images, numbers of neurons or OPCs from the counted nuclei are counted manually. The total neurosphere area is measured using the area of the outline selection of the neurosphere in Fiji. (BC = Brightness and Contrast).

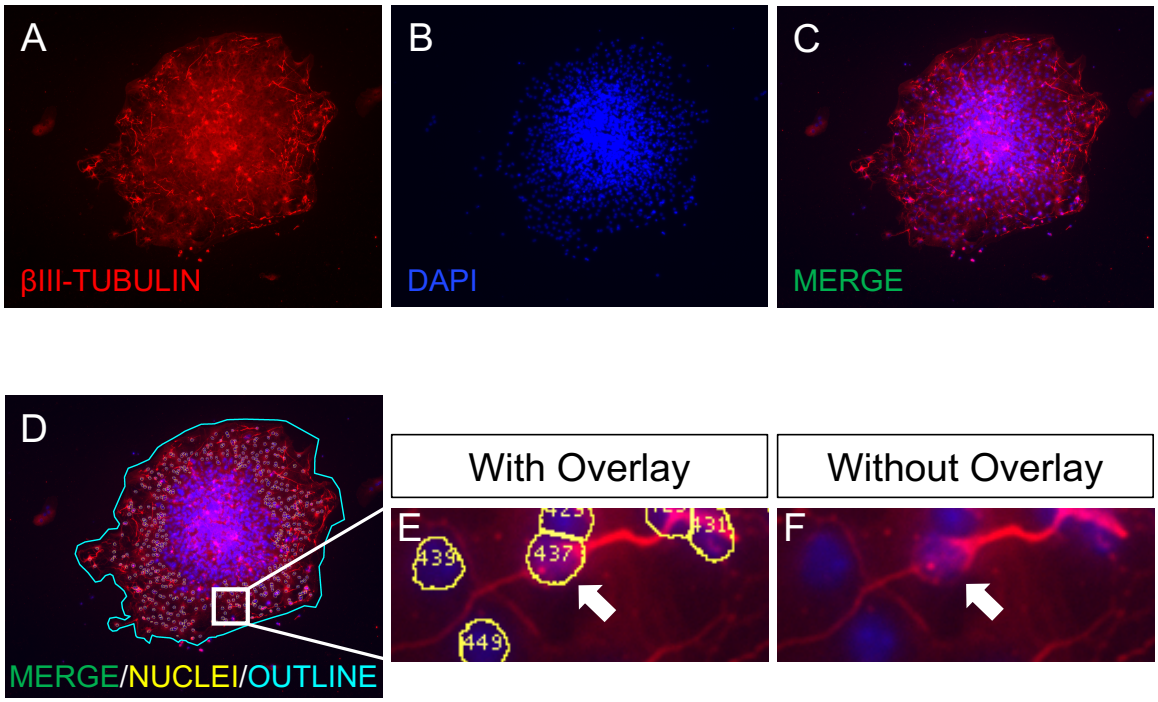

Figure 7: Mouse neurosphere processed using Fiji to count neurons

(A) βIII-Tubulin+ (neuron) staining. (B) DAPI+ (nuclei) staining. (C) Merging of βIII-Tubulin+ and DAPI+ staining. (D) Merging of βIII-Tubulin+ and DAPI+ staining, with the outlined nuclei in yellow by the program, and the perimeter selection created manually by the researcher in cyan. (E) A magnified area of image D with one example of a neuron. The yellow outline of nuclei with numbers is the overlay created by the program. (F) Identical area shown in image E without the counted nuclei overlay, showing the same neuron that was counted.

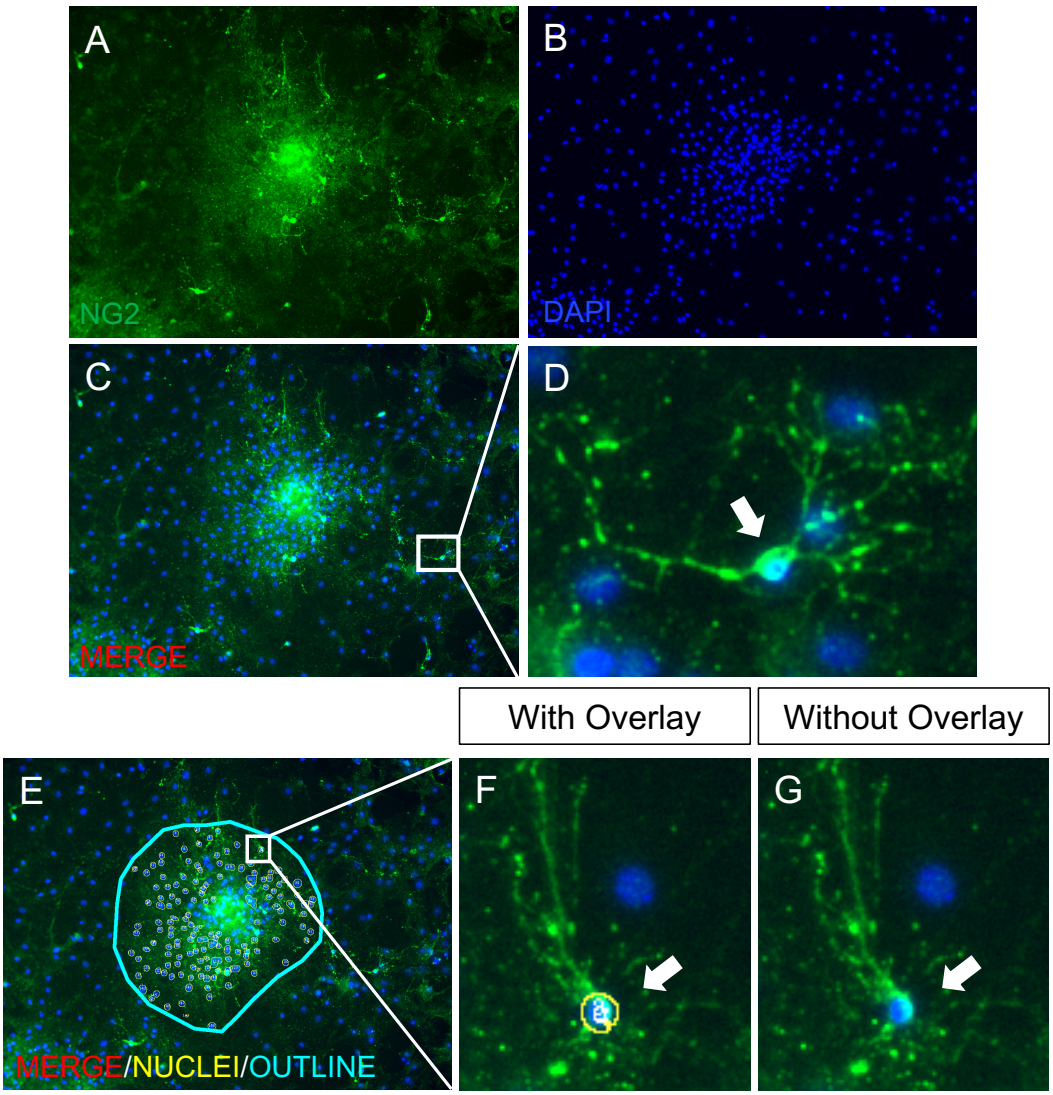

Figure 8: Mouse neurosphere processed using Fiji to count OPCs

(A) NG2+ (OPC) staining. (B) DAPI+ (nuclei) staining. (C) Merging of NG2+ and DAPI+ staining. (D) A magnified area of image C with one example of an OPC. (E) Merging of NG2+ and DAPI+ staining, with the outlined nuclei in yellow by the program, and the perimeter selection created manually by the researcher in cyan. (F) A magnified area of image E with one example of an OPC counted as part of the nuclei counted by the program. The yellow outline of nuclei with numbers is the overlay created by the program (one outline with #9 in center on OPC). (G) Identical area shown in image E without the counted nuclei overlay, showing the same OPC that was counted.

2.10 Myelin Phagocytosis Assay

The myelin phagocytosis assay using primary mouse microglia followed the procedure outlined in Durafourt et al. (Durafourt et al. 2012) with modification. Whole mouse brain myelin was isolated using an earlier protocol (Norton and Poduslo 1973) with modification. Briefly, white matter from whole brains of C57BL/6 mice were mechanically homogenized in 0.32M sucrose. To isolate myelin, the homogenized white matter underwent repeated sucrose density centrifugation and osmotic shocks. Primary mouse microglia were isolated using the mild trypsinization method as described above, and placed into the 8-well permanox chamber slides. Mouse microglia were either untreated, treated with 30nM of negative control mimic, or treated with 30nM of miR-146a mimic for 48 hours as described above. Then, 25µg/mL of isolated myelin was added to the cells for 24 hours. After 24 hours, the cells were fixed with 4% PFA for 15 minutes at room temperature. Primary antibodies against myelin basic protein (MBP) (1:200, Cat. # 808401, Mouse IgG2b, BioLegend) and ionized calcium-binding adapter molecule 1 (Iba1) (1:500, Cat. # 019-19741, Anti-Iba1, Rabbit, Wako) were added overnight at 4°C, and secondary antibodies at 1:1000 (Cat. # A11005, Alexa Fluor® 594 goat anti-mouse IgG, Life Technologies, Cat. # A11008, Alexa Fluor® 488 goat anti-rabbit IgG, Life Technologies) for 1 hour at room temperature. In a double-blind experiment, pictures were taken of each treatment group from multiple fields of view (5-10) and counted. The average percentage of myelin positive cells from all pictures of each treatment well was

calculated and graphed. All work pertaining to the phagocytosis assay and the subsequent immunohistochemistry and cell counting for the phagocytosis assay was conducted by Dylan Galloway.

2.11 Statistical Analysis

Statistical analyses were performed using GraphPad Prism Version 6.0g. Data is presented as mean +/- standard error of the mean. One-way analysis of variance was conducted, and the particular post hoc test used is mentioned in the figure description. $p<0.05$ was considered significant.

Chapter 3 - Results

3.1 Proof of MicroRNA Transfection

3.1.1 MiR-146a mimic can be successfully transfected into primary mouse BMDMs and primary mouse microglia using Lipofectamine RNAiMAX

To determine if a miR-146a mimic could be successfully transfected into primary mouse BMDMs and microglia, RT-qPCR was performed for miR-146a following transfection and LPS stimulation. LPS stimulation alone had a negligible effect on miR-146a expression compared to untreated cells (not shown). Elevated miR-146a expression was measured in both cell types compared to the negative control (Figure 9). The data suggests that primary mouse BMDMs transfected with 10nM and 30nM of a miR-146a mimic can have a higher expression of miR-146a compared to cells transfected with a negative control mimic (30nM). Similar results were also observed in primary mouse microglia.

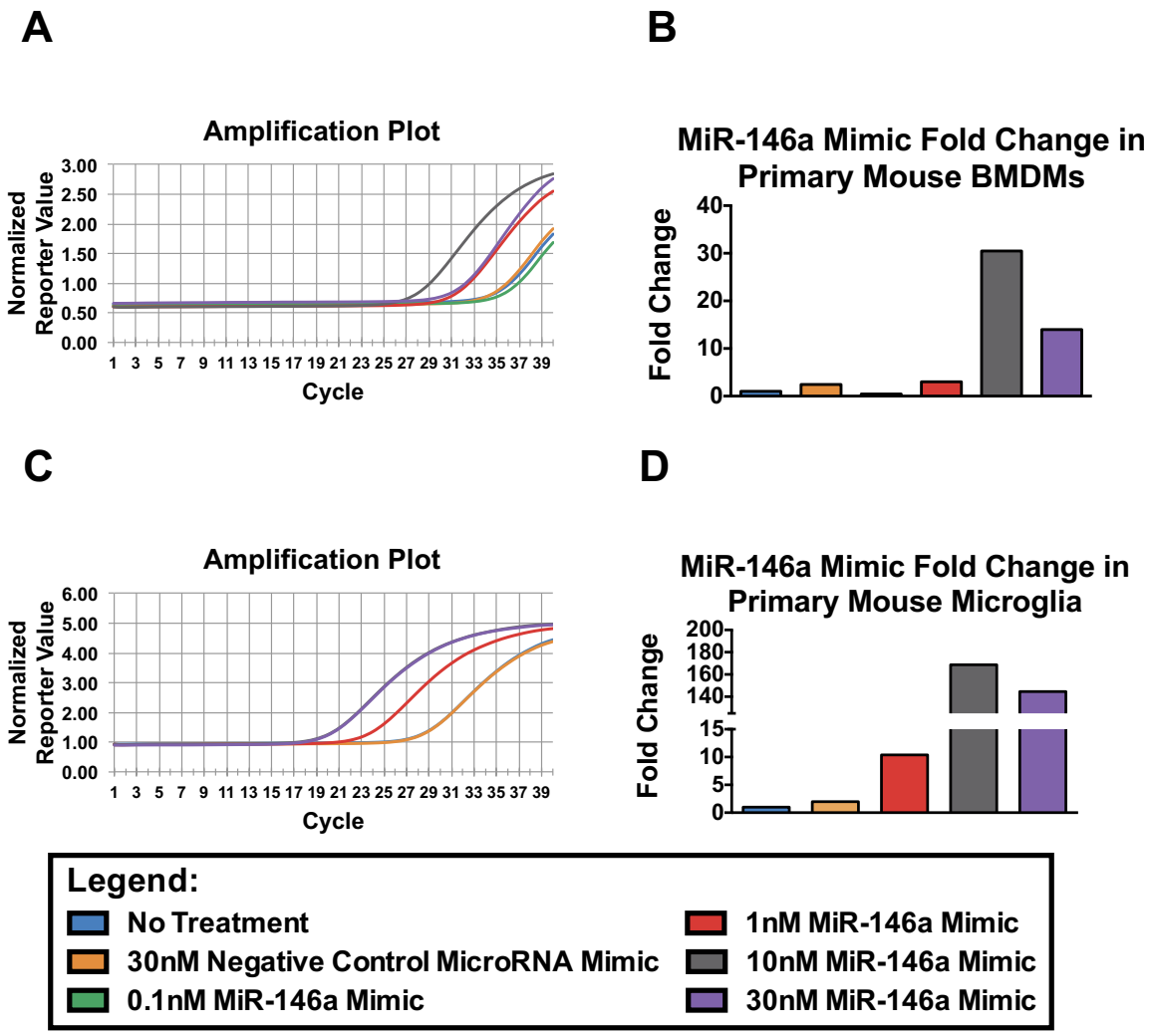

Figure 9: Transfection of miR-146a mimic into primary mouse BMDMs and microglia using Lipofectamine RNAiMAX

RT-qPCR probing for miR-146a expression was performed on primary mouse BMDMs and microglia that were untreated, treated with 30nM of NC miRNA with LPS stimulation, and either 0.1nM, 1nM, 10nM, and 30nM miR-146a mimic with LPS stimulation. LPS stimulation alone had a negligible effect on miR-146a fold change compared to untreated cells (not shown). (A) Amplification plot of miR-146a mimic on a representative technical set of primary mouse BMDMs. (B) Fold change of miR-146a mimic in primary mouse BMDMs using the $2^{-\Delta\Delta CT}$ method. (C) Amplification plot of miR-146a mimic on a representative technical set of primary mouse microglia. (D) Fold change of miR-146a expression in primary mouse microglia using the $2^{-\Delta\Delta CT}$ method. n = 1 for primary mouse BMDMs and primary mouse microglia in technical duplicate.

3.1.2 MicroRNAs can be successfully transfected into human THP-1 macrophages using Lipofectamine RNAiMAX

To provide evidence for the successful transfection of a miR-146a mimic into human THP-1 macrophages, Cy3-labelled microRNA (30nM) was transfected into THP-1 macrophages for 48 hours. The mean fluorescence intensity of the labeled microRNA was measured using flow cytometry. Compared to untransfected cells, a higher fluorescent signal was detected in cells transfected with Cy3-labelled microRNA (Figure 10), suggesting that microRNAs can be successfully transfected with microRNAs.

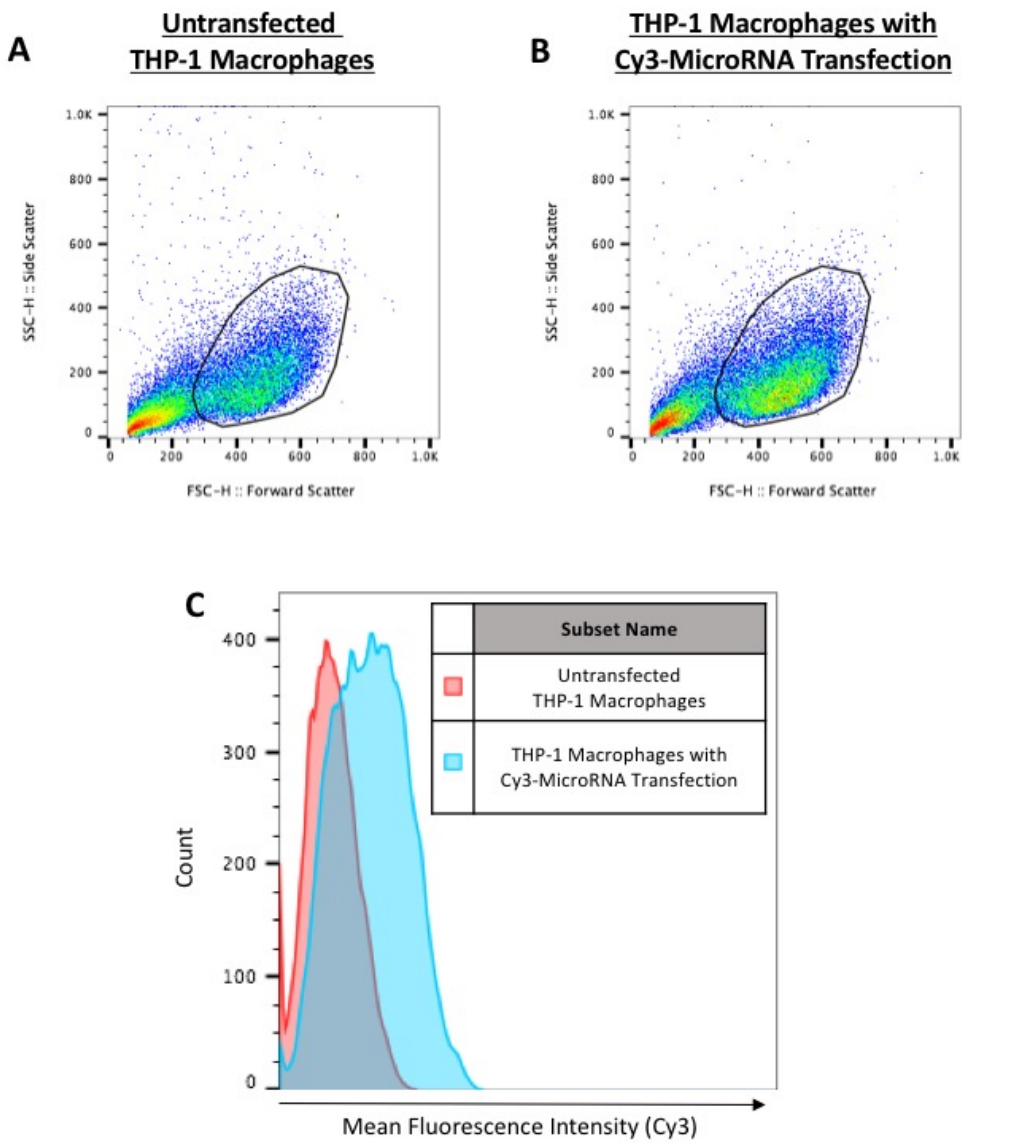

Figure 10: MicroRNA mimics can be successfully transfected into THP-1 macrophages using Lipofectamine RNAiMAX

To provide evidence that microRNAs can be successfully transfected into THP-1 macrophages, THP-1 macrophages were either untreated or transfected with a Cy3-labelled microRNA for 48 hours. The cells were subsequently collected and analyzed using flow cytometry. (A) Collection of THP-1 macrophages that were not transfected. (B) Collection of THP-1 macrophages that were transfected with the Cy3-labeled microRNA. In images A and B, the cells were gated identically. (C) Histogram of number of gated cells counted versus the recorded Cy3 signal for both untransfected and Cy3-transfected cells. There is a higher shift in the Cy3 signal from cells transfected with Cy3-microRNA compared to those that were untreated. n = 1 for THP-1 macrophages.

3.2 Assessing Inflammatory Response of Primary Mouse Myeloid Cells Transfected with a MiR-146a Mimic

3.2.1 ELISAs

3.2.1.1 TNF production decreases in LPS-stimulated primary mouse BMDMs transfected with a miR-146a mimic

A statistically significant decrease in TNF (Figure 11 A), but not IL-6 (Figure 11 B) production was measured in mouse BMDMs that were transfected with 30nM of miR-146a mimic with LPS stimulation compared to the negative control.

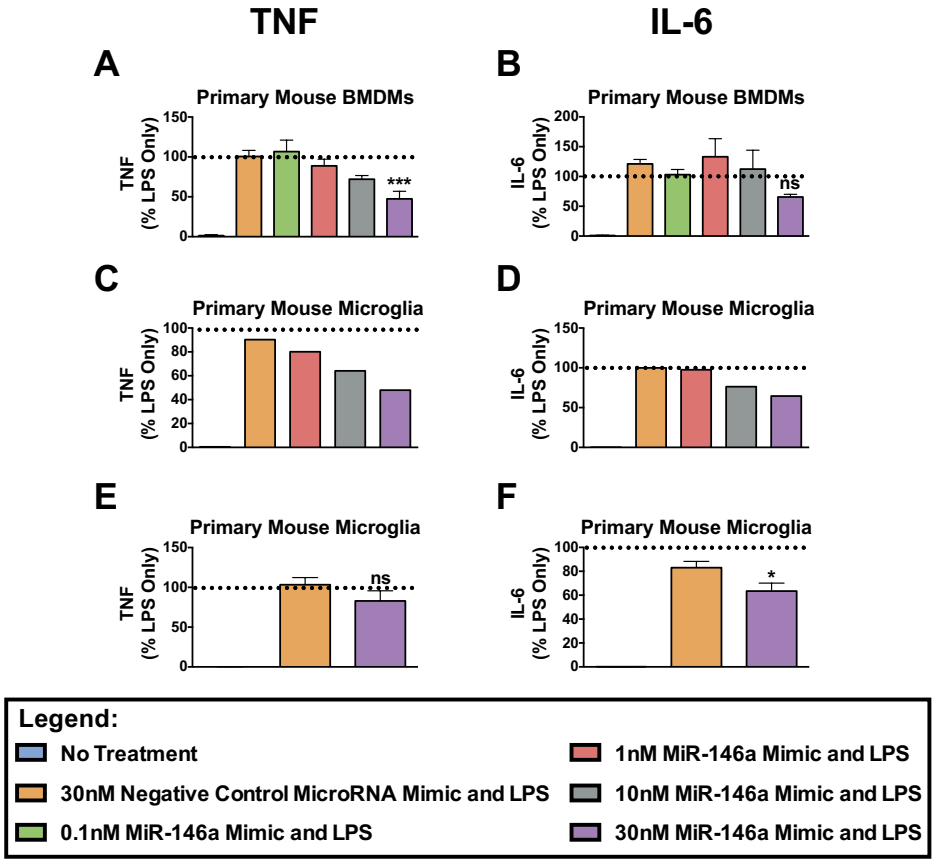

Figure 11: MiR-146a significantly decreases TNF in primary mouse BMDMs and IL-6 in primary mouse microglia after 6 hours under M1-polarizing conditions

(A) Compared to the negative control, miR-146a mimic significantly decreased TNF production by primary mouse BMDMs that were transfected with 30nM of miR-146a mimic with LPS stimulation. (B) Compared to the negative control, miR-146a mimic did not significantly decrease IL-6 production by primary mouse BMDMs in any of the cells treated with miR-146a mimic with LPS stimulation. In the first experiment using primary mouse microglia, the initial result suggested that miR-146a, compared to the negative control, could significantly decrease TNF (C) and IL-6 (D) production in these cells. However, when the experiment was repeated, IL-6 (F), but not TNF (E), was significantly reduced by 30nM of miR-146a mimic with LPS stimulation compared to the negative control. All data is normalized as a percentage of the LPS Only response for each mouse experiment. Error bars represent the mean +/- standard error of the mean of independent experiments. One-way analysis of variance with Dunnett's post hoc test was used to determine group differences. *p<0.05, ***p<0.001 compared to 30nM NC microRNA mimic with LPS stimulation. (A) n = 4-5, (B) n = 4-5, (C) n = 1, (D) n = 1, (E) n = 5, (F) n = 5.

3.2.1.2 IL-6 production decreases in LPS-stimulated primary mouse microglia transfected with a miR-146a mimic

A preliminary experiment using primary mouse microglia and a range of miR-146a mimic concentrations (1-30nM) suggested that LPS-stimulated cells transfected with 30nM may reduce TNF (Figure 11 C) and IL-6 production (Figure 11 D) the most compared to the negative control, and the other miR-146a mimic concentrations. Additional experiments were then performed in four independent sets of primary microglia, and a statistically significant decrease in IL-6 production (Figure 11 F) was observed. No statistically significant decrease was observed for TNF (Figure 11 E).

3.2.2 Western Blots

3.2.2.1 iNOS expression may increase upon LPS stimulation, but may not change in LPS-stimulated primary mouse BMDMs transfected with a miR-146a mimic

While a possible increase in iNOS levels was observed upon LPS stimulation alone, iNOS expression (Figure 12 A and B) may not differ in primary mouse BMDMs that were treated with either a miR-146a mimic or negative control mimic.

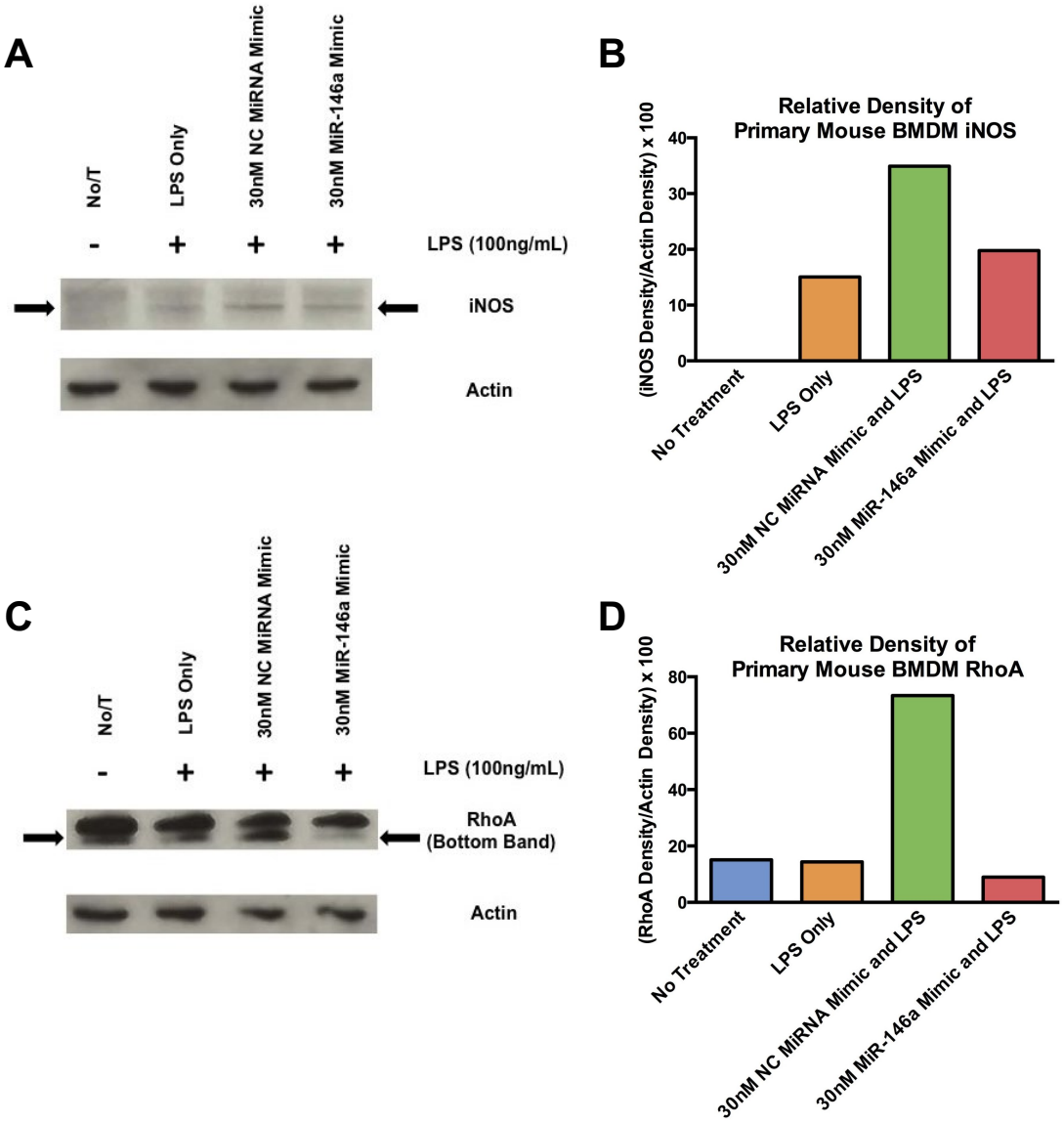

Figure 12: MiR-146a may decrease RhoA, but not iNOS, in primary mouse BMDMs after 6 hours under M1-polarizing conditions

(A) iNOS blot for primary mouse BMDMs. (B) Graph of relative densities of iNOS bands in A. No iNOS band was clearly detected under no treatment conditions; however, upon stimulation with LPS, a stronger iNOS band was observed. Although the data suggests miR-146a decreased iNOS production compared to the negative control, both were higher than the LPS Only control. (C) RhoA blot for primary mouse BMDMs. (D) Graph of relative densities of RhoA bands in C. The data suggests that RhoA in LPS-stimulated cells transfected with a miR-146a mimic (30nM) may decrease compared to the negative control, LPS only control, and untreated cells. Both blots used the same samples. n = 1.

3.2.2.2 RhoA expression may decrease in LPS-stimulated primary mouse BMDMs transfected with a miR-146a mimic

In primary mouse BMDMs, RhoA expression (Figure 12 C and D) may decrease in LPS-stimulated cells transfected with a miR-146a mimic (30nM) compared to all other treatment groups, including untreated cells, LPS only, and LPS-stimulated cells transfected with a negative control mimic (30nM).

3.3 Assessing Inflammatory Response of Human Myeloid Cells Transfected with a MiR-146a Mimic

3.3.1 ELISAs

3.3.1.1 TNF and IL-6 production may decrease in LPS-stimulated THP-1 macrophages transfected with a miR-146a mimic

For technical reasons, including the validation of microRNA transfection and its expected results (as previously documented in the literature), initial experiments were performed in the THP-1 cell line (n = 1) prior to applying methodologies in primary human myeloid cells. A suggested decrease in both TNF and IL-6 production was measured in THP-1 macrophages that were transfected with a miR-146a mimic (10nM & 30nM) compared to the negative control (30nM) (Figure 13).

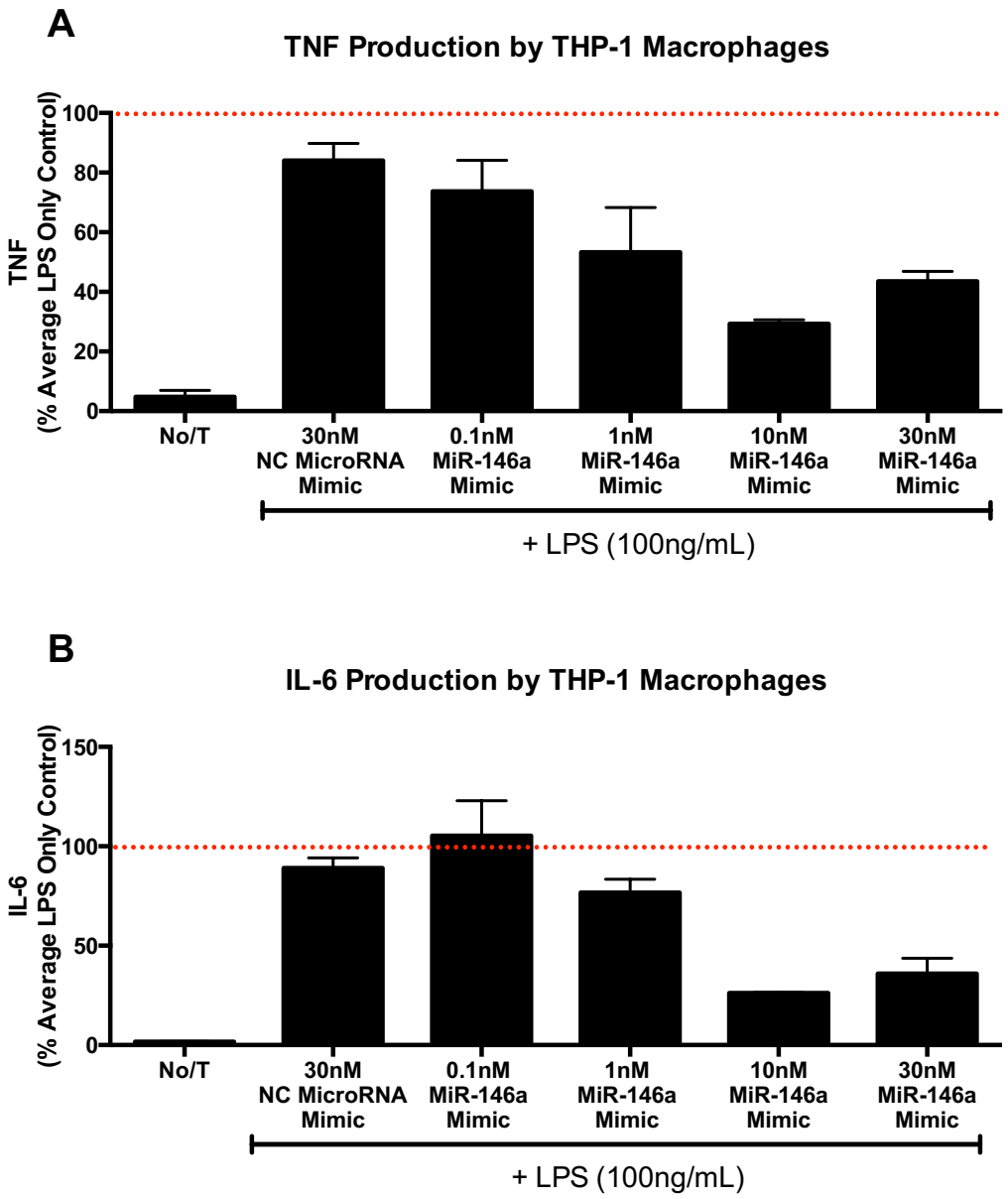

Figure 13: MiR-146a may decrease TNF and IL-6 production by THP-1 macrophages after 6 hours under M1-polarizing conditions

Compared to the negative control, there was a suggested decrease in TNF (A) and IL-6 (B) production in LPS-stimulated THP-1 macrophages that were transfected with either 10nM or 30nM of miR-146a mimic. All data was normalized as a percentage of the average LPS Only response. Error bars represent the mean +/- standard error of the mean of technical replicates. n = 1 performed in technical duplicate.

3.3.1.2 TNF production decreases in LPS-stimulated primary human MDMs transfected with a miR-146a mimic

A statistically significant decrease in TNF production was measured in LPS-stimulated primary human MDMs transfected with a miR-146a mimic (30nM) compared to control (Figure 14 A). No statistically significant difference in IL-6 production was observed (Figure 14 B).

3.3.1.3 TNF production may decrease in LPS-stimulated primary human fetal microglia transfected with a miR-146a mimic

TNF production may decrease in LPS-stimulated primary human fetal microglia transfected with a miR-146a mimic (1nM) compared to controls; however, due to a small sample size at this time (n = 2 – 4), the current result was not statistically significant (Figure 14 C). There was potentially no difference in IL-6 production using the current sample size (n = 1 – 3) (Figure 14 D).

3.3.1.4 TNF production may decrease in LPS-stimulated primary human adult microglia transfected with a miR-146a mimic

TNF production may decrease in LPS-stimulated primary human adult microglia transfected with a miR-146a mimic (1nM, 10nM, and 30nM) compared to control mimic; however, due to a small sample size (n = 1 – 2), the result was not statistically significant at this time (Figure 14 E). There was potentially no difference in IL-6 production using the current sample size (n = 1 – 2) (Figure 14 F).

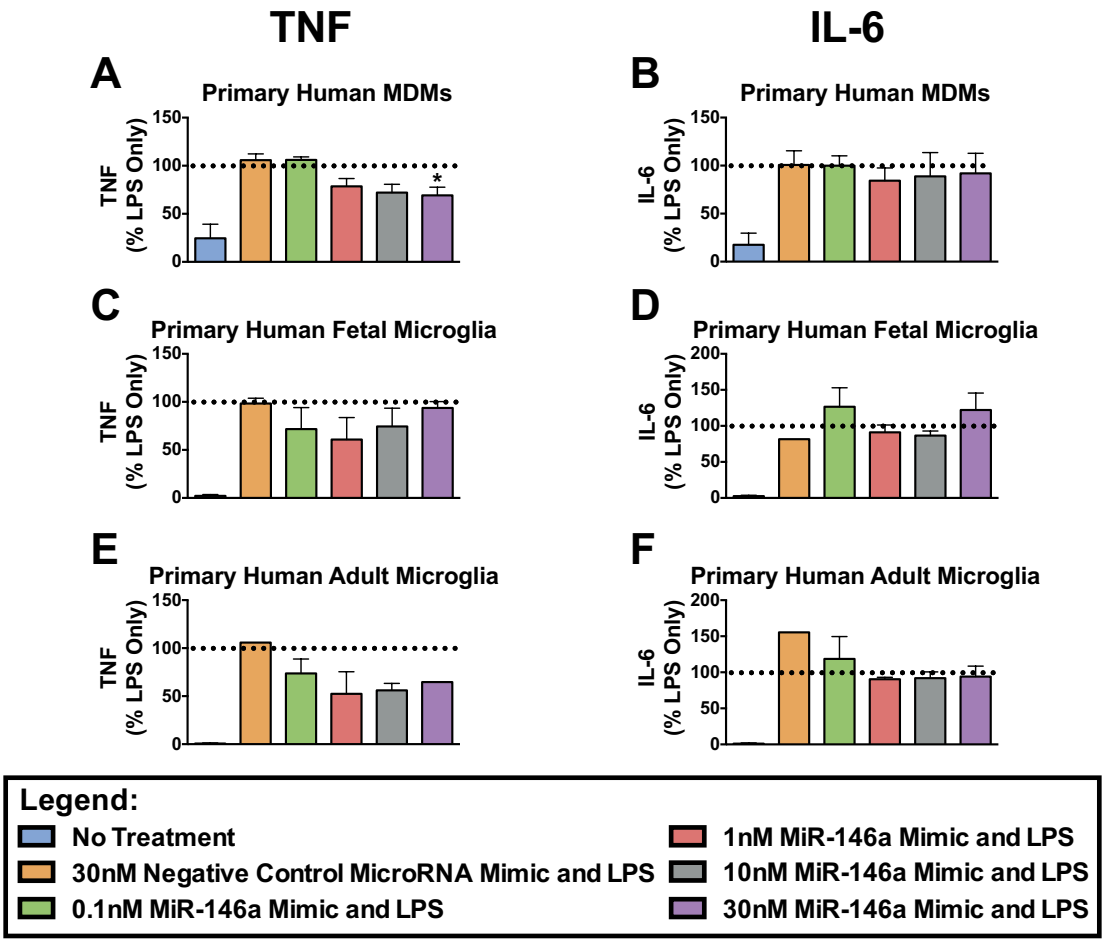

Figure 14: MiR-146a may decrease TNF, but not IL-6, in primary human monocyte-derived macrophages, fetal microglia, and adult microglia, after 6 hours under M1-polarizing conditions

MiR-146a mimic (30nM) significantly decreased TNF (A), but not IL-6 (B), production by human MDMs after LPS stimulation, compared to the negative control (n = 5 for A and B). At this time, miR-146a may reduce TNF production (C) by human fetal microglia after stimulation with LPS compared to the negative control (n = 2 - 4), whereas miR-146a may not affect IL-6 production (D) after LPS stimulation (n = 1 – 3). In human adult microglia, miR-146a may potentially reduce TNF (E), but not IL-6 (F), production when cells are stimulated with LPS, compared to the LPS Only and/or the negative control (n = 1 – 2 for E, n = 1 – 2 for F). All data was normalized as a percentage of the LPS Only response for each experiment. Error bars represent the mean +/- standard error of the mean of independent experiments. One-way analysis of variance with Dunnett's post hoc test was used to determine group differences. *p<0.05 compared to 30nM of NC microRNA Mimic with LPS stimulation.

3.3.2 Western Blots

3.3.2.1 iNOS expression may not change in LPS-stimulated primary human MDMs transfected with miR-146a mimic

The western blot probed for iNOS using primary humans MDMs suggests that there may be no difference in iNOS expression between LPS-stimulated primary human MDMs transfected with a miR-146a mimic (0.1nM, 1nM, 10nM) compared to negative control microRNA mimic (30nM) (Figure 15 A and B).

3.3.2.2 RhoA expression may decrease in LPS-stimulated primary human MDMs transfected with a miR-146a mimic

Compared to cells treated with either LPS only or LPS-stimulated negative control microRNA mimic (30nM), RhoA may decrease in a dose-dependent manner in LPS-stimulated primary human MDMs transfected with miR-146a mimic (Figure 15 C and D).

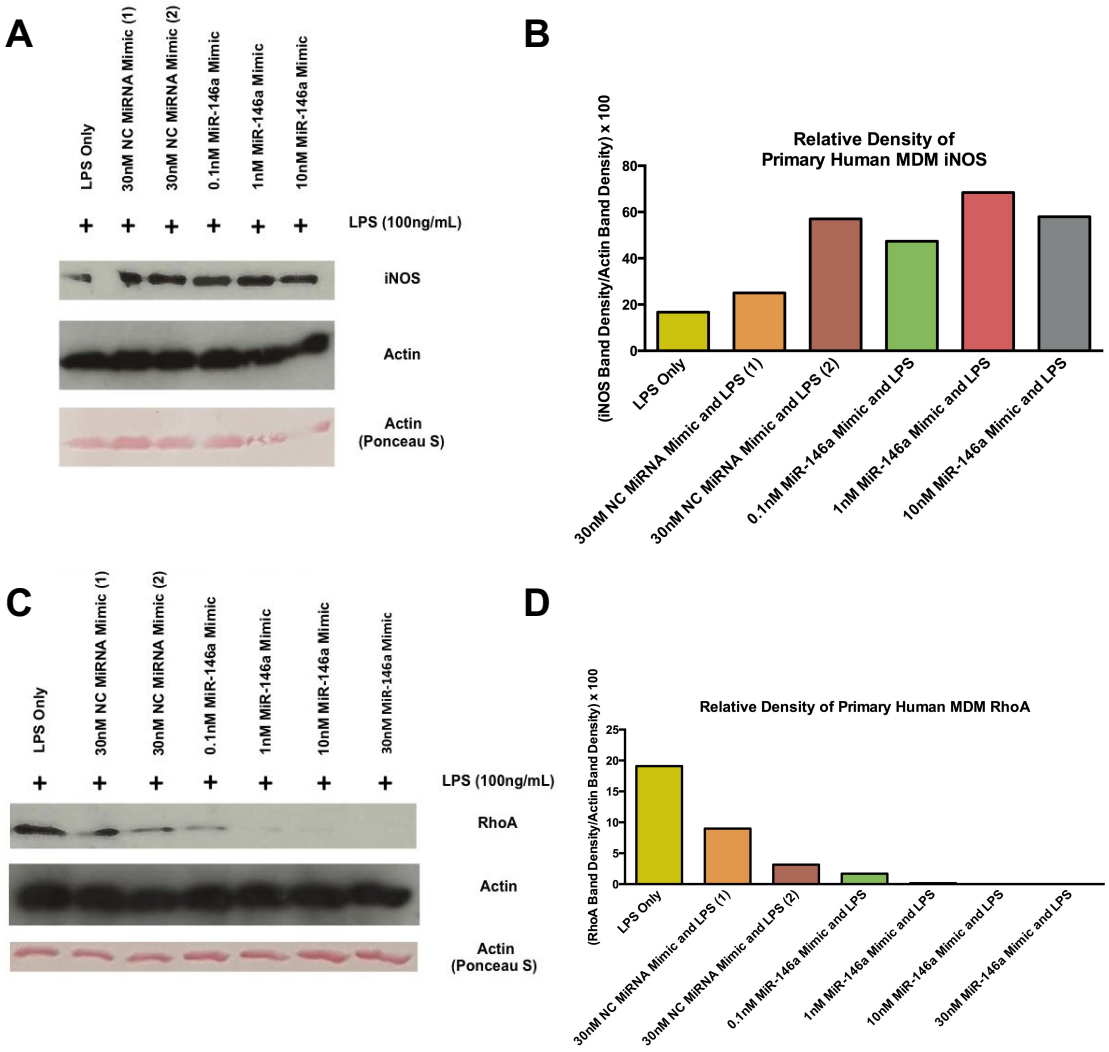

Figure 15: MiR-146a may decrease RhoA, but not iNOS, in primary human MDMs after 6 hours under M1-polarizing conditions

(A) iNOS blot for primary human MDMs. (B) Graph of relative densities of blots in A. The data suggests that iNOS expression by primary human MDMs treated with miR-146a mimic and LPS does not decrease compared to the negative control. (C) RhoA blot for primary human MDMs. (D) Graph of relative densities of RhoA bands in C. RhoA expression may decrease in primary human MDMs treated with 1nm, 10nM, and 30nM of miR-146a mimic with LPS stimulation compared to the 30nM NC miRNA mimic control, and the LPS only control. Both blots used the same samples. n = 1.

3.3.2.3 iNOS expression may not change in LPS-stimulated primary human fetal microglia transfected with a miR-146a mimic

Compared to no treatment, iNOS expression may increase upon LPS stimulation; however, among all LPS-stimulated cells, there may be no difference in iNOS expression (Figure 16 A and B).

3.3.2.4 RhoA expression may not change in LPS-stimulated primary human fetal microglia transfected with miR-146a mimic

Compared to LPS-stimulated cells transfected with a negative control microRNA mimic (10nM), there may be no difference in RhoA expression in LPS-stimulated primary human fetal microglia transfected with a miR-146a mimic (0.1nM, 1nM, 10nM, 30nM) (Figure 16 C and D).

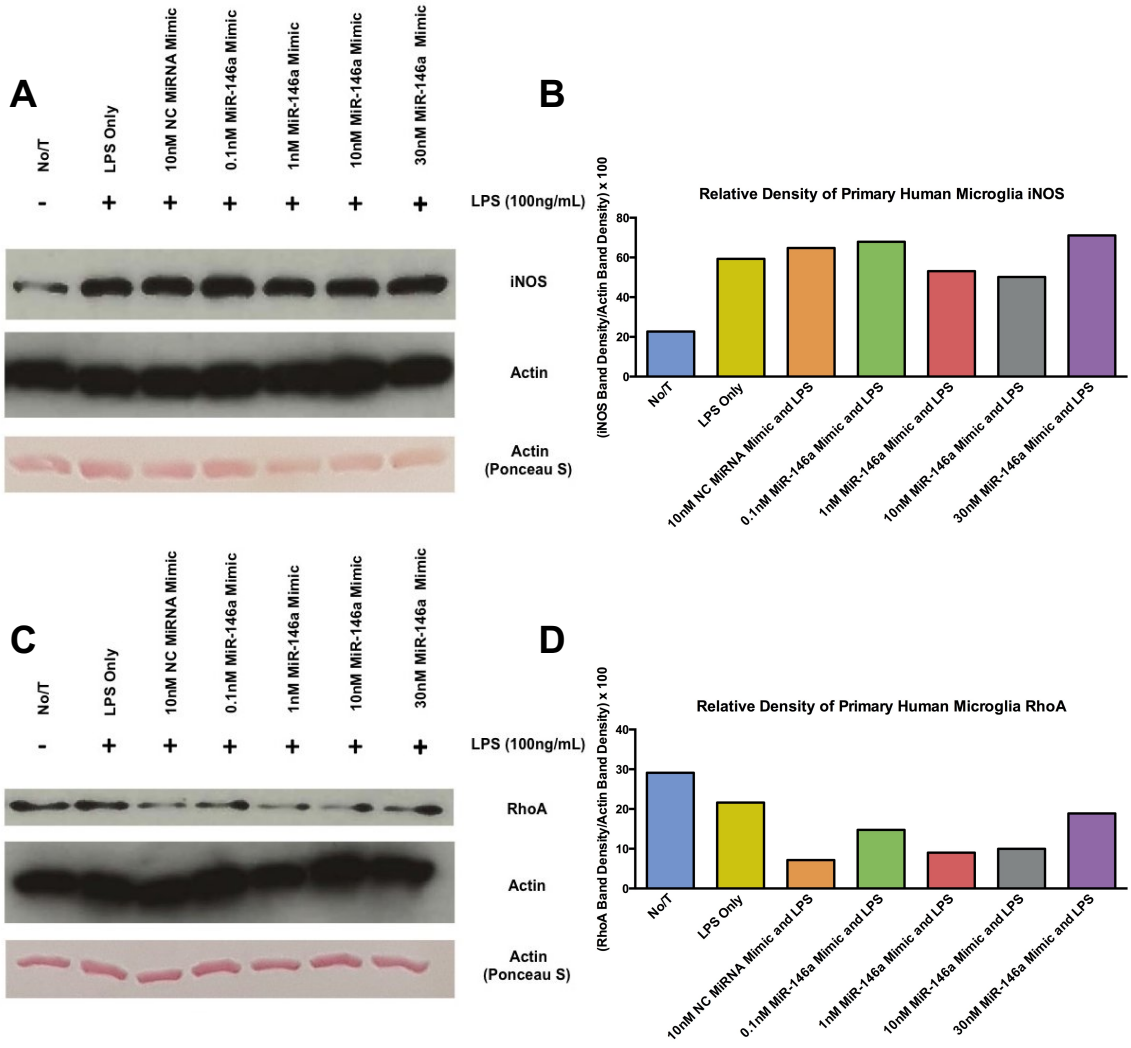

Figure 16: MiR-146a may not alter iNOS or RhoA expression in primary human fetal microglia after 6 hours under M1-polarizing conditions

(A) iNOS blot for primary human fetal microglia. (B) Graph of relative densities of iNOS bands in A. The data suggests that iNOS may increase to a similar degree in all treatment groups with LPS stimulation compared to untreated cells; however, there is potentially no difference in iNOS expression in cells treated with a miR-146a mimic compared to the negative control or to cells treated with LPS only. (C) RhoA blot for primary human fetal microglia. (D) Relative densities of RhoA bands in C. The data suggests that RhoA expression in cells transfected with miR-146a mimic with LPS stimulation may decrease compared to the no treatment and LPS only control; however, RhoA expression by cells treated with the various concentrations of miR-146a mimic with LPS stimulation may be similar to the RhoA expression found in cells treated with 10nM NC microRNA mimic with LPS stimulation. Both blots used the same samples. n = 1.

3.4 Assessing Indirect Effect of Primary Mouse BMDMs Transfected with miR-146a Mimic and LPS Stimulation on Neural Stem Cell Development

3.4.1 Supernatants derived from LPS-stimulated murine BMDMs transfected with a miR-146a mimic did not affect neurogenesis *in vitro*

The supernantants applied to murine neurospheres were taken from experiments (LPS-stimulated BMDMs transfected with a miR-146a mimic) where a statistically significant decrease in TNF was measured (Figure 17 A). The supernatants included both samples from previous experiments (Figure 11 A) in addition to newly generated validated supernatants. To determine whether supernatants influenced the total number of cells within individual neurospheres, the total number of nuclei counted within each neurosphere by the program was tallied. No differences in the number of total nuclei were observed (Figure 17 B). To determine whether supernatants influenced the total number of neurons (defined by βIII-Tubulin+ cells), the total number of neurons (from counted nuclei) within individual neurospheres was tallied. No statistically significant differences were measured across treatment groups (Figure 17 C). To determine whether a potential increase in neurogenesis was due to a mere increase in overall neurosphere size, the effect of the supernatants on individual neurosphere area was measured. No differences were observed using supernatants derived from the miR-146a mimic *vs.* negative control mimic (Figure 17 D). To normalize the total number of neurons per neurosphere, the number of βIII-Tubulin+ cells was

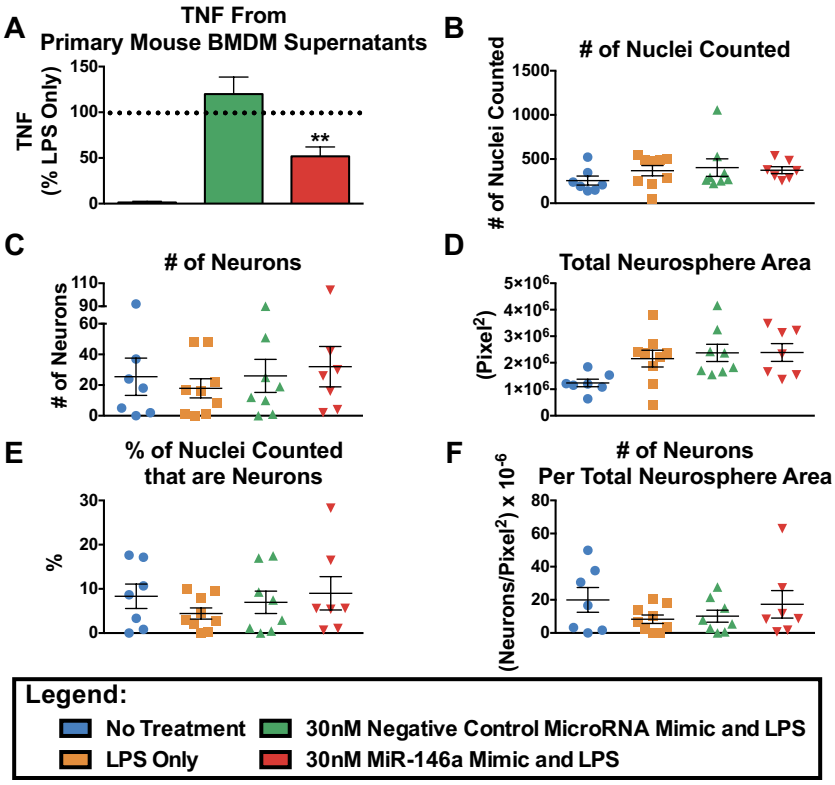

Figure 17: Neurogenesis analysis from primary mouse neurospheres cultured with supernatant from miR-146a-transfected primary mouse BMDMs with M1-polarizing conditions

The procedure for the neuron neurosphere assay is described in the Materials and Methods section. (A) In all neurosphere differentiation assays, all primary mouse BMDM supernantants derived from LPS-stimulated cells transfected with a mir-146a mimic had a statistically significant decrease in TNF levels compared to negative control (n = 5). (B) There is no statistically significant difference in the number of nuclei counted within a neurosphere between treatment groups. (C) There was no statistically significant difference between numbers of differentiated neurons grown in supernatants derived from LPS-stimulated BMDMs transfected with miR-146a mimic compared to controls. (D) No statistically significant differences were observed between neurosphere areas using supernatants from the negative control or miR-146a mimic. (E) There was no statistically significant difference in the number of nucleated neurons within neurospheres cultured in supernatant from mouse BMDMs transfected with miR-146a mimic compared to controls. (F) There is no statistically significant increase in neuron density in neurospheres that were cultured in supernatant from LPS-stimulated mouse BMDMs transfected with miR-146a mimic compared to controls. Error bars represent the mean +/- standard error of the mean. One-way analysis of variance with Dunnett's post hoc test was used to determine group differences. $^{**}p<0.01$ compared to 30nM NC MicroRNA Mimic with LPS stimulation.

divided by the number of total nuclei counted, which provided the percentage of total cells that were neurons (Figure 17 E). Similar to the total number of neurons (Figure 17 C), no differences in neurogenesis were observed. Likewise, to normalize the total number of neurons based on neurosphere size, the number of βIII-Tubulin+ cells was divided by the neurosphere area. Upon normalization for neurosphere size, there were no statistically significant differences between the experimental groups *vs.* controls (Figure 17 F). Figure 18 illustrates a representative set of mouse neurospheres that were analyzed for neuron differentiation.

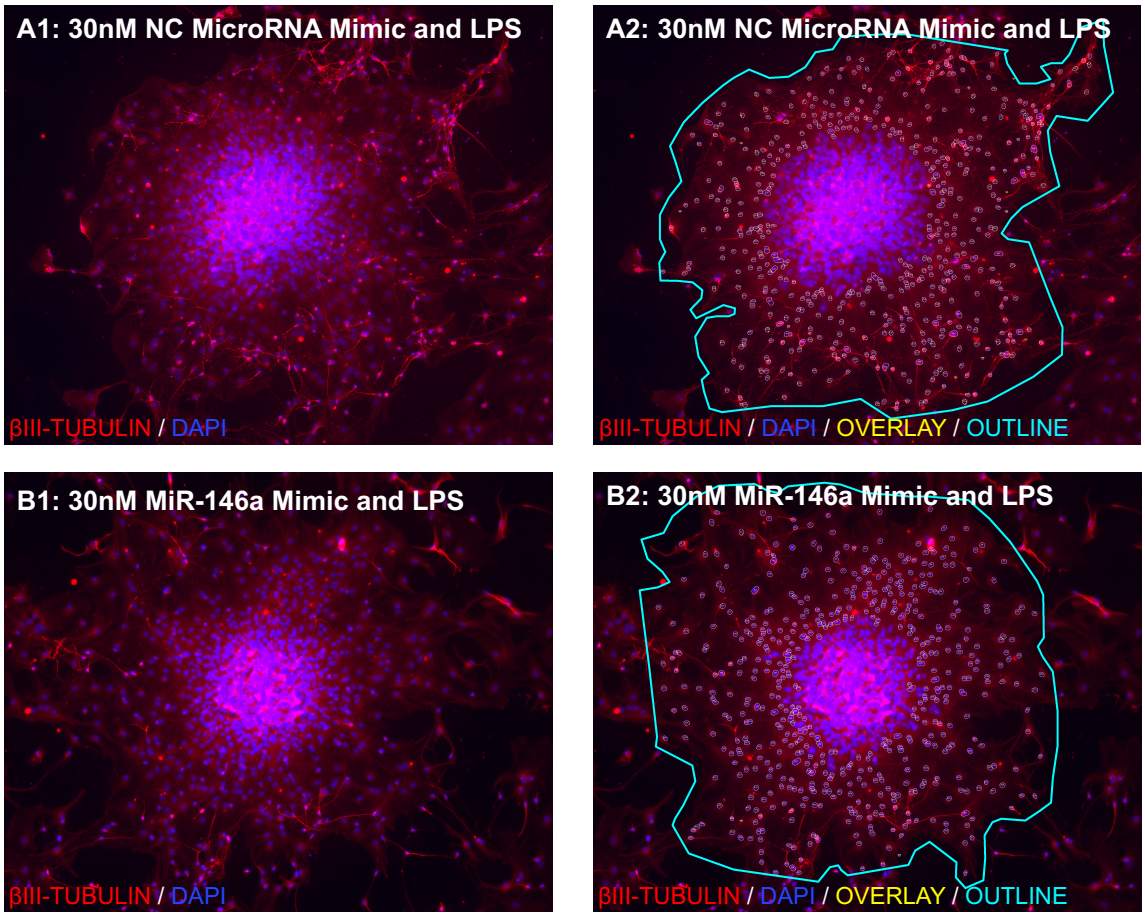

Figure 18: Mouse neurospheres cultured in media from LPS-stimulated mouse BMDMs transfected with miR-146a mimic had no effect on neuron differentiation

(A1) Single mouse neurosphere cultured in media from mouse BMDMs that was transfected with 30nM of NC microRNA mimic and stimulated with LPS for 6 hours. (A2) Identical neurosphere in image A1, with the counted nuclei overlay by the program, and the outline of the neurosphere drawn by the researcher. (B1) Single mouse neurosphere cultured in media from mouse BMDMs that was transfected with 30nM of miR-146a mimic and stimulated with LPS for 6 hours. (B2) Identical neurosphere in image B1, with the counted nuclei overlay by the program, and the outline of the neurosphere drawn by the researcher.

3.4.2 Supernatants derived from LPS-stimulated murine BMDMs transfected with a miR-146a mimic did not affect oligodendrogenesis *in vitro*

The supernantants applied to murine neurospheres were taken from experiments (LPS-stimulated murine BMDMs transfected with a miR-146a mimic) where a decrease in TNF was measured (Figure 19 A). The supernatants were from newly generated validated supernatants that were not part of Figure 11 A. To determine whether supernatants influenced the total number of cells within individual neurospheres, the total number of nuclei counted by the program within each neurosphere was tallied. No differences in the number of total nuclei were observed (Figure 19 B). To determine whether supernatants influenced the total number of OPCs (defined by NG2+ cells), the total number of OPCs (from counted nuclei) within individual neurospheres was tallied. No statistically significant differences were measured across treatment groups (Figure 19 C). Similar to the previous experiment, to determine whether the individual supernatants influenced overall neurosphere size, the effect of the supernatants on individual neurosphere area was measured. No differences were observed across all experimental conditions (Figure 19 D). To normalize the total number of OPCs per neurosphere, the number of NG2+ cells was divided by the number of total nuclei counted, which provided the percentage of total cells that were OPCs (Figure 19 E). No differences were observed. To normalize the total number of OPCs based on neurosphere size, the number of NG2+ cells was divided by the neurosphere area. Upon normalization for neurosphere size, there

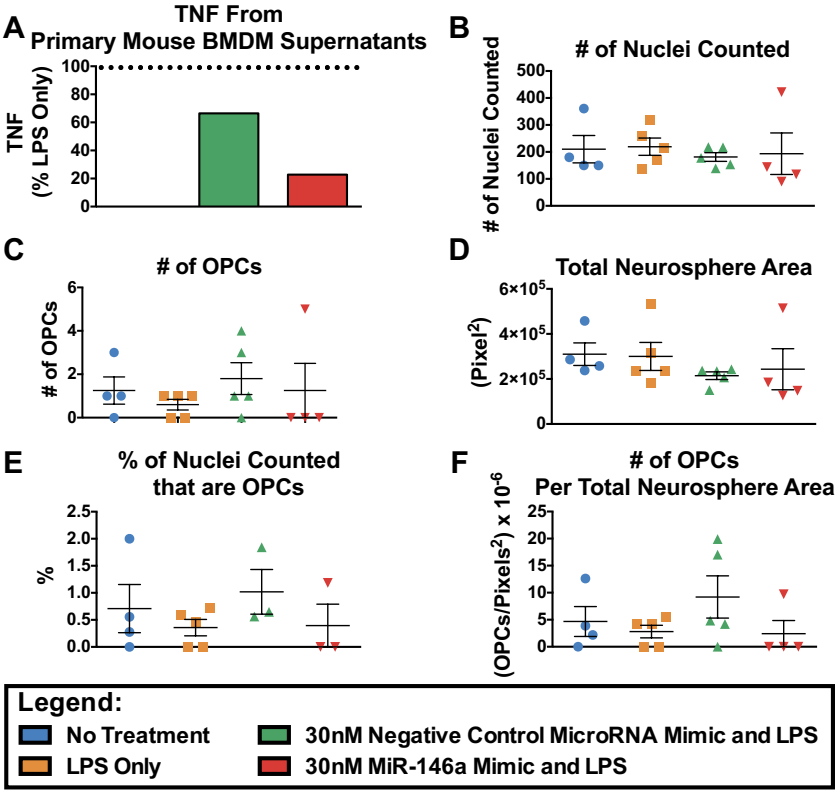

Figure 19: Oligodendrogenesis analysis from primary mouse neurospheres cultured with supernatant from miR-146a-transfected primary mouse BMDMs with M1-polarizing conditions

The procedure for the OPC neurosphere assay is described in the Methods and Materials section. (A) In all neurosphere differentiation assays, the primary mouse BMDM supernatant derived from LPS-stimulated cells transfected with a miR-146a mimic had a decrease in TNF compared to negative control (n = 1). (B) There was no statistically significant difference in the number of nuclei counted within a neurosphere between treatment groups. (C) There was no significant difference in the number of differentiated OPCs grown in supernatants derived from LPS-stimulated BMDMs transfected with miR-146a mimic compared to controls. (D) There was no significant difference in the total area of a neurosphere between treatment groups. (E) There was no significant difference in the number of nucleated OPCs in neurospheres between different treatment groups. (F) There is no significant difference in neuron density in neurospheres between treatment groups. Error bars represent the mean +/- standard error of the mean. One-way analysis of variance with Dunnett's post hoc test was used to determine group differences.

were no statistically significant differences between the experimental groups *vs.* controls (Figure 19 F). Figure 20 illustrates a representative set of mouse neurospheres that were analyzed for OPC differentiation.

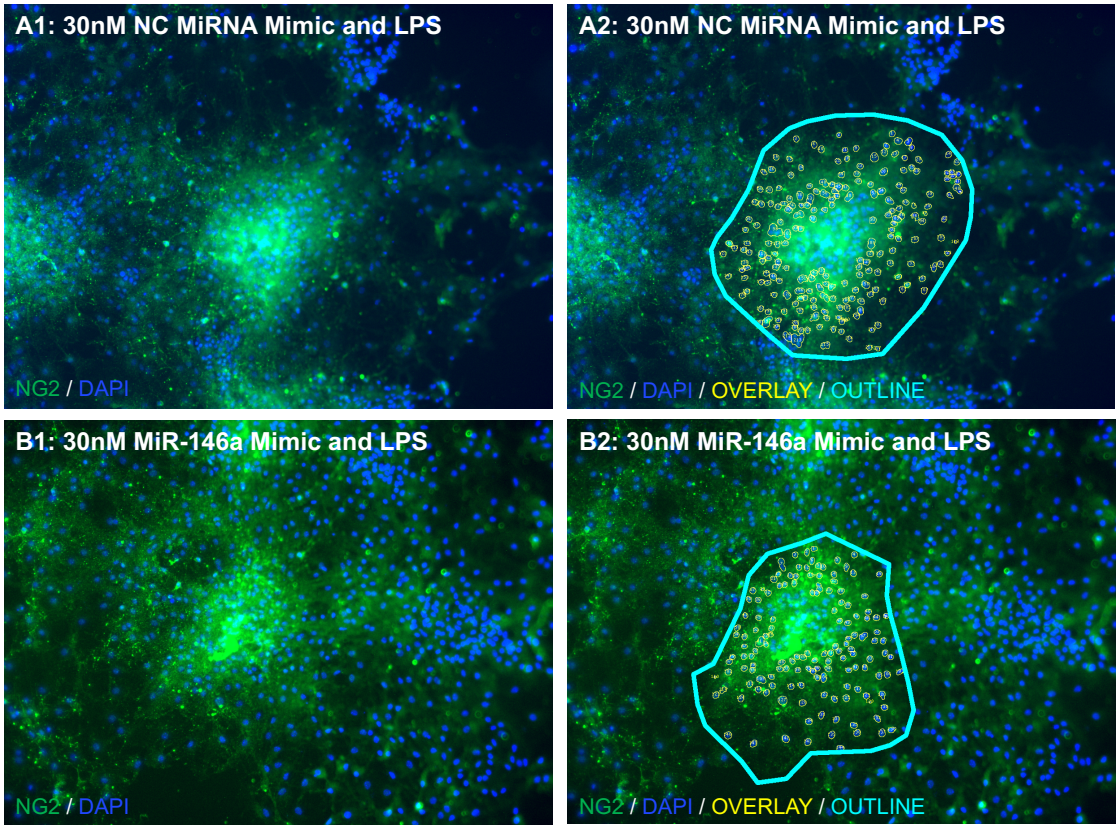

Figure 20: Mouse neurospheres cultured in media from LPS-stimulated mouse BMDMs transfected with miR-146a mimic had no effect on OPC differentiation

(A1) Single mouse neurosphere cultured in media from mouse BMDMs that was transfected with 30nM of NC microRNA mimic and stimulated with LPS for 6 hours. (A2) Identical neurosphere in image A1, with the counted nuclei overlay by the program, and the outline of the neurosphere drawn by the researcher. (B1) Single mouse neurosphere cultured in media from mouse BMDMs that was transfected with 30nM of miR-146a mimic and stimulated with LPS for 6 hours. (B2) Identical neurosphere in image B1, with the counted nuclei overlay by the program, and the outline of the neurosphere drawn by the researcher.

3.5 MiR-146a Increases Phagocytosis of Myelin by Unstimulated Primary Mouse Microglia

To assess the potential effect of miR-146a in myelin phagocytosis by myeloid cells, a preliminary experiment was conducted using primary mouse microglia. Cells were either untreated, or 30nM of miR-146a mimic/negative control mimic was transfected into unstimulated primary mouse microglia, and subsequently cultured with myelin fragments *in vitro*. As shown in Figure 21, there was a statistically significant increase in the number of myelin-positive mouse microglia that were transfected with miR-146a mimic compared to the negative control.

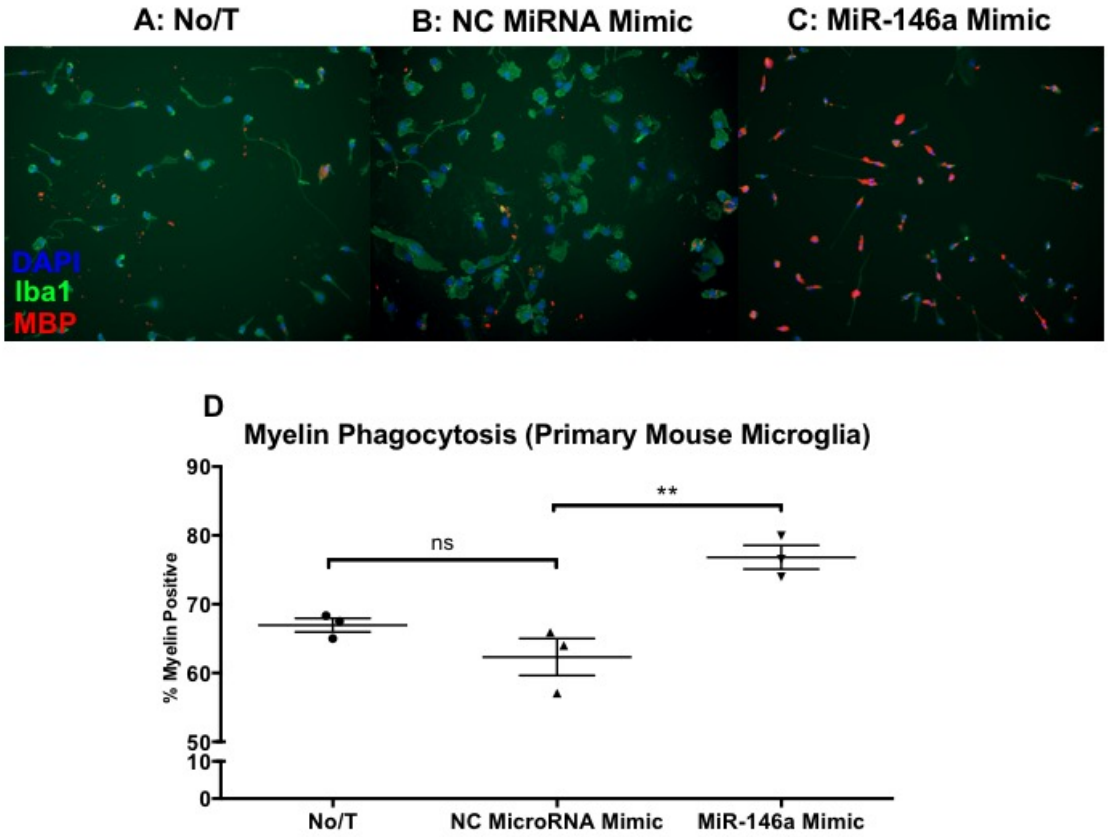

Figure 21: Myelin phagocytosis increases in miR-146a-transfected primary mouse microglia

(A) Image of untreated primary mouse microglia with myelin fragments. (B) Image of primary mouse microglia transfected with 30nM of negative control microRNA mimic with myelin fragments. (C) Image of primary mouse microglia transfected with 30nM of miR-146a mimic with myelin fragments. (D) Percentage of myelin positive primary mouse microglia compared to treatments. A statistically significant increase in myelin positive primary mouse microglia was seen in microglia transfected with miR-146a mimic compared to the negative control. Error bars represent the mean +/- standard error of the mean. One-way analysis of variance with Dunnett's post hoc test was used to determine group differences. ** $p<0.01$ compared to 30nM NC Mimic with LPS stimulation. Work was conducted by Dylan Galloway.

Chapter 4 - Discussion

The objective of this thesis was to investigate a potential role for miR-146a in altering inflammation, cell differentiation, and tissue regenerative responses in the context of MS. Previous work has demonstrated that miR-146a is an inflammatory-resolving microRNA that indirectly decreases inflammation through a negative feedback mechanism (Boldin et al. 2011; Taganov et al. 2006). A failure of the body to increase levels of miR-146a may be suggestive of an abnormal or altered pathophysiological response that fails to "halt" inflammation, thus indirectly promoting a pro-inflammatory response. It has been recently demonstrated that miR-146a levels may decrease in CD68+ myeloid cells (macrophages/microglia) within parenchymal MS lesions exhibiting active demyelination (Moore et al. 2013) and may suggest that during chronic active demyelination, miR-146a expression within myeloid cells may be insufficient to resolve chronic inflammation and demyelination. To overcome this potentially pathological *in situ* observation, I hypothesized that elevating miR-146a within pro-inflammatory myeloid cells during active demyelinating lesions may lead to the polarization of these cells towards an anti-inflammatory and tissue-regenerative phenotype, thus promoting remyelination and recovery.

To test this hypothesis, I performed several *in vitro* experiments using both primary mouse and human myeloid cell populations (macrophages and microglia). Specifically, all cells were transfected with a miR-146a mimic, and subsequently polarized toward an "M1" pro-inflammatory phenotype, which models the activation phenotype often observed within active demyelinating MS

lesions (Vogel et al. 2013). To assess whether increasing miR-146a expression within these cells resulted in a direct effect on cell phenotype and function, experiments were performed to measure production of pro-inflammatory cytokines (TNF and IL-6) and gene expression (iNOS and RhoA). Since it has been previously demonstrated that soluble factors derived from activated myeloid cells can significantly influence the growth of both neurons and oligodendrocyte progenitor cells (Moore et al. 2015; Pool et al. 2011), experiments were also performed to assess whether altered miR-146a levels within myeloid cells had an indirect effect on neurogenesis and oligodendrogenesis. The ability of miR-146a to impact phagocytosis of myelin by myeloid cells, a critical requirement to promote remyelination within MS lesions, was also performed.

In M1-polarized mouse BMDMs, human MDMs, and human fetal/adult microglia, a similar result was obtained: increased miR-146a expression suggested a decrease in TNF production, but not IL-6 (Figure 11 and Figure 14). In contrast, in M1-polarized mouse microglia, the results were opposite: miR-146a was suggested to decrease IL-6, but not TNF (Figure 11). In both mouse and human macrophages, miR-146a may decrease RhoA expression, but may not affect iNOS expression (Figure 12 and Figure 15). In human fetal microglia, miR-146a may have no effect on RhoA or iNOS expression (Figure 16). Supernatants collected from miR-146a-transfected pro-inflammatory mouse macrophages did not significantly affect neurogenesis (Figure 17) or oligodendrogenesis (Figure 19) *in vitro*. Finally, increased miR-146a levels resulted in an increase in the phagocytosis of myelin in resting mouse microglia

(Figure 21). The following sections will discuss these findings in the context of the current literature and its significance to MS.

The first inflammatory cytokine examined was tumour necrosis factor (TNF). M1 cells are often characterized by elevated TNF expression (Mantovani et al. 2004), which is a highly relevant cytokine in MS pathology. In rodents, TNF accelerates experimental autoimmune encephalomyelitis (EAE) onset and promoted inflammatory cell recruitment to the CNS (Kruglov et al. 2011). TNF also promotes demyelination, myelin sheath dilation, and death of oligodendrocytes and neurons (Selmaj and Raine 1988a; Selmaj and Raine 1988b). In addition, TNF suppresses phagocytosis of toxic myelin fragments (Brück et al. 1992), blocks neuronal development from NSCs/neurogenesis (Liu et al. 2005; Monje et al. 2003), and damages primary human oligodendrocytes *in vitro* (D'Souza et al. 1996). The detection of TNF in human CSF was variable in MS studies. Some studies indicated that TNF levels in the CSF were rarely detected, regardless of pathological state (Franciotta et al. 1989; Gallo et al. 1989; Malmestrom et al. 2006; Peter et al. 1991; Vladic et al. 2002). On the other hand, elevated TNF levels in the CSF have been detected in MS patient samples compared to controls (Maimone et al. 1991; Sharief and Hentges 1991; Tsukada et al. 1991) and was more frequently detected in active MS compared to other neurological diseases (Hauser et al. 1990). In serum, TNF was rarely detected in MS serum or in controls (Franciotta et al. 1989; Gallo et al. 1989; Maimone et al. 1991; Malmestrom et al. 2006; Peter et al. 1991; Vladic et al. 2002). In the context of both CSF and serum TNF levels, since the majority of these studies

were performed 25+ years ago, the failure to detect TNF might have been due to technical limitations, including a possible lack of robust ELISAs. In other studies, if TNF was readily detectable in the serum of MS patients, there was no significant increase compared to controls (Tsukada et al. 1991). Despite these mixed results, TNF expression in both MS lesions and PBMCs has a more convincing role in MS pathophysiology. For example, elevated TNF mRNA has been reported in several studies, including: 1) PBMCs from patients with active RRMS compared to stable RRMS and non-inflammatory neurologic disease controls (Rieckmann et al. 1994); 2) PBMCs from clinically active RRMS patients and RRMS patients with active lesions compared to stable RRMS patients and healthy controls (Rieckmann et al. 1995); 3) PBMCs from MS patients compared to healthy controls (Navikas et al. 1996a); 4) PBMCs preceding clinical symptoms of a relapse in RRMS patients (Rieckmann et al. 1995); and 5) whole blood from MS patients experiencing a relapse compared to healthy controls (Kahl et al. 2002). In active MS lesions, TNF protein/mRNA increases have also been observed (Cannella and Raine 1995; Selmaj et al. 1991; Woodroofe and Cuzner 1993), including within macrophages/microglia (Cannella and Raine 1995; Selmaj et al. 1991; Woodroofe and Cuzner 1993). Taken together, I suggest that reducing TNF during active demyelination in MS may encourage oligodendrocyte/neuron viability, remyelination, and recovery.

The ability of miR-146a to influence TNF expression has been previously examined in rodent studies. A majority of studies using the murine macrophage cell line, RAW264.7, have found that miR-146a led to a decrease in TNF protein

or mRNA following infection with mycobacteria (Li et al. 2013b), hypoxia/reoxygenation (Jiang et al. 2014), or stimulation with LPS and IFNγ (Huang et al. 2016). In one study, following LPS activation, increased miR-146a levels did not decrease TNF protein or mRNA compared to controls (He et al. 2014). In an additional murine macrophage cell line (J774 cells), delivery of a miR-146a mimic also decreased TNF protein (Gao et al. 2015b). A reduction of TNF protein and/or mRNA due to a miR-146a mimic transfection was also observed in both pro-inflammatory primary murine peritoneal macrophages (Gao et al. 2015a) and murine BMDMs (He et al. 2016). In an *in vitro* model of Lyme arthritis, BMDMs derived from miR-146a-knockout mice and subsequently infected with the bacteria *Borrelia burgdorferi in vitro* had increased TNF production compared to controls (Lochhead et al. 2014). In summary, a majority of the studies suggest that increasing miR-146a levels under pro-inflammatory states leads to decreased TNF production in mouse macrophages, a result that I also observed in primary mouse BMDMs (Figure 11). However, this did not translate to primary mouse microglia (Figure 11). While this thesis did not investigate the possible mechanisms responsible for this discrepancy between myeloid cell subsets in mice, differences in inflammatory pathways between the cell types may exist. A possible explanation could include that signalling pathways modulating pro-inflammatory cytokine release, via miR-146a, is more tightly regulated in brain-derived microglia compared to macrophages.

In addition to animal studies, the effect of miR-146a on TNF production has also been investigated in human cells. Using the transformed THP-1

monocyte/monocyte-derived macrophage (MDM) human cell line, miR-146a decreased TNF mRNA/protein under pro-inflammatory conditions (Li et al. 2016a; Liu et al. 2014; Nahid et al. 2009; Nahid et al. 2013; Pauley et al. 2011). These results are consistent with the suggested reduction in TNF production in M1-polarized THP-1 MDMs transfected with a miR-146a mimic (Figure 13). In an *in vitro* model of viral-induced encephalitis, miR-146a also decreased TNF protein produced by cultured human CHME3 microglia cell lines infected with a strain of the Japanese encephalitis virus (JEV) (Sharma et al. 2015). In this thesis, I am the first to report that these results have been replicated in healthy primary human pro-inflammatory MDMs transfected with a miR-146a mimic (Figure 14). In addition, although speculative at this time, miR-146a may decrease TNF production from M1 human adult microglia (in agreement with the literature above), although miR-146a may have no effect on TNF production from M1 human fetal microglia. This suggests that the developmental age of human microglia may alter the ability of miR-146a to affect TNF production in this cell type. Using primary healthy human cells, these results are a more accurate representation of the role of miR-146a in humans compared to transformed cell lines or cells derived from diseased individuals. Based on these findings from primary human and mouse cells, I conclude that further testing of oligodendrocyte/neuron viability, remyelination, and recovery in MS, in the context of miR-146a, is warranted.

In addition to TNF, I was also interested in investigating whether increasing miR-146a in pro-inflammatory myeloid cells had an effect on IL-6. First

discovered as a B cell differentiation factor (Hirano et al. 1986), IL-6 has several biological roles related to the immune, cardiovascular, nervous, and endocrine systems (Kishimoto et al. 1995). Most commonly, IL-6 is considered to be a pro-inflammatory molecule with elevated expression in M1-polarized cells (Mantovani et al. 2004); however, several studies have also highlighted the pleiotropic nature of IL-6, which has been demonstrated to have both pro- and anti-inflammatory properties (Scheller et al. 2011).

Similar to TNF, IL-6 is relevant in MS pathophysiology. Evidence of increased IL-6 expression is observed in both MS and its animal models. In rodent EAE, IL-6 cytokine/mRNA expression is increased in the CNS (Gijbels et al. 1990; Kennedy et al. 1992; Okuda et al. 1995) and correlates with disease severity; IL-6 levels also decrease during remyelination (Kennedy et al. 1992; Okuda et al. 1995). The detection of IL-6 in human CSF was variable in MS studies. Some studies indicate that IL-6 levels in the CSF were rarely detected, regardless of pathological state (Hauser et al. 1990; Vladic et al. 2002; Wullschleger et al. 2013). In studies that did detect IL-6, the results were highly variable (Frei et al. 1991; Maimone et al. 1991; Navikas et al. 1996b; Padberg et al. 1999; Stelmasiak et al. 2001; Stelmasiak et al. 2000). In serum, some studies suggested that IL-6 was rarely detected in MS and control samples (Malmestrom et al. 2006; Vladic et al. 2002). In other studies, if serum IL-6 was readily detectable, a similar variability was observed (Frei et al. 1991; Maimone et al. 1991; Navikas et al. 1996b; Padberg et al. 1999; Stelmasiak et al. 2001). In whole PBMCs, there is some evidence to suggest that IL-6 is altered in MS. One

study by Rieckmann et al. found evidence to suggest that IL-6 mRNA was significantly increased in patients with active RRMS compared to stable disease (Rieckmann et al. 1994), however, no correlation between relapses and activity were noted in a follow-up study (Rieckmann et al. 1995). In a separate study, it was suggested that blood monocytes derived from MS patients may be “primed”, as cultured unstimulated blood monocytes from MS patients spontaneously produced significantly higher IL-6 concentrations compared to controls (Maimone et al. 1993).

In MS lesions, Woodroofe et al. found that IL-6 mRNA expression was present in inflammatory perivascular lesions, regardless of whether demyelination was minimal or extensive (Woodroofe and Cuzner 1993); however, IL-6 mRNA levels were higher in inflammatory lesions with extensive demyelination (Woodroofe and Cuzner 1993). In a study by Maimone et al., a similar observation was noted; IL-6 protein expression was elevated in both acute and chronic active plaques, but reduced in chronically silent plaques (Maimone et al. 1997). Interestingly, in a study comparing lesion activity, the highest total number of IL-6 protein-expressing cells included astrocytes and macrophages/microglia within inactive demyelinated lesions; a positive correlation was observed between the numbers of IL-6 protein-expressing cells and the numbers of oligodendrocytes (Schönrock et al. 2000). As the authors noted, this study suggested that the presence of IL-6-expressing cells may encourage oligodendrocyte survival and viability.

Similar to other inflammatory diseases, the role of IL-6 in the context of MS pathology is complex as it appears to have both pro- and anti-inflammatory properties. IL-6 has an anti-inflammatory effect on monocytes/macrophages by increasing the production of anti-inflammatory cytokines IL-4 and IL-10 (Duluc et al. 2007; Frisdal et al. 2011), which promote an anti-inflammatory phenotype in microglia and macrophages. Furthermore, IL-6 increases the expression of several genes associated with the M2-polarized phenotype of monocytes/macrophages (Duluc et al. 2007; Frisdal et al. 2011; Roca et al. 2009), which has been suggested to be beneficial during MS recovery (Miron et al. 2013; Peferoen et al. 2015; Vogel et al. 2013). IL-6 also has an anti-inflammatory effect on OPCs/oligodendrocytes. There is evidence that IL-6 bound with its soluble receptor encourages rodent OPC differentiation into mature oligodendrocytes and survival *in vitro* (Valerio et al. 2002), and either IL-6 alone or IL-6 bound with its soluble receptor rescued oligodendrocytes from excitotoxic injury *in vitro* while preserving and encouraging myelin production (Pizzi et al. 2004). Although IL-6 can negatively affect rodent neurogenesis *in vitro* (Monje et al. 2003), there is evidence to suggest that IL-6 can have an anti-inflammatory effect on neurons by promoting neuronal and axonal regeneration (Ali et al. 2000; Cafferty et al. 2004; Cao et al. 2006; Fisher et al. 2001; Hirota et al. 1996; Pizzi et al. 2004; Zhong et al. 1999). In the context of animal models of MS, manipulating IL-6 expression using relevant animal models has not yielded conclusive results. Using the Theiler's Murine Encephalomyelitis Virus (TMEV) model of demyelination, systemic administration of IL-6 before or after the viral

infection reduced demyelination (Rodriguez et al. 1994); however, rodents orally gavaged with tocilizumab (Actemra®) (antihuman IL-6 receptor antibody that blocks IL-6 activity) during rodent EAE suppressed disease activity (Brod and Bauer 2014), suggesting that blocking IL-6 signalling may be beneficial in treating MS. Taken together, as IL-6 signalling appears to be important in MS biology, I investigated whether increasing miR-146a expression in macrophages and microglia had an effect on IL-6 production.

In murine studies, the effect of miR-146a on IL-6 production has been previously investigated. Similar to the TNF result, using miR-146a knockout mice, untreated BMDMs had a basally higher IL-6 mRNA expression compared to wild-type (Zhao et al. 2013). In addition, transfection of a miR-146a mimic also decreased IL-6 protein/mRNA in the RAW264.7 mouse macrophage cell line when exposed to either hypoxia/reoxygenation (Jiang et al. 2014), LPS (He et al. 2014), or a strain of *Mycobacterium bovis* (Li et al. 2013b). In addition, BMDMs derived from miR-146a knockout mice secreted higher concentrations of IL-6 *in vitro* compared to controls when subsequently infected with the *Borrelia burgdorferi* bacterium (Lochhead et al. 2014). *In vitro*, pre-miR-146a reduced IL-6 production in the murine BV-2 microglia cell line (Gushue 2014) upon stimulation with toll-like receptor 2 (TLR2) agonist heat-killed *Listeria monocytogenes* (HKLM) bacteria. A dual-luciferase assay has also suggested that the 3'-untranslated region of IL-6 mRNA is a direct target of pre-miR-146a (Zhou et al. 2015). Based on these findings, I investigated whether miR-146a might also decrease IL-6 in primary mouse macrophages and microglia. MiR-146a

significantly decreased IL-6 cytokine production in M1-polarized mouse microglia, however, it had no significant effect on M1 mouse macrophages (Figure 11). In addition, the differences between miR-146a regulating IL-6 between mouse BMDMs and microglia may indicate that the miR-146a/IL-6 pathway is more tightly regulated in mouse macrophages compared to mouse microglia.

The effect of miR-146a on IL-6 expression has been previously examined in human studies. Using THP-1 monocytes/MDMs, miR-146a reduced IL-6 mRNA under pro-inflammatory conditions (Li et al. 2016a; Nahid et al. 2009; Pauley et al. 2011). These results are consistent with the suggested reduction of IL-6 production by M1-polarized pro-inflammatory THP-1 MDMs in this thesis (Figure 13). MiR-146a also decreased IL-6 in a human CHME3 microglia cell line infected with a strain of the Japanese encephalitis virus (Sharma et al. 2015); however, in contrast to the cell line, the current results suggest that miR-146a does not alter IL-6 production from M1-polarized primary human MDMs, and may not alter IL-6 production from M1-polarized primary human fetal/adult microglia (Figure 14). This discrepancy between primary cells and cell lines may be explained by the lack of genetic and phenotypic variability between cells within a cell line. In contrast, primary human cells often possess greater heterogeneity, thus often leading to more variability, particularly when assessing immune responses.

Following the assessment of miR-146a to influence inflammatory cytokine production in pro-inflammatory mouse and human macrophages and microglia, I sought to elucidate a possible mechanism by measuring the protein expression

of two genes that have been previously validated as a target of miR-146a, inducible nitric oxide synthase (iNOS) and RhoA (Gushue 2014; Liu et al. 2016; Wu et al. 2015). As discussed below, both iNOS and RhoA are relevant proteins in MS pathology and their inhibition may encourage remyelination.

iNOS (also known as NOS2) is one of three known subtypes of nitric oxidase synthase (NOS); the others being neuronal (nNOS or NOS1) and endothelial (eNOS and NOS3) (Ghasemi and Fatemi 2014). Typically, when iNOS is induced, usually by infection, inflammatory stimuli, and/or bacterial products, NO is produced, which can destroy viral and microbial pathogens, and in some cases, can potentially be cytotoxic (Aktan 2004). In murine EAE, iNOS mRNA production in the CNS is primarily expressed in infiltrating macrophages and positively correlates with EAE severity (Okuda et al. 1995). In MS lesions, iNOS mRNA is also increased in myeloid-lineage cells (Bagasra et al. 1995; Bö et al. 1994a; Hooper et al. 1997). In rodents, NO has been reported to have many pathological functions, including: 1) disrupting/increasing BBB permeability (Mayhan 2000; Shukla et al. 1995; Shukla et al. 1996); 2) promoting damage and death to oligodendrocytes (Merrill et al. 1993; Mitrovic et al. 1994; Mitrovic et al. 1995; Mitrovic et al. 1996); and 3) preventing neuronal electrical conduction and promoting neuronal damage (Bonfoco et al. 1995; Garthwaite et al. 2002; Redford et al. 1997; Shrager et al. 1998). In humans, NO decreases MBP gene expression in primary myelinating oligodendrocytes *in vitro* (Jana and Pahan 2013). iNOS and nicotinamide adenine dinucleotide phosphate (NADPH) oxidase by rodent microglia can lead to the production of NO and superoxide to form

peroxynitrite, which kills rodent oligodendrocytes (Li et al. 2005). Given the pathophysiological relevance of iNOS in MS pathology, inhibiting iNOS may be beneficial in preventing demyelination and neurodegeneration. In rodents, inhibition of iNOS through drug administration using inhibitors of iNOS (tricyclodecan-9-yl-xanthogenate (D609) or aminoguanidine) or an antisense oligodeoxynucleotide to iNOS mRNA prevented EAE induction and/or reduced EAE symptoms (Ding et al. 1998; Hooper et al. 1997; Pozza et al. 2000).

The direct effect of miR-146a on iNOS expression has been previously investigated in both murine macrophage and microglia cell lines, and *in vivo*. *In vitro*, miR-146a decreased iNOS mRNA (Li et al. 2016b) and protein (Huang et al. 2016) in pro-inflammatory RAW264.7 mouse macrophages, and decreased iNOS mRNA in pro-inflammatory rat macrophages from the Kupffer cell line (He et al. 2016). Pre-miR-146a also reduced iNOS protein in mouse BV-2 microglia following stimulation with the TLR2 agonist HKLM bacteria (Gushue 2014). Using the cuprizone-induced model of demyelination, mice continuously infused with Cy3-labeled miR-146a mimic into the corpus callosum had reduced iNOS protein (Zhang et al. 2017). Collectively, these studies provide strong evidence to suggest that miR-146a is likely to decrease iNOS in pro-inflammatory macrophages and microglia; however, in my current results, transfection of a miR-146a mimic in primary mouse BMDMs was suggested to have no effect on iNOS production (Figure 12). This discrepancy may be due to the kinetics of iNOS expression. The current experiment measured iNOS levels after 6hrs of LPS stimulation; however, previous studies have measured iNOS protein at later

time points, such as 12hrs using LPS and IFN γ (Huang et al. 2016) or 24hrs using TLR2 agonist HKLM (Gushue 2014). The 6hr time-point was originally selected as the most-optimal time-point to assay pro-inflammatory cytokine production,which are rapidly released upon stimulation in general. It is possible that had the experiment continued beyond 6hrs, the LPS-only and negative controls would continue producing iNOS, while cells transfected with a miR-146a mimic would produce less iNOS over time. Future experiments should examine iNOS expression in miR-146a-transfected cells at later time-points.

The effect of miR-146a on iNOS production has been previously investigated in pro-inflammatory M1 human THP-1 MDMs; however, similar experiments have not been performed in primary healthy human MDMs and microglia. MiR-146a decreased iNOS protein in M1-polarized THP-1 MDMs (Li et al. 2016a). For the first time, in primary cells from healthy volunteers, there is evidence to suggest that miR-146a may not decrease iNOS protein in M1-polarized primary human MDMs and fetal microglia 6hrs after LPS stimulation (Figure 15 and Figure 16). Similar to mouse studies, the inability of miR-146a to reduce iNOS may be due to the 6hr time-point. Following stimulation, a longer time-point (12-48hrs) may be required. For example, Li et al. investigated iNOS expression 24hrs after pro-inflammatory stimulated miR-146a-transfected THP-1 MDMs (Li et al. 2016a). Furthermore, in a kinetic study of iNOS using mixed human glial cultures containing both astrocytes and microglia, Ding et al. found that iNOS protein started to peak beginning at the 24-48hr time-point following stimulation with interleukin-1 β (IL-1β) and IFNγ (Ding et al. 1997).

RhoA was also examined in pro-inflammatory mouse and human myeloid cells as a possible downstream target of miR-146a. Part of the Ras superfamily of Rho GTPases (Rojas et al. 2012), most Rho (**R**as-**ho**mologous (Ridley 2001)) GTPases function as switches in biological processes by converting between active (GTP-bound) and inactive (GDP-bound) conformation states, thus regulating several signalling transduction pathways (Hall 2012). In the Rho subfamily, there are three isoforms: RhoA, RhoB, and RhoC (Bustelo et al. 2007; Wheeler and Ridley 2004). Rho A/B/C are well-known for their roles in regulating cell shape and movement by altering actomyosin contractility, actin polymerization, microtubules, and cell adhesion (Ridley et al. 2003; Wheeler and Ridley 2004). In the literature, RhoA is the most highly studied. As a regulator of several signal transduction pathways, RhoA regulates the Rho/Rho kinase pathway (Amano et al. 2010). Inhibition of RhoA translation is therefore likely to prevent the activation of Rho-kinase downstream and has been previously investigated in MS. In CNS lesions of EAE mice, RhoA expression is positively correlated with EAE severity (Zhang et al. 2008). In MS, a high number of RhoA+ cells were also detected in active MS lesions; RhoA+ cells were reduced in chronic lesions and absent in control brains (Zhang et al. 2008). In both EAE and MS lesions, the majority of RhoA+ cells were macrophages/microglia (Zhang et al. 2008). As mentioned previously, remyelination in the CNS occurs most efficiently following the clearance of cellular debris and myelin fragments *via* phagocytosis. Phagocytosis of myelin by primary mouse microglia has been previously reported to be increased following inhibition of RhoA (Gitik et al.

2010). In both unstimulated J774 murine macrophages and primary mouse macrophages, overexpression of RhoA inhibited phagocytosis of apoptotic thymocytes (Nakaya et al. 2006; Tosello-Trampont et al. 2003). Inhibiting RhoA may also decrease the migration of monocytes/macrophages across the BBB by inhibiting diapedesis across transendothelial membranes/endothelial monolayers (Honing et al. 2004; Worthylake et al. 2001). In addition to implicating RhoA, targeting the Rho/Rho-associated protein kinase pathway has also been suggested to improve MS and EAE pathology. In EAE, selective inhibitors of Rho-associated protein kinase (ROCK) improved clinical severity, decreased demyelination, reduced the number of inflammatory foci in the spinal cord, and shifted mouse macrophages/microglia from an M1 to an M2 phenotype (Hou et al. 2012; Liu et al. 2013). In addition to directly targeting RhoA, activation of the Rho/ROCK pathway inhibits axonal regeneration, neurite growth, and synaptogenesis (Chen et al. 2015; Liu et al. 2015). Collectively, inhibiting RhoA and/or the Rho/ROCK pathway in inflammatory monocytes and macrophages (*via* expression of miR-146a) may limit their movement across the BBB during active demyelination, increase the clearance of myelin and cellular debris, and promote remyelination and recovery in MS.

To date, the ability of miR-146a to influence RhoA expression in primary mouse and human macrophages and microglia has not been examined. In both primary mouse and human MDMs, there is evidence to suggest that miR-146a may reduce RhoA expression (Figure 12 and Figure 15); there is also evidence to suggest that miR-146a has no effect on RhoA in primary human fetal microglia

(Figure 16). A possible reason for the observed difference between blood-derived macrophages and microglia may indicate that the ability of miR-146a to influence RhoA expression is more tightly regulated in human microglia compared to mouse BMDMs and/or human MDMs. Although speculative, one could argue that the reason RhoA is more tightly regulated in microglia compared to MDMs is due to the innate differences in cellular function. For example, microglia are "tissue-resident macrophages" of the CNS, where they specifically develop and reside only in the CNS throughout their life cycle. As a permanent resident of the CNS, it can be argued that their function is closely in tandem with the health of the CNS. If their functionality could be quickly and easily altered, such as quickly increasing or decreasing RhoA expression without being tightly regulated, it could quickly alter the homeostatic balance of the CNS. On the other hand, MDMs are short-lived, do not reside within the CNS, and originate as circulating blood monocytes in the blood. MDMs can be considered more adaptable/plastic than microglia in the sense that they must be able to enter a wide range of tissues upon immune challenge, a mechanism that can be controlled acutely by microRNAs.

Based on my results and the current literature, the following signalling cascade between miR-146a, RhoA, and TNF was proposed. Previous studies have noted that LPS stimulates the toll-like receptor 4 (TLR4) in macrophages (Li and Cherayil 2003; Wu et al. 2009). When TLR4 is activated, TNF protein can be produced through the myeloid differentiation primary response 88 (MyD88) dependent pathway (Li et al. 2013a). This pathway requires IRAK1 and TRAF6,

leading to the activation of NF-kB and the production of inflammatory cytokines, including TNF (Li et al. 2013a). Previously, RhoA has also been found to increase in human monocytes after LPS stimulation (Chen et al. 2002), and there is evidence to suggest that it is also involved in the activation of NF-kB in human monocytes/macrophages (Chen et al. 2002; Huang et al. 2009). MiR-146a has been previously known to be a potential target of IRAK1 and TRAF6 (Taganov et al. 2006) and RhoA in luciferase assays (Liu et al. 2016; Wu et al. 2015). My results suggest that expressing miR-146a may lead to a reduction of both RhoA and TNF in LPS-stimulated primary mouse BMDMs and human MDMs. Therefore, it is possible that endogenous increases in miR-146a levels within these cells causes an inhibition of RhoA, IRAK1, and TRAF6, which consequently curbs the production of TNF protein. This proposed scheme is illustrated in Figure 22.

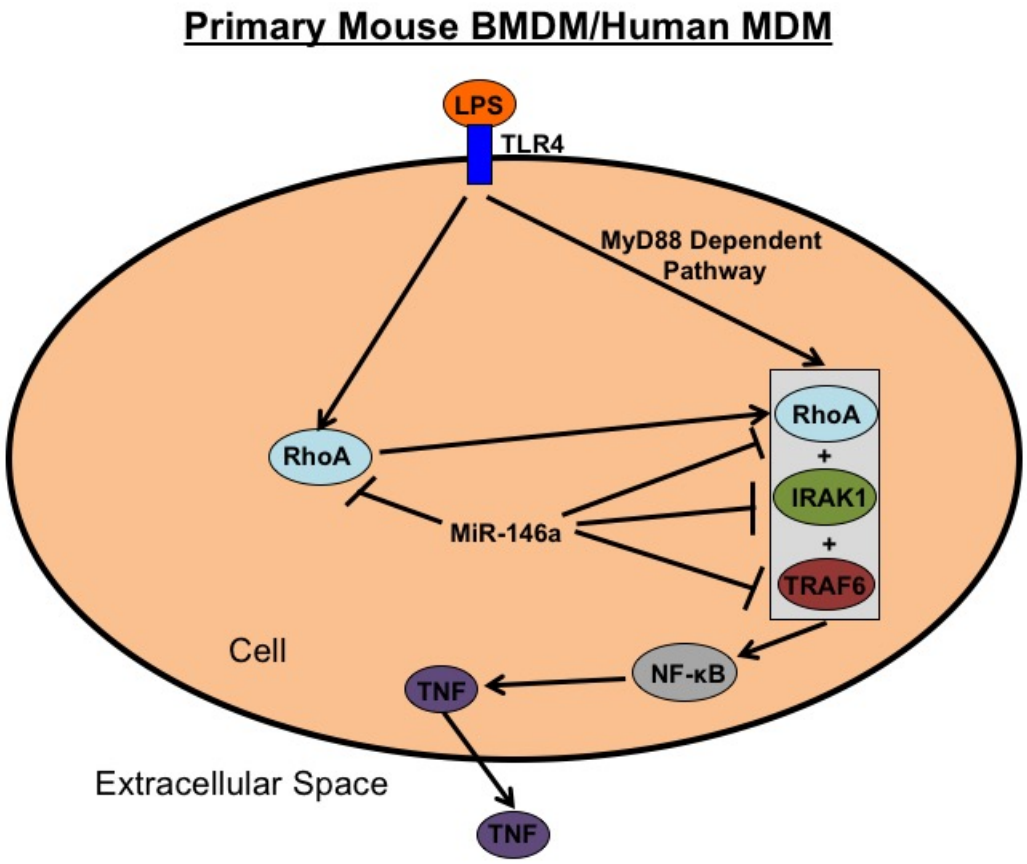

Figure 22: Proposed scheme of signalling pathways between miR-146a, TNF, and RhoA in either primary mouse BMDMs or human MDMs after 6 hours of LPS stimulation

Based on the current literature (Chen et al. 2002; Huang et al. 2009; Li et al. 2013a; Liu et al. 2016; Taganov et al. 2006; Wu et al. 2015), and the results from miR-146a-transfected primary mouse and human cells with LPS stimulation, the following scheme was proposed. When LPS triggers TLR4, the MyD88 dependent pathway is activated. RhoA may increase due to LPS stimulation, and is required, along with IRAK1 and TRAF6, to activate NF-κB, which leads to the production of TNF. However, an increase in endogenous miR-146a may inhibit the production of RhoA/IRAK1/TRAF6, and therefore reducing the amount of TNF produced and released into the extracellular space.

The effect of miR-146a on myelin phagocytosis in primary mouse and human myeloid cells has not been previously investigated; however, it has been examined in cell lines. MiR-146a-transfected RAW264.7 mouse macrophages, when infected with the *Mycobacterium bovis* bacillus Calmette-Guérin (*M. bovis* BCG), had no effect on the phagocytosis of fluorescently labelled *M. bovis* BCG (Li et al. 2016b). However, THP-1 monocytes transfected with pre-miR-146a increased their phagocytosis of *Escherichia coli* bacteria (Pauley et al. 2011). In preliminary experiments, transfection of a miR-146a mimic increased myelin phagocytosis in unstimulated primary mouse microglia (Figure 21), suggesting that miR-146a exerts an anti-inflammatory role and has the potential to promote the clearance of myelin debris.

As previously mentioned, the recruitment of neural stem/progenitor cells and OPCs occurs during remyelination and is required to promote neurogenesis, oligodendrogenesis, and repair (Chang et al. 2008; Di Bello et al. 1999; Nait-Oumesmar et al. 1999; Nait-Oumesmar et al. 2007; Picard-Riera et al. 2002; Xing et al. 2014). *In vitro*, neuronal differentiation was increased following transfection of a miR-146a mimic in mouse neural stem cells (Mei et al. 2011). Increased MBP+ OPCs has also been observed in both primary rat embryonic OPCs and in the N20.1 mouse OPC cell line transfected with a miR-146a mimic (Santra et al. 2014). *In vivo*, in a mouse model of cuprizone-induced demyelination, Cy3–labelled miR-146a continuously infused into the corpus collosum targeted OPCs, increased differentiation into myelinating oligodendrocytes, and promoted remyelination (Zhang et al. 2017). Collectively,

these studies suggest that miR-146a may directly promote neurogenesis and/or oligodendrogenesis. Since it is known that soluble factors released from activated myeloid cells (both rodent and human) can directly influence neurogenesis and oligodendrogenesis, I examined whether the differences I observed in myeloid cells following transfection with a miR-146a mimic had an indirect effect on neuronal and/or oligodendrocyte cell fate. This thesis examined the *indirect* effect of miR-146a on neurogenesis/oligodendrogenesis *via* myeloid cells, specifically from mouse BMDMs. Using supernatants collected from LPS-stimulated miR-146a-transfected mouse macrophages, no significant effect on either neurogenesis or oligodendrogenesis was observed (Figure 17 and Figure 19). *In vitro* experiments, by design, serve as a model of biological processes occurring *in vivo* and possess inherent limitations. Although supernatants derived from miR-146a-transfected mouse macrophages did not significantly affect neurogenesis and/or oligodendrogenesis directly within the confines of this model, it is possible that under pro-inflammatory conditions, increased miR-146a expression within myeloid cells *in vivo* may directly influence neurogenesis and oligodendrogenesis (as observed in previous studies). For example, miR-146a is thought to promote phagocytosis of myelin fragments in myeloid cells. As previously mentioned, the clearance of toxic myelin fragments is required for neural stem cell/OPC survival. As found in this study using mouse microglia (Figure 21), there is evidence that miR-146a transfected cells may increase phagocytosis of myelin fragments. Furthermore, as least in evidence in mouse BMDMs (Figure 12) and human MDMs (Figure 15), limiting RhoA expression in

pro-inflammatory macrophages by miR-146a could also increase phagocytosis of myelin (Gitik et al. 2010) and apoptotic cells (Nakaya et al. 2006; Tosello-Trampont et al. 2003), which is associated with inhibiting RhoA. Another way miR-146a-transfected cells could influence OPC and neural stem cell fate is through the reduction of pro-inflammatory cytokine signalling towards other cells. As seen in both primary mouse and human macrophages and microglia, a reduction in TNF could help in curbing pro-inflammatory signalling toward other cells that provide growth factors and support to neural stem cells during active demyelination, especially astrocytes. This effect of curbing pro-inflammatory responses from myeloid cells to other cells could also be improved by the maintaining of a strong IL-6 response, which has been shown to induce anti-inflammatory IL-4 (Frisdal et al. 2011) and IL-10 (Duluc et al. 2007; Frisdal et al. 2011), promote the M2 anti-inflammatory phenotype (Duluc et al. 2007; Frisdal et al. 2011; Roca et al. 2009), and increase phagocytosis of apoptotic cells (Frisdal et al. 2011). Although ROS production was not measured in these cells, and collected only 6 hours post-stimulation (a very acute time-point), a potential lack of ROS production may help to explain why no differences were observed in either neurogenesis or oligodendrogenesis.

Chapter 5 - Future Directions

There are limitations to the current study. All experiments were performed *in vitro*, which may not accurately reflect activities *in vivo*. Furthermore, due to time and availability of resources (e.g. primary human brain tissue), experiments with n<3 will need to be repeated to determine if the suggested effects by miR-146a are indeed biologically and statistically significant.

In continuing to explore how miR-146a is relevant to MS pathophysiology, remyelination, and CNS repair, there are several potential steps forward. These steps can be broadly classified under two categories: 1) modifications to the current experiments, and 2) developing experiments outside the scope of this thesis. Each category will be briefly discussed.

The first set of future directions fall under modifications to the described experiments. The first modification would be performing additional TNF and IL-6 ELISAs on human fetal and adult microglia experiments to determine whether transfection of a miR-146a mimic has a statistically significant effect on TNF and IL-6 production. Unfortunately, these cells are difficult to obtain, and therefore only a few samples were available for use. The second modification would be to continue to measure TNF, IL-6, iNOS, and RhoA production in M1-polarized myeloid cells transfected with a miR-146a mimic at various time points (at 6hrs and beyond), with an n = 3 for a single time point. Due to the unexpected lack of effect of miR-146a on cytokine and gene production in some primary cells compared to previous studies, it may suggest that the interactions between miR-146a and possible target genes is kinetically different. Examining cytokine and/or

gene production at other time points (*e.g.* 24-96hrs), may provide additional insight. The final modification to the current experiments would be to assess the ability of miR-146a to influence myelin phagocytosis in mouse and human microglia initially polarized towards either a pro-inflammatory (M1) or anti-inflammatory (M2) phenotype. It is possible that miR-146a may have a different effect on cells originally polarized towards an activated phenotype (compared to naïve cells), which is typically seen in MS lesions and during active demyelination.

Besides modifying existing experiments, there are also several additional experiments that could be performed to expand the scope of this investigation. First, laser-capture microdissection could be used to examine any differences in miR-146a levels between different types of lesions in untreated RRMS patients, or in other MS types, such as untreated SPMS or PPMS patients. Such differences in expression of this anti-inflammatory microRNA is already evident from PBMCs of untreated RRMS patients (higher), compared to untreated SPMS and PPMS patients (lower than RRMS and similar to controls) (Fenoglio et al. 2011). By examining differences in this microRNA between lesions of different MS types, it may reveal that miR-146a has a role to play in: 1) the stages of demyelinating and remyelinating lesions; 2) the transition from RRMS to SPMS; and 3) remission incidence and frequency. Second, the effect of a miR-146a mimic could be examined in the lysolecithin model of demyelination. Although effect of miR-146a has been previously examined in a cuprizone demyelination model with several potentially therapeutic benefits (Zhang et al. 2017), cuprizone

is orally administered in chow, and demyelinates several white matter areas in the brain (Denic et al. 2011). One advantage of the lysolecithin model over the cuprizone model is that one can measure and control demyelination and remyelination within defined anatomic regions of the CNS (Denic et al. 2011; Lassmann and Bradl 2017). It also has a pre-defined, predictable timeline of pathology when demyelination and remyelination peak (Keough et al. 2015). In addition to the lysolecithin model, it would also be interesting to examine the effect of miR-146a administered to EAE mice, however, route of administration and the dosing of microRNA mimics remains a significant barrier for *in vivo* applications. Third, it would be interesting to assess the effect of miR-146a on ROS production, both in primary mouse and human blood-derived macrophages and microglia. Although examining iNOS expression is important, ROS are the actual compounds that can kill cells critical for remyelination. Examining the amount of ROS produced by miR-146a-transfected primary myeloid cells would be important to determine if miR-146a could limit excessive ROS production and encourage the survival of these cells. Fourth, assessing myelin and apoptotic phagocytosis by miR-146a-transfected primary M1 mouse/human microglia and blood-derived macrophages would be interesting to determine if miR-146a had an effect on clearing debris, which is required for remyelination. Fifth, it would be interesting to assess the effect of miR-146a on the shift from M1 to M2 phenotypes in mouse/human microglia/blood-derived macrophages using traditional M1 markers (such as CD80 and CCR7) and M2 markers (such as CD23, CD163, CD206, and CD209) by flow cytometry (Durafourt et al. 2012).

Finally, another experiment could be assessing miR-146a-transfected M1-polarized mouse microglia and human MDMs/microglia on neurogenesis/oligodendrogenesis *in vitro,* and possibly assessing the types of neurons that can be generated. Since this thesis only examined the effect of miR-146a-transfected murine BMDMs on mouse NSCs, additional experiments could be performed to assess how miR-146a may indirectly improve neurogenesis/oligodendrogenesis using mouse *microglia*. Furthermore, the ability of miR-146a-transfected primary human microglia and/or MDMs on human NSCs could also be assessed.

Chapter 6 - Conclusion

This thesis investigated the therapeutic potential of promoting miR-146a expression within macrophages and microglia in the context of MS pathophysiology, remyelination, and CNS repair. In pro-inflammatory myeloid cells, increasing miR-146a expression resulted in functions that could be interpreted as being anti-inflammatory and beneficial for promoting remyelination. Overexpression of miR-146a suggested a decrease in pro-inflammatory TNF but little or no effect on IL-6. Overexpression of miR-146a also suggested that it had no effect on iNOS production, but may decrease RhoA expression in both mouse and human blood-derived macrophages after 6 hours of LPS stimulation. Unstimulated primary mouse microglia that were transfected with miR-146a mimic increased myelin phagocytosis compared to negative control. Finally, *in vitro* experiments suggest that supernatants collected from LPS-stimulated mouse BMDMs transfected with a miR-146a mimic do not affect neurogenesis or oligodendrogenesis.

Bibliography

2012. Setting new standards in multiple sclerosis care and research. Lancet Neurol 11:835.

Aktan F. 2004. iNOS-mediated nitric oxide production and its regulation. Life Sci 75:639-53.

Ali C, Nicole O, Docagne F, Lesne S, MacKenzie ET, Nouvelot A, Buisson A, Vivien D. 2000. Ischemia-induced interleukin-6 as a potential endogenous neuroprotective cytokine against NMDA receptor-mediated excitotoxicity in the brain. J Cereb Blood Flow Metab 20:956-66.

Amano M, Nakayama M, Kaibuchi K. 2010. Rho-kinase/ROCK: A key regulator of the cytoskeleton and cell polarity. Cytoskeleton (Hoboken) 67:545-54.

Babar IA, Cheng CJ, Booth CJ, Liang X, Weidhaas JB, Saltzman WM, Slack FJ. 2012. Nanoparticle-based therapy in an in vivo microRNA-155 (miR-155)-dependent mouse model of lymphoma. Proc Natl Acad Sci U S A 109:E1695-704.

Bagasra O, Michaels FH, Zheng YM, Bobroski LE, Spitsin SV, Fu ZF, Tawadros R, Koprowski H. 1995. Activation of the inducible form of nitric oxide synthase in the brains of patients with multiple sclerosis. Proc Natl Acad Sci U S A 92:12041-5.

Baker D, Amor S. 2015. Mouse models of multiple sclerosis: lost in translation? Curr Pharm Des 21:2440-52.

Barkhof F, Brück W, De Groot CJ, Bergers E, Hulshof S, Geurts J, Polman CH, van der Valk P. 2003. Remyelinated lesions in multiple sclerosis: magnetic resonance image appearance. Arch Neurol 60:1073-81.

Bartel DP. 2004. MicroRNAs: genomics, biogenesis, mechanism, and function. Cell 116:281-97.

Bhaumik D, Scott GK, Schokrpur S, Patil CK, Campisi J, Benz CC. 2008. Expression of microRNA-146 suppresses NF-κB activity with reduction of metastatic potential in breast cancer cells. Oncogene 27:5643-7.

Blank T, Prinz M. 2014. NF-κB signaling regulates myelination in the CNS. Front Mol Neurosci 7:47.

Bö L, Dawson TM, Wesselingh S, Mörk S, Choi S, Kong PA, Hanley D, Trapp BD. 1994a. Induction of nitric oxide synthase in demyelinating regions of multiple sclerosis brains. Ann Neurol 36:778-86.

Bö L, Mörk S, Kong PA, Nyland H, Pardo CA, Trapp BD. 1994b. Detection of MHC class II-antigens on macrophages and microglia, but not on astrocytes and endothelia in active multiple sclerosis lesions. J Neuroimmunol 51:135-46.

Boldin MP, Taganov KD, Rao DS, Yang L, Zhao JL, Kalwani M, Garcia-Flores Y, Luong M, Devrekanli A, Xu J and others. 2011. miR-146a is a significant brake on autoimmunity, myeloproliferation, and cancer in mice. J Exp Med 208:1189-201.

Bonfoco E, Krainc D, Ankarcrona M, Nicotera P, Lipton SA. 1995. Apoptosis and necrosis: two distinct events induced, respectively, by mild and intense insults with *N*-methyl-D-aspartate or nitric oxide/superoxide in cortical cell cultures. Proc Natl Acad Sci U S A 92:7162-6.

Bonnan M. 2015. Intrathecal IgG synthesis: a resistant and valuable target for future multiple sclerosis treatments. Mult Scler Int 2015:296184.

Boyle EA, McGeer PL. 1990. Cellular immune response in multiple sclerosis plaques. Am J Pathol 137:575-84.

Brod SA, Bauer VL. 2014. Ingested (oral) tocilizumab inhibits EAE. Cytokine 68:86-93.

Brück W, Brück Y, Friede RL. 1992. TNF-α suppresses CR3-mediated myelin removal by macrophages. J Neuroimmunol 38:9-17.

Brück W, Porada P, Poser S, Rieckmann P, Hanefeld F, Kretzschmar HA, Lassmann H. 1995. Monocyte/macrophage differentiation in early multiple sclerosis lesions. Ann Neurol 38:788-96.

Bustelo XR, Sauzeau V, Berenjeno IM. 2007. GTP-binding proteins of the Rho/Rac family: regulation, effectors and functions in vivo. Bioessays 29:356-70.

Butovsky O, Ziv Y, Schwartz A, Landa G, Talpalar AE, Pluchino S, Martino G, Schwartz M. 2006. Microglia activated by IL-4 or IFN-gamma differentially induce neurogenesis and oligodendrogenesis from adult stem/progenitor cells. Mol Cell Neurosci 31:149-60.

Cafferty WB, Gardiner NJ, Das P, Qiu J, McMahon SB, Thompson SW. 2004. Conditioning injury-induced spinal axon regeneration fails in interleukin-6 knock-out mice. J Neurosci 24:4432-43.

Caldeira C, Oliveira AF, Cunha C, Vaz AR, Falcão AS, Fernandes A, Brites D. 2014. Microglia change from a reactive to an age-like phenotype with the time in culture. Front Cell Neurosci 8:152.

Cameron JE, Yin Q, Fewell C, Lacey M, McBride J, Wang X, Lin Z, Schaefer BC, Flemington EK. 2008. Epstein-Barr virus latent membrane protein 1 induces cellular MicroRNA miR-146a, a modulator of lymphocyte signaling pathways. J Virol 82:1946-58.

Cannella B, Raine CS. 1995. The adhesion molecule and cytokine profile of multiple sclerosis lesions. Ann Neurol 37:424-35.

Cao Z, Gao Y, Bryson JB, Hou J, Chaudhry N, Siddiq M, Martinez J, Spencer T, Carmel J, Hart RB and others. 2006. The cytokine interleukin-6 is sufficient but not necessary to mimic the peripheral conditioning lesion effect on axonal growth. J Neurosci 26:5565-73.

Chandran S, Hunt D, Joannides A, Zhao C, Compston A, Franklin RJM. 2008. Myelin repair: the role of stem and precursor cells in multiple sclerosis. Philosophical Transactions of the Royal Society B: Biological Sciences 363:171.

Chang A, Smith MC, Yin X, Fox RJ, Staugaitis SM, Trapp BD. 2008. Neurogenesis in the chronic lesions of multiple sclerosis. Brain 131:2366-75.

Chastain EM, Duncan DS, Rodgers JM, Miller SD. 2011. The role of antigen presenting cells in multiple sclerosis. Biochim Biophys Acta 1812:265-74.

Chen C, Yu JZ, Zhang Q, Zhao YF, Liu CY, Li YH, Yang WF, Ma CG, Xiao BG. 2015. Role of Rho Kinase and Fasudil on Synaptic Plasticity in Multiple Sclerosis. Neuromolecular Med 17:454-65.

Chen LY, Zuraw BL, Liu FT, Huang S, Pan ZK. 2002. IL-1 receptor-associated kinase and low molecular weight GTPase RhoA signal molecules are required for bacterial lipopolysaccharide-induced cytokine gene transcription. J Immunol 169:3934-9.

Chen Y, Zhu X, Zhang X, Liu B, Huang L. 2010. Nanoparticles modified with tumor-targeting scFv deliver siRNA and miRNA for cancer therapy. Mol Ther 18:1650-6.

Chistiakov DA, Myasoedova VA, Revin VV, Orekhov AN, Bobryshev YV. 2018. The impact of interferon-regulatory factors to macrophage differentiation and polarization into M1 and M2. Immunobiology 223:101-111.

Choi JY, Kim JY, Kim JY, Park J, Lee WT, Lee JE. 2017. M2 Phenotype Microglia-derived Cytokine Stimulates Proliferation and Neuronal Differentiation of Endogenous Stem Cells in Ischemic Brain. Exp Neurobiol 26:33-41.

Cramer SP, Simonsen H, Frederiksen JL, Rostrup E, Larsson HB. 2014. Abnormal blood-brain barrier permeability in normal appearing white matter in multiple sclerosis investigated by MRI. Neuroimage Clin 4:182-9.

Cross AH, Manning PT, Keeling RM, Schmidt RE, Misko TP. 1998. Peroxynitrite formation within the central nervous system in active multiple sclerosis. Journal of Neuroimmunology 88:45-56.

Cui JG, Li YY, Zhao Y, Bhattacharjee S, Lukiw WJ. 2010. Differential regulation of interleukin-1 receptor-associated kinase-1 (IRAK-1) and IRAK-2 by microRNA-146a and NF-kappaB in stressed human astroglial cells and in Alzheimer disease. J Biol Chem 285:38951-60.

Cuzner ML, Hayes GM, Newcombe J, Woodroofe MN. 1988. The nature of inflammatory components during demyelination in multiple sclerosis. J Neuroimmunol 20:203-9.

D'Souza SD, Alinauskas KA, Antel JP. 1996. Ciliary neurotrophic factor selectively protects human oligodendrocytes from tumor necrosis factor-mediated injury. J Neurosci Res 43:289-98.

Damasceno A, Damasceno BP, Cendes F. 2014. The clinical impact of cerebellar grey matter pathology in multiple sclerosis. PLoS One 9:e96193.

Denic A, Johnson AJ, Bieber AJ, Warrington AE, Rodriguez M, Pirko I. 2011. The relevance of animal models in multiple sclerosis research. Pathophysiology 18:21-9.

Di Bello IC, Dawson MR, Levine JM, Reynolds R. 1999. Generation of oligodendroglial progenitors in acute inflammatory demyelinating lesions of the rat brain stem is associated with demyelination rather than inflammation. J Neurocytol 28:365-81.

Ding M, St Pierre BA, Parkinson JF, Medberry P, Wong JL, Rogers NE, Ignarro LJ, Merrill JE. 1997. Inducible nitric-oxide synthase and nitric oxide production in human fetal astrocytes and microglia. A kinetic analysis. J Biol Chem 272:11327-35.

Ding M, Zhang M, Wong JL, Rogers NE, Ignarro LJ, Voskuhl RR. 1998. Antisense knockdown of inducible nitric oxide synthase inhibits induction of experimental autoimmune encephalomyelitis in SJL/J mice. J Immunol 160:2560-4.

Doxaki C, Kampranis SC, Eliopoulos AG, Spilianakis C, Tsatsanis C. 2015. Coordinated Regulation of miR-155 and miR-146a Genes during Induction of Endotoxin Tolerance in Macrophages. J Immunol 195:5750-61.

Duluc D, Delneste Y, Tan F, Moles MP, Grimaud L, Lenoir J, Preisser L, Anegon I, Catala L, Ifrah N and others. 2007. Tumor-associated leukemia inhibitory factor and IL-6 skew monocyte differentiation into tumor-associated macrophage-like cells. Blood 110:4319-30.

Durafourt BA, Moore CS, Blain M, Antel JP. 2013. Isolating, culturing, and polarizing primary human adult and fetal microglia. Methods Mol Biol 1041:199-211.

Durafourt BA, Moore CS, Zammit DA, Johnson TA, Zaguia F, Guiot MC, Bar-Or A, Antel JP. 2012. Comparison of polarization properties of human adult microglia and blood-derived macrophages. Glia 60:717-27.

Dziedzic T, Metz I, Dallenga T, König FB, Müller S, Stadelmann C, Brück W. 2010. Wallerian degeneration: a major component of early axonal pathology in multiple sclerosis. Brain Pathol 20:976-85.

Fairweather D, Cihakova D. 2009. Alternatively activated macrophages in infection and autoimmunity. J Autoimmun 33:222-30.

Fenoglio C, Cantoni C, De Riz M, Ridolfi E, Cortini F, Serpente M, Villa C, Comi C, Monaco F, Mellesi L and others. 2011. Expression and genetic analysis of miRNAs involved in CD4+ cell activation in patients with multiple sclerosis. Neurosci Lett 504:9-12.

Ferguson B, Matyszak MK, Esiri MM, Perry VH. 1997. Axonal damage in acute multiple sclerosis lesions. Brain 120 (Pt 3):393-9.

Ferreira T, Rasband WS. 2012. ImageJ User Guide - IJ 1.46r. Retrieved on March 31, 2018, from: https://imagej.nih.gov/ij/docs/guide/146.html.

Fischer MT, Sharma R, Lim JL, Haider L, Frischer JM, Drexhage J, Mahad D, Bradl M, van Horssen J, Lassmann H. 2012. NADPH oxidase expression in active multiple sclerosis lesions in relation to oxidative tissue damage and mitochondrial injury. Brain 135:886-99.

Fischer MT, Wimmer I, Höftberger R, Gerlach S, Haider L, Zrzavy T, Hametner S, Mahad D, Binder CJ, Krumbholz M and others. 2013. Disease-specific molecular events in cortical multiple sclerosis lesions. Brain 136:1799-815.

Fisher J, Mizrahi T, Schori H, Yoles E, Levkovitch-Verbin H, Haggiag S, Revel M, Schwartz M. 2001. Increased post-traumatic survival of neurons in IL-6-

knockout mice on a background of EAE susceptibility. J Neuroimmunol 119:1-9.

Fortini AS, Sanders EL, Weinshenker BG, Katzmann JA. 2003. Cerebrospinal fluid oligoclonal bands in the diagnosis of multiple sclerosis. Isoelectric focusing with IgG immunoblotting compared with high-resolution agarose gel electrophoresis and cerebrospinal fluid IgG index. Am J Clin Pathol 120:672-5.

Franciotta DM, Grimaldi LM, Martino GV, Piccolo G, Bergamaschi R, Citterio A, Melzi d'Eril GV. 1989. Tumor necrosis factor in serum and cerebrospinal fluid of patients with multiple sclerosis. Ann Neurol 26:787-9.

Franco R, Fernández-Suárez D. 2015. Alternatively activated microglia and macrophages in the central nervous system. Prog Neurobiol 131:65-86.

Franklin RJ, ffrench-Constant C. 2008. Remyelination in the CNS: from biology to therapy. Nat Rev Neurosci 9:839-55.

Frei K, Fredrikson S, Fontana A, Link H. 1991. Interleukin-6 is elevated in plasma in multiple sclerosis. J Neuroimmunol 31:147-53.

Friedman RC, Farh KK, Burge CB, Bartel DP. 2009. Most mammalian mRNAs are conserved targets of microRNAs. Genome Res 19:92-105.

Frisdal E, Lesnik P, Olivier M, Robillard P, Chapman MJ, Huby T, Guerin M, Le Goff W. 2011. Interleukin-6 protects human macrophages from cellular cholesterol accumulation and attenuates the proinflammatory response. J Biol Chem 286:30926-36.

Gallo P, Piccinno MG, Krzalic L, Tavolato B. 1989. Tumor necrosis factor alpha (TNF α) and neurological diseases. Failure in detecting TNF alpha in the cerebrospinal fluid from patients with multiple sclerosis, AIDS dementia complex, and brain tumours. J Neuroimmunol 23:41-4.

Gandhi R. 2015. miRNA in multiple sclerosis: search for novel biomarkers. Mult Scler 21:1095-103.

Gao J, Wang D, Liu D, Liu M, Ge Y, Jiang M, Liu Y, Zheng D. 2015a. Tumor necrosis factor-related apoptosis-inducing ligand induces the expression of proinflammatory cytokines in macrophages and re-educates tumor-associated macrophages to an antitumor phenotype. Mol Biol Cell 26:3178-89.

Gao M, Wang X, Zhang X, Ha T, Ma H, Liu L, Kalbfleisch JH, Gao X, Kao RL, Williams DL and others. 2015b. Attenuation of Cardiac Dysfunction in Polymicrobial Sepsis by MicroRNA-146a Is Mediated via Targeting of IRAK1 and TRAF6 Expression. J Immunol 195:672-82.

Garo LP, Murugaiyan G. 2016. Contribution of MicroRNAs to autoimmune diseases. Cell Mol Life Sci 73:2041-51.

Garthwaite G, Goodwin DA, Batchelor AM, Leeming K, Garthwaite J. 2002. Nitric oxide toxicity in CNS white matter: an in vitro study using rat optic nerve. Neuroscience 109:145-55.

Gay FW, Drye TJ, Dick GW, Esiri MM. 1997. The application of multifactorial cluster analysis in the staging of plaques in early multiple sclerosis. Identification and characterization of the primary demyelinating lesion. Brain 120 (Pt 8):1461-83.

Gelfand JM. 2014. Multiple sclerosis: diagnosis, differential diagnosis, and clinical presentation. Handb Clin Neurol 122:269-90.

Ghasemi M, Fatemi A. 2014. Pathologic role of glial nitric oxide in adult and pediatric neuroinflammatory diseases. Neurosci Biobehav Rev 45:168-82.

Gijbels K, Van Damme J, Proost P, Put W, Carton H, Billiau A. 1990. Interleukin 6 production in the central nervous system during experimental autoimmune encephalomyelitis. Eur J Immunol 20:233-5.

Gitik M, Reichert F, Rotshenker S. 2010. Cytoskeleton plays a dual role of activation and inhibition in myelin and zymosan phagocytosis by microglia. FASEB J 24:2211-21.

Goldschmidt T, Antel J, König FB, Brück W, Kuhlmann T. 2009. Remyelination capacity of the MS brain decreases with disease chronicity. Neurology 72:1914-21.

Gray E, Thomas TL, Betmouni S, Scolding N, Love S. 2008a. Elevated activity and microglial expression of myeloperoxidase in demyelinated cerebral cortex in multiple sclerosis. Brain Pathol 18:86-95.

Gray E, Thomas TL, Betmouni S, Scolding N, Love S. 2008b. Elevated myeloperoxidase activity in white matter in multiple sclerosis. Neurosci Lett 444:195-8.

Guo H, Ingolia NT, Weissman JS, Bartel DP. 2010. Mammalian microRNAs predominantly act to decrease target mRNA levels. Nature 466:835-40.

Gushue S. 2014. Regulation of a prion-induced immune response by miRNA-146a [Masters Thesis]. Winnipeg, Manitoba: University of Manitoba. Retrieved on December 15, 2017, from: http://hdl.handle.net/1993/24032 or https://mspace.lib.umanitoba.ca/xmlui/handle/1993/24032

Haider L, Fischer MT, Frischer JM, Bauer J, Höftberger R, Botond G, Esterbauer H, Binder CJ, Witztum JL, Lassmann H. 2011. Oxidative damage in multiple sclerosis lesions. Brain 134:1914-24.

Hall A. 2012. Rho family GTPases. Biochem Soc Trans 40:1378-82.

Hauser SL, Doolittle TH, Lincoln R, Brown RH, Dinarello CA. 1990. Cytokine accumulations in CSF of multiple sclerosis patients: frequent detection of interleukin-1 and tumor necrosis factor but not interleukin-6. Neurology 40:1735-9.

Häusler SF, Keller A, Chandran PA, Ziegler K, Zipp K, Heuer S, Krockenberger M, Engel JB, Hönig A, Scheffler M and others. 2010. Whole blood-derived miRNA profiles as potential new tools for ovarian cancer screening. Br J Cancer 103:693-700.

Hayes GM, Woodroofe MN, Cuzner ML. 1988. Microglia express MHC class II in normal and demyelinating human white matter. Ann N Y Acad Sci 540:501-3.

He H, Jazdzewski K, Li W, Liyanarachchi S, Nagy R, Volinia S, Calin GA, Liu CG, Franssila K, Suster S and others. 2005. The role of microRNA genes in papillary thyroid carcinoma. Proc Natl Acad Sci U S A 102:19075-80.

He X, Tang R, Sun Y, Wang YG, Zhen KY, Zhang DM, Pan WQ. 2016. MicroR-146 blocks the activation of M1 macrophage by targeting signal transducer and activator of transcription 1 in hepatic schistosomiasis. EBioMedicine 13:339-347.

He Y, Sun X, Huang C, Long XR, Lin X, Zhang L, Lv XW, Li J. 2014. MiR-146a regulates IL-6 production in lipopolysaccharide-induced RAW264.7 macrophage cells by inhibiting Notch1. Inflammation 37:71-82.

Hedström AK, Bäärnhielm M, Olsson T, Alfredsson L. 2009. Tobacco smoking, but not Swedish snuff use, increases the risk of multiple sclerosis. Neurology 73:696-701.

Hirano T, Yasukawa K, Harada H, Taga T, Watanabe Y, Matsuda T, Kashiwamura S, Nakajima K, Koyama K, Iwamatsu A and others. 1986. Complementary DNA for a novel human interleukin (BSF-2) that induces B lymphocytes to produce immunoglobulin. Nature 324:73-6.

Hirota H, Kiyama H, Kishimoto T, Taga T. 1996. Accelerated Nerve Regeneration in Mice by upregulated expression of interleukin (IL) 6 and IL-6 receptor after trauma. J Exp Med 183:2627-34.

Hollenbach JA, Oksenberg JR. 2015. The immunogenetics of multiple sclerosis: A comprehensive review. J Autoimmun 64:13-25.

Honing H, van den Berg TK, van der Pol SM, Dijkstra CD, van der Kammen RA, Collard JG, de Vries HE. 2004. RhoA activation promotes transendothelial migration of monocytes via ROCK. J Leukoc Biol 75:523-8.

Hooper DC, Bagasra O, Marini JC, Zborek A, Ohnishi ST, Kean R, Champion JM, Sarker AB, Bobroski L, Farber JL and others. 1997. Prevention of

experimental allergic encephalomyelitis by targeting nitric oxide and peroxynitrite: implications for the treatment of multiple sclerosis. Proc Natl Acad Sci U S A 94:2528-33.

Hou SW, Liu CY, Li YH, Yu JZ, Feng L, Liu YT, Guo MF, Xie Y, Meng J, Zhang HF and others. 2012. Fasudil ameliorates disease progression in experimental autoimmune encephalomyelitis, acting possibly through antiinflammatory effect. CNS Neurosci Ther 18:909-17.

Housley WJ, Pitt D, Hafler DA. 2015. Biomarkers in multiple sclerosis. Clin Immunol 161:51-8.

Huang C, Liu XJ, QunZhou, Xie J, Ma TT, Meng XM, Li J. 2016. MiR-146a modulates macrophage polarization by inhibiting Notch1 pathway in RAW264.7 macrophages. Int Immunopharmacol 32:46-54.

Huang X, Chen LY, Doerner AM, Pan WW, Smith L, Huang S, Papadimos TJ, Pan ZK. 2009. An atypical protein kinase C (PKC zeta) plays a critical role in lipopolysaccharide-activated NF-kappa B in human peripheral blood monocytes and macrophages. J Immunol 182:5810-5.

Huang X, Schwind S, Yu B, Santhanam R, Wang H, Hoellerbauer P, Mims A, Klisovic R, Walker AR, Chan KK and others. 2013. Targeted delivery of microRNA-29b by transferrin-conjugated anionic lipopolyplex

nanoparticles: a novel therapeutic strategy in acute myeloid leukemia. Clin Cancer Res 19:2355-67.

Irvine KA, Blakemore WF. 2008. Remyelination protects axons from demyelination-associated axon degeneration. Brain 131:1464-77.

Jana M, Pahan K. 2013. Down-regulation of Myelin Gene Expression in Human Oligodendrocytes by Nitric Oxide: Implications for Demyelination in Multiple Sclerosis. J Clin Cell Immunol 4.

Jeffery ND, Blakemore WF. 1997. Locomotor deficits induced by experimental spinal cord demyelination are abolished by spontaneous remyelination. Brain 120 (Pt 1):27-37.

Jiang M, Xiang Y, Wang D, Gao J, Liu D, Liu Y, Liu S, Zheng D. 2012. Dysregulated expression of miR-146a contributes to age-related dysfunction of macrophages. Aging Cell 11:29-40.

Jiang W, Kong L, Ni Q, Lu Y, Ding W, Liu G, Pu L, Tang W, Kong L. 2014. miR-146a ameliorates liver ischemia/reperfusion injury by suppressing IRAK1 and TRAF6. PLoS One 9:e101530.

Junker A, Krumbholz M, Eisele S, Mohan H, Augstein F, Bittner R, Lassmann H, Wekerle H, Hohlfeld R, Meinl E. 2009. MicroRNA profiling of multiple sclerosis lesions identifies modulators of the regulatory protein CD47. Brain 132:3342-52.

Kahl KG, Kruse N, Toyka KV, Rieckmann P. 2002. Serial analysis of cytokine mRNA profiles in whole blood samples from patients with early multiple sclerosis. J Neurol Sci 200:53-5.

Keirstead HS, Blakemore WF. 1997. Identification of post-mitotic oligodendrocytes incapable of remyelination within the demyelinated adult spinal cord. J Neuropathol Exp Neurol 56:1191-201.

Kennedy MK, Torrance DS, Picha KS, Mohler KM. 1992. Analysis of cytokine mRNA expression in the central nervous system of mice with experimental autoimmune encephalomyelitis reveals that IL-10 mRNA expression correlates with recovery. J Immunol 149:2496-505.

Keough MB, Jensen SK, Yong VW. 2015. Experimental demyelination and remyelination of murine spinal cord by focal injection of lysolecithin. J Vis Exp.

Kidd D, Barkhof F, McConnell R, Algra PR, Allen IV, Revesz T. 1999. Cortical lesions in multiple sclerosis. Brain 122 (Pt 1):17-26.

Kishimoto T, Akira S, Narazaki M, Taga T. 1995. Interleukin-6 family of cytokines and gp130. Blood 86:1243-54.

Kobayashi M, Konishi H, Takai T, Kiyama H. 2015. A DAP12-dependent signal promotes pro-inflammatory polarization in microglia following nerve injury and exacerbates degeneration of injured neurons. Glia 63:1073-82.

Koch M, Kingwell E, Rieckmann P, Tremlett H. 2009. The natural history of primary progressive multiple sclerosis. Neurology 73:1996-2002.

Koch M, Kingwell E, Rieckmann P, Tremlett H, Neurologists UMC. 2010. The natural history of secondary progressive multiple sclerosis. J Neurol Neurosurg Psychiatry 81:1039-43.

Kotter MR, Li WW, Zhao C, Franklin RJ. 2006. Myelin impairs CNS remyelination by inhibiting oligodendrocyte precursor cell differentiation. J Neurosci 26:328-32.

Kruglov AA, Lampropoulou V, Fillatreau S, Nedospasov SA. 2011. Pathogenic and protective functions of TNF in neuroinflammation are defined by its expression in T lymphocytes and myeloid cells. J Immunol 187:5660-70.

Kuhlmann T, Lingfeld G, Bitsch A, Schuchardt J, Brück W. 2002. Acute axonal damage in multiple sclerosis is most extensive in early disease stages and decreases over time. Brain 125:2202-12.

Kuhlmann T, Miron V, Cui Q, Wegner C, Antel J, Brück W. 2008. Differentiation block of oligodendroglial progenitor cells as a cause for remyelination failure in chronic multiple sclerosis. Brain 131:1749-58.

Kurtzke JF. 1983. Rating neurologic impairment in multiple sclerosis: an expanded disability status scale (EDSS). Neurology 33:1444-52.

Kutzelnigg A, Lucchinetti CF, Stadelmann C, Brück W, Rauschka H, Bergmann M, Schmidbauer M, Parisi JE, Lassmann H. 2005. Cortical demyelination and diffuse white matter injury in multiple sclerosis. Brain 128:2705-12.

Lagos-Quintana M, Rauhut R, Lendeckel W, Tuschl T. 2001. Identification of novel genes coding for small expressed RNAs. Science 294:853-8.

Lampron A, Larochelle A, Laflamme N, Prefontaine P, Plante MM, Sanchez MG, Yong VW, Stys PK, Tremblay ME, Rivest S. 2015. Inefficient clearance of myelin debris by microglia impairs remyelinating processes. J Exp Med 212:481-95.

Larochelle C, Alvarez JI, Prat A. 2011. How do immune cells overcome the blood-brain barrier in multiple sclerosis? FEBS Lett 585:3770-80.

Larochelle C, Uphaus T, Prat A, Zipp F. 2016. Secondary Progression in Multiple Sclerosis: Neuronal Exhaustion or Distinct Pathology? Trends Neurosci 39:325-339.

Lassmann H, Bradl M. 2017. Multiple sclerosis: experimental models and reality. Acta Neuropathol 133:223-244.

Lau NC, Lim LP, Weinstein EG, Bartel DP. 2001. An abundant class of tiny RNAs with probable regulatory roles in Caenorhabditis elegans. Science 294:858-62.

Lee RC, Ambros V. 2001. An extensive class of small RNAs in Caenorhabditis elegans. Science 294:862-4.

Lee RC, Feinbaum RL, Ambros V. 1993. The C. elegans heterochronic gene lin-4 encodes small RNAs with antisense complementarity to lin-14. Cell 75:843-54.

Lescher J, Paap F, Schultz V, Redenbach L, Scheidt U, Rosewich H, Nessler S, Fuchs E, Gärtner J, Brück W and others. 2012. MicroRNA regulation in experimental autoimmune encephalomyelitis in mice and marmosets resembles regulation in human multiple sclerosis lesions. J Neuroimmunol 246:27-33.

Levin LI, Munger KL, O'Reilly EJ, Falk KI, Ascherio A. 2010. Primary infection with the Epstein-Barr virus and risk of multiple sclerosis. Ann Neurol 67:824-30.

Li D, Duan M, Feng Y, Geng L, Li X, Zhang W. 2016a. MiR-146a modulates macrophage polarization in systemic juvenile idiopathic arthritis by targeting INHBA. Mol Immunol 77:205-12.

Li J, Baud O, Vartanian T, Volpe JJ, Rosenberg PA. 2005. Peroxynitrite generated by inducible nitric oxide synthase and NADPH oxidase mediates microglial toxicity to oligodendrocytes. Proc Natl Acad Sci U S A 102:9936-41.

Li J, Lee DS, Madrenas J. 2013a. Evolving Bacterial Envelopes and Plasticity of TLR2-Dependent Responses: Basic Research and Translational Opportunities. Front Immunol 4:347.

Li M, Wang J, Fang Y, Gong S, Li M, Wu M, Lai X, Zeng G, Wang Y, Yang K and others. 2016b. microRNA-146a promotes mycobacterial survival in macrophages through suppressing nitric oxide production. Sci Rep 6:23351.

Li Q, Cherayil BJ. 2003. Role of Toll-like receptor 4 in macrophage activation and tolerance during Salmonella enterica serovar Typhimurium infection. Infect Immun 71:4873-82.

Li S, Yue Y, Xu W, Xiong S. 2013b. MicroRNA-146a represses mycobacteria-induced inflammatory response and facilitates bacterial replication via targeting IRAK-1 and TRAF-6. PLoS One 8:e81438.

Li Y, VandenBoom TG, 2nd, Wang Z, Kong D, Ali S, Philip PA, Sarkar FH. 2010. miR-146a suppresses invasion of pancreatic cancer cells. Cancer Res 70:1486-95.

Liu C, Li Y, Yu J, Feng L, Hou S, Liu Y, Guo M, Xie Y, Meng J, Zhang H and others. 2013. Targeting the shift from M1 to M2 macrophages in experimental autoimmune encephalomyelitis mice treated with fasudil. PLoS One 8:e54841.

Liu J, Gao HY, Wang XF. 2015. The role of the Rho/ROCK signaling pathway in inhibiting axonal regeneration in the central nervous system. Neural Regen Res 10:1892-6.

Liu Q, Wang W, Yang X, Zhao D, Li F, Wang H. 2016. MicroRNA-146a inhibits cell migration and invasion by targeting RhoA in breast cancer. Oncol Rep 36:189-96.

Liu YP, Lin HI, Tzeng SF. 2005. Tumor necrosis factor-alpha and interleukin-18 modulate neuronal cell fate in embryonic neural progenitor culture. Brain Res 1054:152-8.

Liu Z, Zhou G, Deng X, Yu Q, Hu Y, Sun H, Wang Z, Chen H, Jia C, Wang D. 2014. Analysis of miRNA expression profiling in human macrophages responding to Mycobacterium infection: induction of the immune regulator miR-146a. J Infect 68:553-61.

Livak KJ, Schmittgen TD. 2001. Analysis of relative gene expression data using real-time quantitative PCR and the 2(-Delta Delta C(T)) Method. Methods 25:402-8.

Lochhead RB, Ma Y, Zachary JF, Baltimore D, Zhao JL, Weis JH, O'Connell RM, Weis JJ. 2014. MicroRNA-146a provides feedback regulation of lyme arthritis but not carditis during infection with Borrelia burgdorferi. PLoS Pathog 10:e1004212.

Londin E, Loher P, Telonis AG, Quann K, Clark P, Jing Y, Hatzimichael E, Kirino Y, Honda S, Lally M and others. 2015. Analysis of 13 cell types reveals evidence for the expression of numerous novel primate- and tissue-specific microRNAs. Proc Natl Acad Sci U S A 112:E1106-15.

Lu LF, Boldin MP, Chaudhry A, Lin LL, Taganov KD, Hanada T, Yoshimura A, Baltimore D, Rudensky AY. 2010. Function of miR-146a in controlling Treg cell-mediated regulation of Th1 responses. Cell 142:914-29.

Lublin FD, Reingold SC. 1996. Defining the clinical course of multiple sclerosis: results of an international survey. National Multiple Sclerosis Society (USA) Advisory Committee on Clinical Trials of New Agents in Multiple Sclerosis. Neurology 46:907-11.

Lublin FD, Reingold SC, Cohen JA, Cutter GR, Sørensen PS, Thompson AJ, Wolinsky JS, Balcer LJ, Banwell B, Barkhof F and others. 2014. Defining the clinical course of multiple sclerosis: the 2013 revisions. Neurology 83:278-86.

Lucchinetti C, Brück W, Parisi J, Scheithauer B, Rodriguez M, Lassmann H. 1999. A quantitative analysis of oligodendrocytes in multiple sclerosis lesions. A study of 113 cases. Brain 122 (Pt 12):2279-95.

Lucchinetti C, Brück W, Parisi J, Scheithauer B, Rodriguez M, Lassmann H. 2000. Heterogeneity of multiple sclerosis lesions: implications for the pathogenesis of demyelination. Ann Neurol 47:707-17.

Lukiw WJ, Zhao Y, Cui JG. 2008. An NF-kappaB-sensitive micro RNA-146a-mediated inflammatory circuit in Alzheimer disease and in stressed human brain cells. J Biol Chem 283:31315-22.

Lunemann JD, Jelcic I, Roberts S, Lutterotti A, Tackenberg B, Martin R, Munz C. 2008. EBNA1-specific T cells from patients with multiple sclerosis cross react with myelin antigens and co-produce IFN-gamma and IL-2. J Exp Med 205:1763-73.

Maimone D, Gregory S, Arnason BG, Reder AT. 1991. Cytokine levels in the cerebrospinal fluid and serum of patients with multiple sclerosis. J Neuroimmunol 32:67-74.

Maimone D, Guazzi GC, Annunziata P. 1997. IL-6 detection in multiple sclerosis brain. J Neurol Sci 146:59-65.

Maimone D, Reder AT, Gregory S. 1993. T cell lymphokine-induced secretion of cytokines by monocytes from patients with multiple sclerosis. Cell Immunol 146:96-106.

Malmestrom C, Andersson BA, Haghighi S, Lycke J. 2006. IL-6 and CCL2 levels in CSF are associated with the clinical course of MS: implications for their possible immunopathogenic roles. J Neuroimmunol 175:176-82.

Mantovani A, Sica A, Sozzani S, Allavena P, Vecchi A, Locati M. 2004. The chemokine system in diverse forms of macrophage activation and polarization. Trends Immunol 25:677-86.

Martinez FO, Helming L, Gordon S. 2009. Alternative activation of macrophages: an immunologic functional perspective. Annu Rev Immunol 27:451-83.

Martinez FO, Sica A, Mantovani A, Locati M. 2008. Macrophage activation and polarization. Front Biosci 13:453-61.

Mayhan WG. 2000. Nitric oxide donor-induced increase in permeability of the blood-brain barrier. Brain Res 866:101-8.

McFarland HF, Frank JA, Albert PS, Smith ME, Martin R, Harris JO, Patronas N, Maloni H, McFarlin DE. 1992. Using gadolinium-enhanced magnetic resonance imaging lesions to monitor disease activity in multiple sclerosis. Ann Neurol 32:758-66.

McKay KA, Kwan V, Duggan T, Tremlett H. 2015. Risk factors associated with the onset of relapsing-remitting and primary progressive multiple sclerosis: a systematic review. Biomed Res Int 2015:817238.

Meamar R, Nematollahi S, Dehghani L, Mirmosayyeb O, Shayegannejad V, Basiri K, Tanhaei AP. 2016. The role of stem cell therapy in multiple sclerosis: An overview of the current status of the clinical studies. Adv Biomed Res 5:46.

Mei J, Bachoo R, Zhang CL. 2011. MicroRNA-146a inhibits glioma development by targeting Notch1. Mol Cell Biol 31:3584-92.

Merrill JE, Ignarro LJ, Sherman MP, Melinek J, Lane TE. 1993. Microglial cell cytotoxicity of oligodendrocytes is mediated through nitric oxide. J Immunol 151:2132-41.

Michell-Robinson MA, Touil H, Healy LM, Owen DR, Durafourt BA, Bar-Or A, Antel JP, Moore CS. 2015. Roles of microglia in brain development, tissue maintenance and repair. Brain 138:1138-59.

Miller D, Barkhof F, Montalban X, Thompson A, Filippi M. 2005. Clinically isolated syndromes suggestive of multiple sclerosis, part I: natural history, pathogenesis, diagnosis, and prognosis. Lancet Neurol 4:281-8.

Miller E. 2012. Multiple sclerosis. Adv Exp Med Biol 724:222-38.

Miller L. 2010. Analyzing gels and western blots with ImageJ. Retrieved on March 31, 2018, from: http://lukemiller.org/index.php/2010/11/analyzing-gels-and-western-blots-with-image-j/.

Minohara M, Matsuoka T, Li W, Osoegawa M, Ishizu T, Ohyagi Y, Kira J. 2006. Upregulation of myeloperoxidase in patients with opticospinal multiple sclerosis: positive correlation with disease severity. J Neuroimmunol 178:156-60.

Miron VE, Boyd A, Zhao JW, Yuen TJ, Ruckh JM, Shadrach JL, van Wijngaarden P, Wagers AJ, Williams A, Franklin RJ and others. 2013. M2 microglia and macrophages drive oligodendrocyte differentiation during CNS remyelination. Nat Neurosci 16:1211-8.

Mitchell PS, Parkin RK, Kroh EM, Fritz BR, Wyman SK, Pogosova-Agadjanyan EL, Peterson A, Noteboom J, O'Briant KC, Allen A and others. 2008. Circulating microRNAs as stable blood-based markers for cancer detection. Proc Natl Acad Sci U S A 105:10513-8.

Mitrovic B, Ignarro LJ, Montestruque S, Smoll A, Merrill JE. 1994. Nitric oxide as a potential pathological mechanism in demyelination: its differential effects on primary glial cells in vitro. Neuroscience 61:575-85.

Mitrovic B, Ignarro LJ, Vinters HV, Akers MA, Schmid I, Uittenbogaart C, Merrill JE. 1995. Nitric oxide induces necrotic but not apoptotic cell death in oligodendrocytes. Neuroscience 65:531-9.

Mitrovic B, Parkinson J, Merrill JE. 1996. An in Vitro Model of Oligodendrocyte Destruction by Nitric Oxide and Its Relevance to Multiple Sclerosis. Methods 10:501-13.

Monje ML, Toda H, Palmer TD. 2003. Inflammatory blockade restores adult hippocampal neurogenesis. Science 302:1760-5.

Moore CS, Cui QL, Warsi NM, Durafourt BA, Zorko N, Owen DR, Antel JP, Bar-Or A. 2015. Direct and indirect effects of immune and central nervous system-resident cells on human oligodendrocyte progenitor cell differentiation. J Immunol 194:761-72.

Moore CS, Milner R, Nishiyama A, Frausto RF, Serwanski DR, Pagarigan RR, Whitton JL, Miller RH, Crocker SJ. 2011. Astrocytic tissue inhibitor of metalloproteinase-1 (TIMP-1) promotes oligodendrocyte differentiation and enhances CNS myelination. J Neurosci 31:6247-54.

Moore CS, Rao VT, Durafourt BA, Bedell BJ, Ludwin SK, Bar-Or A, Antel JP. 2013. miR-155 as a multiple sclerosis-relevant regulator of myeloid cell polarization. Ann Neurol 74:709-20.

Motsch N, Pfuhl T, Mrazek J, Barth S, Grasser FA. 2007. Epstein-Barr virus-encoded latent membrane protein 1 (LMP1) induces the expression of the cellular microRNA miR-146a. RNA Biol 4:131-7.

Multiple Sclerosis International Federation. 2013a. Atlas of MS 2013 [Database]. London: MS International Federation. Retrieved on April 13, 2018, (Updated Link) from: https://www.msif.org/about-us/who-we-are-and-what-we-do/advocacy/atlas/.

Multiple Sclerosis International Federation. 2013b. Atlas of MS 2013: Mapping Multiple Sclerosis Around the World. London: Multiple Sclerosis International Federation. Retrieved on April 13, 2018, (Updated Link) from: http://www.msif.org/wp-content/uploads/2014/09/Atlas-of-MS.pdf or https://www.msif.org/about-us/who-we-are-and-what-we-do/advocacy/atlas/

Munger KL, Levin LI, Hollis BW, Howard NS, Ascherio A. 2006. Serum 25-hydroxyvitamin D levels and risk of multiple sclerosis. JAMA 296:2832-8.

Murray PD, McGavern DB, Sathornsumetee S, Rodriguez M. 2001. Spontaneous remyelination following extensive demyelination is associated with improved neurological function in a viral model of multiple sclerosis. Brain 124:1403-16.

Nahid MA, Pauley KM, Satoh M, Chan EK. 2009. miR-146a is critical for endotoxin-induced tolerance: IMPLICATION IN INNATE IMMUNITY. J Biol Chem 284:34590-9.

Nahid MA, Satoh M, Chan EK. 2015. Interleukin 1beta-Responsive MicroRNA-146a Is Critical for the Cytokine-Induced Tolerance and Cross-Tolerance to Toll-Like Receptor Ligands. J Innate Immun 7:428-40.

Nahid MA, Yao B, Dominguez-Gutierrez PR, Kesavalu L, Satoh M, Chan EK. 2013. Regulation of TLR2-mediated tolerance and cross-tolerance through IRAK4 modulation by miR-132 and miR-212. J Immunol 190:1250-63.

Nait-Oumesmar B, Decker L, Lachapelle F, Avellana-Adalid V, Bachelin C, Baron-Van Evercooren A. 1999. Progenitor cells of the adult mouse subventricular zone proliferate, migrate and differentiate into oligodendrocytes after demyelination. Eur J Neurosci 11:4357-66.

Nait-Oumesmar B, Picard-Riera N, Kerninon C, Decker L, Seilhean D, Hoglinger GU, Hirsch EC, Reynolds R, Baron-Van Evercooren A. 2007. Activation of the subventricular zone in multiple sclerosis: evidence for early glial progenitors. Proc Natl Acad Sci U S A 104:4694-9.

Nakasa T, Miyaki S, Okubo A, Hashimoto M, Nishida K, Ochi M, Asahara H. 2008. Expression of microRNA-146 in rheumatoid arthritis synovial tissue. Arthritis Rheum 58:1284-92.

Nakasa T, Shibuya H, Nagata Y, Niimoto T, Ochi M. 2011. The inhibitory effect of microRNA-146a expression on bone destruction in collagen-induced arthritis. Arthritis Rheum 63:1582-90.

Nakaya M, Tanaka M, Okabe Y, Hanayama R, Nagata S. 2006. Opposite effects of rho family GTPases on engulfment of apoptotic cells by macrophages. J Biol Chem 281:8836-42.

Natrajan MS, de la Fuente AG, Crawford AH, Linehan E, Nunez V, Johnson KR, Wu T, Fitzgerald DC, Ricote M, Bielekova B and others. 2015. Retinoid X receptor activation reverses age-related deficiencies in myelin debris phagocytosis and remyelination. Brain 138:3581-97.

Navikas V, He B, Link J, Haglund M, Söderström M, Fredrikson S, Ljungdahl A, Höjeberg J, Qiao J, Olsson T and others. 1996a. Augmented expression of tumour necrosis factor-alpha and lymphotoxin in mononuclear cells in multiple sclerosis and optic neuritis. Brain 119 (Pt 1):213-23.

Navikas V, Matusevicius D, Söderström M, Fredrikson S, Kivisäkk P, Ljungdahl Å, Höjeberg B, Link H. 1996b. Increased interleukin-6 mRNA expression in blood and cerebrospinal fluid mononuclear cells in multiple sclerosis. J Neuroimmunol 64:63-9.

Newcombe J, Li H, Cuzner ML. 1994. Low density lipoprotein uptake by macrophages in multiple sclerosis plaques: implications for pathogenesis. Neuropathol Appl Neurobiol 20:152-62.

Nimmerjahn A, Kirchhoff F, Helmchen F. 2005. Resting microglial cells are highly dynamic surveillants of brain parenchyma in vivo. Science 308:1314-8.

Norton WT, Poduslo SE. 1973. Myelination in rat brain: method of myelin isolation. J Neurochem 21:749-57.

Okuda Y, Nakatsuji Y, Fujimura H, Esumi H, Ogura T, Yanagihara T, Sakoda S. 1995. Expression of the inducible isoform of nitric oxide synthase in the central nervous system of mice correlates with the severity of actively induced experimental allergic encephalomyelitis. J Neuroimmunol 62:103-12.

Olah M, Amor S, Brouwer N, Vinet J, Eggen B, Biber K, Boddeke HW. 2012. Identification of a microglia phenotype supportive of remyelination. Glia 60:306-21.

Padberg F, Feneberg W, Schmidt S, Schwarz MJ, Körschenhausen D, Greenberg BD, Nolde T, Müller N, Trapmann H, König N and others. 1999. CSF and serum levels of soluble interleukin-6 receptors (sIL-6R and sgp130), but not of interleukin-6 are altered in multiple sclerosis. J Neuroimmunol 99:218-23.

Patani R, Balaratnam M, Vora A, Reynolds R. 2007. Remyelination can be extensive in multiple sclerosis despite a long disease course. Neuropathol Appl Neurobiol 33:277-87.

Paterson MR, Kriegel AJ. 2017. MiR-146a/b: a family with shared seeds and different roots. Physiol Genomics 49:243-252.

Patnaik SK, Yendamuri S, Kannisto E, Kucharczuk JC, Singhal S, Vachani A. 2012. MicroRNA expression profiles of whole blood in lung adenocarcinoma. PLoS One 7:e46045.

Patrikios P, Stadelmann C, Kutzelnigg A, Rauschka H, Schmidbauer M, Laursen H, Sorensen PS, Brück W, Lucchinetti C, Lassmann H. 2006. Remyelination is extensive in a subset of multiple sclerosis patients. Brain 129:3165-72.

Pauley KM, Satoh M, Chan AL, Bubb MR, Reeves WH, Chan EK. 2008. Upregulated miR-146a expression in peripheral blood mononuclear cells from rheumatoid arthritis patients. Arthritis Res Ther 10:R101.

Pauley KM, Stewart CM, Gauna AE, Dupre LC, Kuklani R, Chan AL, Pauley BA, Reeves WH, Chan EK, Cha S. 2011. Altered miR-146a expression in Sjogren's syndrome and its functional role in innate immunity. Eur J Immunol 41:2029-39.

Peferoen LA, Vogel DY, Ummenthum K, Breur M, Heijnen PD, Gerritsen WH, Peferoen-Baert RM, van der Valk P, Dijkstra CD, Amor S. 2015. Activation status of human microglia is dependent on lesion formation stage and remyelination in multiple sclerosis. J Neuropathol Exp Neurol 74:48-63.

Perkin GD, Sethi K, Muller BR. 1983. IgG ratios and oligoclonal IgG in multiple sclerosis and other neurological disorders. J Neurol Sci 60:325-36.

Peter JB, Boctor FN, Tourtellotte WW. 1991. Serum and CSF levels of IL-2, sIL-2R, TNF-alpha, and IL-1 beta in chronic progressive multiple sclerosis: expected lack of clinical utility. Neurology 41:121-3.

Peterson JW, Bö L, Mörk S, Chang A, Trapp BD. 2001. Transected neurites, apoptotic neurons, and reduced inflammation in cortical multiple sclerosis lesions. Ann Neurol 50:389-400.

Picard-Riera N, Decker L, Delarasse C, Goude K, Nait-Oumesmar B, Liblau R, Pham-Dinh D, Baron-Van Evercooren A. 2002. Experimental autoimmune encephalomyelitis mobilizes neural progenitors from the subventricular zone to undergo oligodendrogenesis in adult mice. Proc Natl Acad Sci U S A 99:13211-6.

Pitt D, Werner P, Raine CS. 2000. Glutamate excitotoxicity in a model of multiple sclerosis. Nat Med 6:67-70.

Pizzi M, Sarnico I, Boroni F, Benarese M, Dreano M, Garotta G, Valerio A, Spano P. 2004. Prevention of neuron and oligodendrocyte degeneration by interleukin-6 (IL-6) and IL-6 receptor/IL-6 fusion protein in organotypic hippocampal slices. Mol Cell Neurosci 25:301-11.

Polman CH, Reingold SC, Banwell B, Clanet M, Cohen JA, Filippi M, Fujihara K, Havrdova E, Hutchinson M, Kappos L and others. 2011. Diagnostic criteria

for multiple sclerosis: 2010 revisions to the McDonald criteria. Ann Neurol 69:292-302.

Pool M, Rambaldi I, Durafourt BA, Wright MC, Antel JP, Bar-Or A, Fournier AE. 2011. Myeloid lineage cells inhibit neurite outgrowth through a myosin II-dependent mechanism. J Neuroimmunol 237:101-5.

Pozza M, Bettelli C, Aloe L, Giardino L, Calzà L. 2000. Further evidence for a role of nitric oxide in experimental allergic encephalomyelitis: aminoguanidine treatment modifies its clinical evolution. Brain Res 855:39-46.

Quintana E, Ortega FJ, Robles-Cedeño R, Villar ML, Buxó M, Mercader JM, Alvarez-Cermeño JC, Pueyo N, Perkal H, Fernández-Real JM and others. 2017. miRNAs in cerebrospinal fluid identify patients with MS and specifically those with lipid-specific oligoclonal IgM bands. Mult Scler:1352458516684213.

Redford EJ, Kapoor R, Smith KJ. 1997. Nitric oxide donors reversibly block axonal conduction: demyelinated axons are especially susceptible. Brain 120 (Pt 12):2149-57.

Ridley AJ. 2001. Rho family proteins: coordinating cell responses. Trends Cell Biol 11:471-7.

Ridley AJ, Schwartz MA, Burridge K, Firtel RA, Ginsberg MH, Borisy G, Parsons JT, Horwitz AR. 2003. Cell migration: integrating signals from front to back. Science 302:1704-9.

Rieckmann P, Albrecht M, Kitze B, Weber T, Tumani H, Broocks A, Luer W, Helwig A, Poser S. 1995. Tumor necrosis factor-alpha messenger RNA expression in patients with relapsing-remitting multiple sclerosis is associated with disease activity. Ann Neurol 37:82-8.

Rieckmann P, Albrecht M, Kitze B, Weber T, Tumani H, Broocks A, Luer W, Poser S. 1994. Cytokine mRNA levels in mononuclear blood cells from patients with multiple sclerosis. Neurology 44:1523-6.

Robinson S, Miller RH. 1999. Contact with central nervous system myelin inhibits oligodendrocyte progenitor maturation. Dev Biol 216:359-68.

Roca H, Varsos ZS, Sud S, Craig MJ, Ying C, Pienta KJ. 2009. CCL2 and interleukin-6 promote survival of human CD11b+ peripheral blood mononuclear cells and induce M2-type macrophage polarization. J Biol Chem 284:34342-54.

Rodriguez A, Griffiths-Jones S, Ashurst JL, Bradley A. 2004. Identification of mammalian microRNA host genes and transcription units. Genome Res 14:1902-10.

Rodriguez M, Pavelko KD, McKinney CW, Leibowitz JL. 1994. Recombinant human IL-6 suppresses demyelination in a viral model of multiple sclerosis. J Immunol 153:3811-21.

Rojas AM, Fuentes G, Rausell A, Valencia A. 2012. The Ras protein superfamily: evolutionary tree and role of conserved amino acids. J Cell Biol 196:189-201.

Saba R, Gushue S, Huzarewich RL, Manguiat K, Medina S, Robertson C, Booth SA. 2012. MicroRNA 146a (miR-146a) is over-expressed during prion disease and modulates the innate immune response and the microglial activation state. PLoS One 7:e30832.

Santra M, Zhang ZG, Yang J, Santra S, Santra S, Chopp M, Morris DC. 2014. Thymosin beta4 up-regulation of microRNA-146a promotes oligodendrocyte differentiation and suppression of the Toll-like proinflammatory pathway. J Biol Chem 289:19508-18.

Saura J, Tusell JM, Serratosa J. 2003. High-yield isolation of murine microglia by mild trypsinization. Glia 44:183-9.

Scalfari A, Neuhaus A, Daumer M, Muraro PA, Ebers GC. 2014. Onset of secondary progressive phase and long-term evolution of multiple sclerosis. J Neurol Neurosurg Psychiatry 85:67-75.

Scheller J, Chalaris A, Schmidt-Arras D, Rose-John S. 2011. The pro- and anti-inflammatory properties of the cytokine interleukin-6. Biochim Biophys Acta 1813:878-88.

Schindelin J, Arganda-Carreras I, Frise E, Kaynig V, Longair M, Pietzsch T, Preibisch S, Rueden C, Saalfeld S, Schmid B and others. 2012. Fiji: an open-source platform for biological-image analysis. Nat Methods 9:676-82.

Schindelin J, Rueden CT, Hiner MC, Eliceiri KW. 2015. The ImageJ ecosystem: An open platform for biomedical image analysis. Mol Reprod Dev 82:518-29.

Schmittgen TD, Livak KJ. 2008. Analyzing real-time PCR data by the comparative C(T) method. Nat Protoc 3:1101-8.

Schneider CA, Rasband WS, Eliceiri KW. 2012. NIH Image to ImageJ: 25 years of image analysis. Nat Methods 9:671-5.

Schönrock LM, Gawlowski G, Brück W. 2000. Interleukin-6 expression in human multiple sclerosis lesions. Neurosci Lett 294:45-8.

Schrauder MG, Strick R, Schulz-Wendtland R, Strissel PL, Kahmann L, Loehberg CR, Lux MP, Jud SM, Hartmann A, Hein A and others. 2012. Circulating micro-RNAs as potential blood-based markers for early stage breast cancer detection. PLoS One 7:e29770.

Selmaj K, Raine CS. 1988a. Tumor necrosis factor mediates myelin damage in organotypic cultures of nervous tissue. Ann N Y Acad Sci 540:568-70.

Selmaj K, Raine CS, Cannella B, Brosnan CF. 1991. Identification of lymphotoxin and tumor necrosis factor in multiple sclerosis lesions. J Clin Invest 87:949-54.

Selmaj KW, Raine CS. 1988b. Tumor necrosis factor mediates myelin and oligodendrocyte damage in vitro. Ann Neurol 23:339-46.

Serbina NV, Jia T, Hohl TM, Pamer EG. 2008. Monocyte-mediated defense against microbial pathogens. Annu Rev Immunol 26:421-52.

Sharief MK, Hentges R. 1991. Association between tumor necrosis factor-alpha and disease progression in patients with multiple sclerosis. N Engl J Med 325:467-72.

Sharma N, Verma R, Kumawat KL, Basu A, Singh SK. 2015. miR-146a suppresses cellular immune response during Japanese encephalitis virus JaOArS982 strain infection in human microglial cells. J Neuroinflammation 12:30.

Shi C, Pamer EG. 2011. Monocyte recruitment during infection and inflammation. Nat Rev Immunol 11:762-74.

Shrager P, Custer AW, Kazarinova K, Rasband MN, Mattson D. 1998. Nerve conduction block by nitric oxide that is mediated by the axonal environment. J Neurophysiol 79:529-36.

Shukla A, Dikshit M, Srimal RC. 1995. Nitric oxide modulates blood-brain barrier permeability during infections with an inactivated bacterium. Neuroreport 6:1629-32.

Shukla A, Dikshit M, Srimal RC. 1996. Nitric oxide-dependent blood-brain barrier permeability alteration in the rat brain. Experientia 52:136-40.

Sica A, Erreni M, Allavena P, Porta C. 2015. Macrophage polarization in pathology. Cell Mol Life Sci 72:4111-26.

Smith KJ. 2007. Sodium channels and multiple sclerosis: roles in symptom production, damage and therapy. Brain Pathol 17:230-42.

Smith KJ, Blakemore WF, McDonald WI. 1979. Central remyelination restores secure conduction. Nature 280:395-6.

Smith KJ, Blakemore WF, McDonald WI. 1981. The restoration of conduction by central remyelination. Brain 104:383-404.

Smith ME. 1993. Phagocytosis of myelin by microglia in vitro. J Neurosci Res 35:480-7.

Spickett CM, Jerlich A, Panasenko OM, Arnhold J, Pitt AR, Stelmaszynska T, Schaur RJ. 2000. The reactions of hypochlorous acid, the reactive oxygen species produced by myeloperoxidase, with lipids. Acta Biochim Pol 47:889-99.

Starr T. 2013. Quantification of protein bands using densitometry. Retrieved on March 31, 2018, from: http://www1.med.umn.edu/starrlab_deleteme/prod/groups/med/@pub/@med/@starrlab/documents/content/med_content_370494.html

Stelmasiak Z, Koziol-Montewka M, Dobosz B, Rejdak K. 2001. IL-6 and sIL-6R concentration in the cerebrospinal fluid and serum of MS patients. Med Sci Monit 7:914-8.

Stelmasiak Z, Koziol-Montewka M, Dobosz B, Rejdak K, Bartosik-Psujek H, Mitosek-Szewczyk K, Belniak-Legieć E. 2000. Interleukin-6 concentration in serum and cerebrospinal fluid in multiple sclerosis patients. Med Sci Monit 6:1104-8.

Stys PK, Zamponi GW, van Minnen J, Geurts JJ. 2012. Will the real multiple sclerosis please stand up? Nat Rev Neurosci 13:507-14.

Taganov KD, Boldin MP, Chang KJ, Baltimore D. 2006. NF-kappaB-dependent induction of microRNA miR-146, an inhibitor targeted to signaling proteins of innate immune responses. Proc Natl Acad Sci U S A 103:12481-6.

Tanaka T, Ueno M, Yamashita T. 2009. Engulfment of axon debris by microglia requires p38 MAPK activity. J Biol Chem 284:21626-36.

Tang Y, Luo X, Cui H, Ni X, Yuan M, Guo Y, Huang X, Zhou H, de Vries N, Tak PP and others. 2009. MicroRNA-146A contributes to abnormal activation of the type I interferon pathway in human lupus by targeting the key signaling proteins. Arthritis Rheum 60:1065-75.

Tosello-Trampont AC, Nakada-Tsukui K, Ravichandran KS. 2003. Engulfment of apoptotic cells is negatively regulated by Rho-mediated signaling. J Biol Chem 278:49911-9.

Trapp BD, Peterson J, Ransohoff RM, Rudick R, Mörk S, Bö L. 1998. Axonal transection in the lesions of multiple sclerosis. N Engl J Med 338:278-85.

Tremlett H, Yinshan Z, Devonshire V. 2008. Natural history of secondary-progressive multiple sclerosis. Mult Scler 14:314-24.

Tremlett H, Zhao Y, Devonshire V, Neurologists UBC. 2009. Natural history comparisons of primary and secondary progressive multiple sclerosis reveals differences and similarities. J Neurol 256:374-81.

Tsukada N, Miyagi K, Matsuda M, Yanagisawa N, Yone K. 1991. Tumor necrosis factor and interleukin-1 in the CSF and sera of patients with multiple sclerosis. J Neurol Sci 104:230-4.

University of Washington. 2017. RBC Lysing Solutions and Cell Lysing Procedure. University of Washington, Department of Immunology, Cell Analysis Facility, Seattle WA, USA: University of Washington. Retrieved on March 7, 2017, from: https://depts.washington.edu/flowlab/Cell%20Analysis%20Facility/RBC%20Lysing%20Solutions%20and%20Cell%20Lysing%20Procedure.pdf

Valerio A, Ferrario M, Dreano M, Garotta G, Spano P, Pizzi M. 2002. Soluble interleukin-6 (IL-6) receptor/IL-6 fusion protein enhances in vitro differentiation of purified rat oligodendroglial lineage cells. Mol Cell Neurosci 21:602-15.

van Horssen J, Schreibelt G, Drexhage J, Hazes T, Dijkstra CD, van der Valk P, de Vries HE. 2008. Severe oxidative damage in multiple sclerosis lesions coincides with enhanced antioxidant enzyme expression. Free Radic Biol Med 45:1729-37.

Vladic A, Horvat G, Vukadin S, Sucic Z, Simaga S. 2002. Cerebrospinal fluid and serum protein levels of tumour necrosis factor-alpha (TNF-alpha) interleukin-6 (IL-6) and soluble interleukin-6 receptor (sIL-6R gp80) in multiple sclerosis patients. Cytokine 20:86-9.

Vogel DY, Vereyken EJ, Glim JE, Heijnen PD, Moeton M, van der Valk P, Amor S, Teunissen CE, van Horssen J, Dijkstra CD. 2013. Macrophages in

inflammatory multiple sclerosis lesions have an intermediate activation status. J Neuroinflammation 10:35.

Waschbisch A, Atiya M, Linker RA, Potapov S, Schwab S, Derfuss T. 2011. Glatiramer acetate treatment normalizes deregulated microRNA expression in relapsing remitting multiple sclerosis. PLoS One 6:e24604.

Wheeler AP, Ridley AJ. 2004. Why three Rho proteins? RhoA, RhoB, RhoC, and cell motility. Experimental Cell Research 301:43-49.

Williams K, Ulvestad E, Waage A, Antel JP, McLaurin J. 1994. Activation of adult human derived microglia by myelin phagocytosis in vitro. J Neurosci Res 38:433-43.

Winter J, Jung S, Keller S, Gregory RI, Diederichs S. 2009. Many roads to maturity: microRNA biogenesis pathways and their regulation. Nat Cell Biol 11:228-34.

Wolswijk G. 1998. Chronic stage multiple sclerosis lesions contain a relatively quiescent population of oligodendrocyte precursor cells. J Neurosci 18:601-9.

Woodroofe MN, Cuzner ML. 1993. Cytokine mRNA expression in inflammatory multiple sclerosis lesions: detection by non-radioactive in situ hybridization. Cytokine 5:583-8.

Worthylake RA, Lemoine S, Watson JM, Burridge K. 2001. RhoA is required for monocyte tail retraction during transendothelial migration. J Cell Biol 154:147-60.

Wu D, Cerutti C, Lopez-Ramirez MA, Pryce G, King-Robson J, Simpson JE, van der Pol SM, Hirst MC, de Vries HE, Sharrack B and others. 2015. Brain endothelial miR-146a negatively modulates T-cell adhesion through repressing multiple targets to inhibit NF-kappaB activation. J Cereb Blood Flow Metab 35:412-23.

Wu TT, Chen TL, Chen RM. 2009. Lipopolysaccharide triggers macrophage activation of inflammatory cytokine expression, chemotaxis, phagocytosis, and oxidative ability via a toll-like receptor 4-dependent pathway: validated by RNA interference. Toxicol Lett 191:195-202.

Wu Y, Crawford M, Mao Y, Lee RJ, Davis IC, Elton TS, Lee LJ, Nana-Sinkam SP. 2013. Therapeutic Delivery of MicroRNA-29b by Cationic Lipoplexes for Lung Cancer. Mol Ther Nucleic Acids 2:e84.

Wucherpfennig KW, Strominger JL. 1995. Molecular mimicry in T cell-mediated autoimmunity: viral peptides activate human T cell clones specific for myelin basic protein. Cell 80:695-705.

Wullschleger A, Kapina V, Molnarfi N, Courvoisier DS, Seebach JD, Santiago-Raber ML, Hochstrasser DF, Lalive PH. 2013. Cerebrospinal fluid

interleukin-6 in central nervous system inflammatory diseases. PLoS One 8:e72399.

Xing YL, Roth PT, Stratton JA, Chuang BH, Danne J, Ellis SL, Ng SW, Kilpatrick TJ, Merson TD. 2014. Adult neural precursor cells from the subventricular zone contribute significantly to oligodendrocyte regeneration and remyelination. J Neurosci 34:14128-46.

Ying W, Cheruku PS, Bazer FW, Safe SH, Zhou B. 2013. Investigation of macrophage polarization using bone marrow derived macrophages. J Vis Exp.

Zampetaki A, Willeit P, Drozdov I, Kiechl S, Mayr M. 2012. Profiling of circulating microRNAs: from single biomarkers to re-wired networks. Cardiovasc Res 93:555-62.

Zhang J, Zhang ZG, Lu M, Wang X, Shang X, Elias SB, Chopp M. 2017. MiR-146a promotes remyelination in a cuprizone model of demyelinating injury. Neuroscience 348:252-263.

Zhang K, Zheng J, Bian G, Liu L, Xue Q, Liu F, Yu C, Zhang H, Song B, Chung SK and others. 2015. Polarized Macrophages Have Distinct Roles in the Differentiation and Migration of Embryonic Spinal-cord-derived Neural Stem Cells After Grafting to Injured Sites of Spinal Cord. Molecular Therapy 23:1077-1091.

Zhang Z, Schittenhelm J, Meyermann R, Schluesener HJ. 2008. Lesional accumulation of RhoA(+) cells in brains of experimental autoimmune encephalomyelitis and multiple sclerosis. Neuropathol Appl Neurobiol 34:231-40.

Zhao JL, Rao DS, O'Connell RM, Garcia-Flores Y, Baltimore D. 2013. MicroRNA-146a acts as a guardian of the quality and longevity of hematopoietic stem cells in mice. Elife 2:e00537.

Zhong J, Dietzel ID, Wahle P, Kopf M, Heumann R. 1999. Sensory impairments and delayed regeneration of sensory axons in interleukin-6-deficient mice. J Neurosci 19:4305-13.

Zhou J, Chaudhry H, Zhong Y, Ali MM, Perkins LA, Owens WB, Morales JE, McGuire FR, Zumbrun EE, Zhang J and others. 2015. Dysregulation in microRNA expression in peripheral blood mononuclear cells of sepsis patients is associated with immunopathology. Cytokine 71:89-100.

APPENDIX A: DENSITOMETRY PROCEDURE

Densitometry Procedure Using ImageJ

This procedure is based off of the ImageJ (Schneider et al., 2012) online user guide (IJ 1.46r), Section 30.13 (Ferreira and Rasband, 2012), and tutorials by Luke Miller (Miller 2010) and Tim Starr (Starr, 2013) with modification.

Image Set-Up

1. Scan coloured copies of your x-rayed western blot into a TIFF file of at least 600dpi resolution. Ideally, the blot should be clean with little variation in background.
2. Open scan in ImageJ, and change to Grayscale: Image -> Type -> 8-bit. Save scan as a TIFF file.
3. If the bands of interest are not lined up horizontally, rotate the image. To do this, go to Image -> Transform… -> Rotate… . Check only Preview, set Interpolation to None, set Gridlines to desired number, and adjust the angle accordingly until the bands are horizontal. Positive angles turn image clockwise, negative angles turn image counterclockwise. Once the image is adjusted accordingly, save the image again as a TIFF file.

Measuring Density

4. First, make a rectangular selection of the first vertical lane over the band of interest. Make sure the rectangle is longer vertically than horizontally. Once selected, go to Analyze -> Gels -> Select First Lane (or do Command + 1 on a Mac). A “1” should show up inside your selection.
5. Click inside your selection with the “1”, and drag the copy of your selection over to the next lane over the band. Do not adjust the size of the selection in any way, and don’t worry if your new selection doesn’t line up with the first selection (the program will fix this later). Once you have your selection over the band in the row, go to Analyze -> Gels -> Select Next Lane (or Command + 2 on a Mac). Now, a “2” should appear in your new selection, and the selection should have “snapped” to the same height as the selection for the first lane. Repeat this process for the rest of the vertical lanes.
6. After you select the last lane, make sure the last selection is still “selected” or “highlighted” with the small white squares around the perimeter of the selection (or else the next step will not work). Then, go to Analyze -> Gels -> Plot Lanes (or Command + 3 on a Mac). ImageJ then plots graphs of your bands with the first lane as the top plot, the second lane as the second plot, etc. The bands are displayed as “peaks”.
7. Using the straight line tool, make a straight line from where the peak begins on the left to where the peak ends on the right, the “base” of the peak. This will be subjective, but try to be consistent when choosing when

the peak starts to go up, and where it starts to level out. Note that peaks can vary in width, depending on if the band is wide or narrow. You are trying to remove the “background” from the band.

8. Once you have made straight lines across the bases, choose the “Wand (tracing) tool”, and select the area of the peak that you have enclosed with your line. An outline of the area will appear, and ImageJ will provide you the area of that peak that it measured (the density of the band). Continue clicking on the areas for the rest of the peaks to get the areas of those enclosed peaks. Copy and paste the results into Excel. **Don’t forget** to save the plots as a TIFF file, and take a snapshot of the grayscale image with your lane selections for future reference. A image of a sample peaks and blots for actin is shown below using this technique:

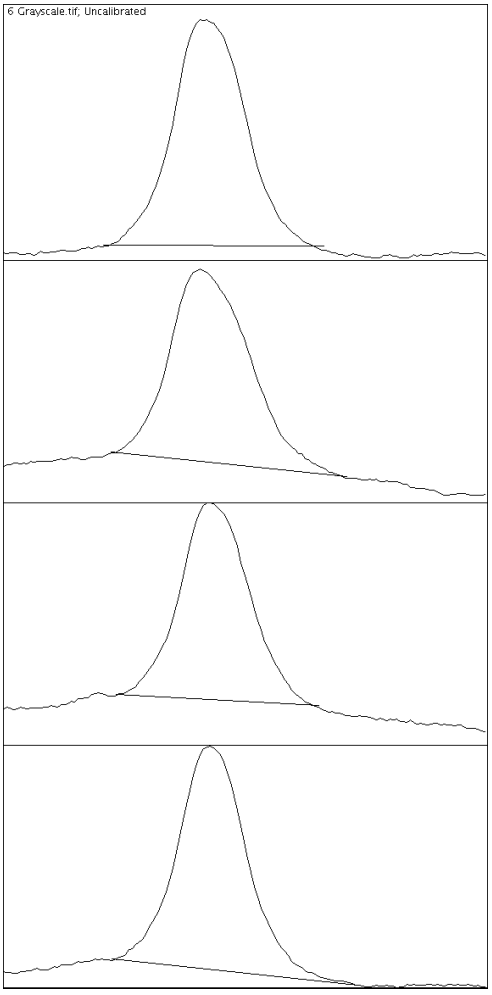

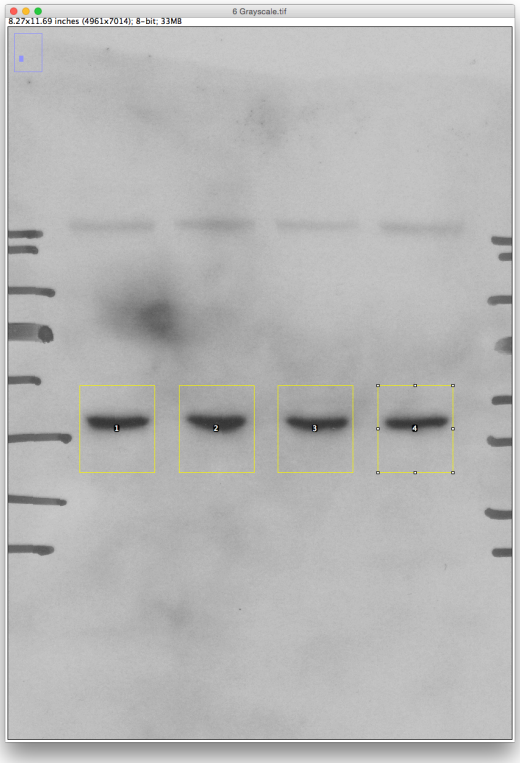

Analysis

9. Repeat the above procedure for other blots, including those with loading controls for your bands (such as actin).
10. Once you have the areas for you band of interest with it's loading control in Excel, perform the following calculation to normalize the band per lane:

$$Relative\ Density\ of Protein\ of\ Interest\ in\ Lane$$

$$= \frac{Density\ of\ Protein\ of\ Interest\ in\ Lane}{Density\ of\ Loading\ Control\ in\ Lane} \times 100$$

11. Graph your relative densities.

References:

Ferreira, T., & Rasband, W. (2012, October 2). *ImageJ User Guide IJ 1.46r*. Retrieved from https://imagej.nih.gov/ij/docs/guide/146.html

Miller, L. (2010, November 10). *Analyzing gels and western blots with ImageJ.* Retrieved from http://lukemiller.org/index.php/2010/11/analyzing-gels-and-western-blots-with-image-j/

Schneider, C. A.; Rasband, W. S. & Eliceiri, K. W. (2012). *NIH Image to ImageJ: 25 years of image analysis. Nature methods, 9*(7), 671-675.

Starr, T. (2013, April 24). *Quantification of protein bands using densitometry.* Retrieved from http://www1.med.umn.edu/starrlab_deleteme/prod/groups/med/@pub/@med/@starrlab/documents/content/med_content_370494.html

APPENDIX B: NEUROSPHERE IMAGE-PROCESSING PROGRAM FOR FIJI SOFTWARE

```
////////////////////////////////////////////////////////////////////////////////////////////////////////////
// PROGRAM TO COUNT NUCLEI IN NEUROSPHERES IN VITRO ////////////////////////////////////////////////////////
////////////////////////////////////////////////////////////////////////////////////////////////////////////

//  *** Please note that any reference to Neurons below, you can replace
//      with Oligodendrocyte Precursor or Progenitor Cell (OPC) Images,
//      depending on if you using OPC images, or other cell types.

//Before Using Program//////////////////////////////////////////////////////////////////////////////////////

// You need to make nine folders on your computer:

 // (1) "Input Uncorrected Nuclei": Has raw .tif files of nuclei channel of neurospheres.
 // (2) "Input Uncorrected Neurons": Has raw .tif file of neuron channel of neurospheres.
 // (3) "Input BC Nuclei Image Directory": (Nothing in here.)
 // (4) "Input BC Neuron Image Directory": (Nothing in here.)
 // (5) "Input Selection Center Directory": Has .roi files of the selection centers of each neurosphere.
 // (6) "Input Selection Outline Directory": Has .roi files of the selection outlines of each neurosphere.
 // (7) "Output Completed Processed Nuclei Directory": (Nothing in here).
 // (8) "Output Composites": (Nothing in here.)
 // (9) "Output Composites without Counted Nuclei": (Nothing in here.)

// NOTE: ALL IMAGES AND SELECTIONS FROM THE SAME NEUROSPHERE MUST BE IN THE SAME ORDER IN EACH FOLDER!

////////////////////////////////////////////////////////////////////////////////////////////////////////////

//Variables/////////////////////////////////////////////////////////////////////////////////////////////////

// Below is a list of the variables used by the program:

inputUncorrectedNuclei = getDirectory("Input Uncorrected Nuclei"); // You choose the folder of the raw .tif file
                                                                   // of nuclei channel.
inputUncorrectedNeuron = getDirectory("Input Uncorrected Neurons"); // You choose the folder of the raw .tif file
                                                                    // of neuron channel.

inputNuclei = getDirectory("Input BC Nuclei Image Directory"); // You choose the folder that will hold the Nuclei
                                                               // images that have Brightness and Contrast
                                                               // automatically corrected.
inputNeuron = getDirectory("Input BC Neuron Image Directory"); // You choose the folder that will hold the Neuron
                                                               // images that have Brightness and Contrast
                                                               // automatically corrected.
inputSelectCenter = getDirectory("Input Selection Center Directory"); // You choose the folder that contains the
                                                                      // .roi files of the Selection Centers of
                                                                      // each neurosphere.
inputSelectOutline = getDirectory("Input Selection Outline Directory"); // You choose the folder that contains the
                                                                        // .roi files of the Selection Outlines of
                                                                        // each neurosphere.

outputNuclei = getDirectory("Output Completed Processed Nuclei Directory"); // You choose the folder that will hold
                                                                             // the .tif overlay image of the counted nuclei.

outputComposites = getDirectory("Output Composites"); // You choose the folder that will hold the final processed composite
                                                      // image WITHOUT the overlay of counted nuclei.
outputComposites2 = getDirectory("Output Composites without Counted Nuclei"); // You choose the folder that will hold the
                                                                               // final processed composite image WITH the
                                                                               // overlay of counted nuclei.

uncorrectedNucleiList = getFileList(inputUncorrectedNuclei); //This returns an array containing the names of the files in
                                                             // your "Input Uncorrected Nuclei" folder.
uncorrectedNeuronList = getFileList(inputUncorrectedNeuron); // This returns an array containing the names of the files
                                                             // in your "Input Uncorrected Neurons" folder.
listNuclei = getFileList(inputNuclei);// This returns an array containing the names of the files in your "Input BC Nuclei
                                      // Image Directory" folder.
listNeuron = getFileList(inputNeuron);// This returns an array containing the names of the files in your "Input BC Neuron
                                      // Image Directory" folder.
listSelectCenter = getFileList(inputSelectCenter); // This returns an array containing the names of the files in your
                                                   // "Input Selection Center Directory" folder.
listSelectOutline = getFileList(inputSelectOutline); // This returns an array containing the names of the files in your
                                                     // "Input Selection Outline Directory" folder.

////////////////////////////////////////////////////////////////////////////////////////////////////////////

//Actual Start to Program///////////////////////////////////////////////////////////////////////////////////

setBatchMode(true);

```

```
77
78 for (i = 0; i < uncorrectedNucleiList.length; i++) { //Note uncorrectedNucleiList.length is the same for all so it's ok!
79
80
81 //Nuclei First
82 open(inputUncorrectedNuclei + uncorrectedNucleiList[i]); // Nuclei first
83 //run("Brightness/Contrast..."); This is automatically adjusting the brightness and contrast.
84 setMinAndMax(0, 65535);
85 call("ij.ImagePlus.setDefault16bitRange", 16);
86
87 run("Enhance Contrast", "saturated=0.35"); // Automatic setting in Fiji.
88 run("Apply LUT");
89
90
91 selectWindow(uncorrectedNucleiList[i]);
92 saveAs("Tiff", inputNuclei+uncorrectedNucleiList[i]); //Now overwrite and save those files in the same location.
93 close();
94
95 open(inputUncorrectedNeuron + uncorrectedNeuronList[i]);
96 //run("Brightness/Contrast..."); Repeat for Neuron Image
97 setMinAndMax(0, 65535);
98 call("ij.ImagePlus.setDefault16bitRange", 16);
99
100 run("Enhance Contrast", "saturated=0.35"); // Automatic setting in Fiji.
101 run("Apply LUT");
102
103
104
105 selectWindow(uncorrectedNeuronList[i]);
106 saveAs("Tiff", inputNeuron+uncorrectedNeuronList[i]); //Now overwrite and save those files in the same location.
107 close();
108
109 //Now, image process the corrected brightness and contrast nuclei and neuron pictures.
110
111
112 open(inputNuclei + uncorrectedNucleiList[i]); // Open B/C Nuclei Image
113
114 run("Subtract Background...", "rolling=0.2 sliding disable"); // Subtract background << PLACE TO ADJUST: Set at this setting.
115
116 setAutoThreshold("Default dark");
117 //run("Threshold...");
118 setThreshold(5495, 63687); // Setting Threshold << PLACE TO ADJUST: Set at this setting.
119 setOption("BlackBackground", false);
120 run("Convert to Mask");
121
122 run("Convert to Mask");
123
124 run("Watershed");
125
126 //Now remove center and outside from this image of the nuclei you are currently processing.
127
128 open(inputSelectCenter + listSelectCenter[i]); // Open up selection center for this image.
129
130
131 setBackgroundColor(0, 0, 0);//These two lines here clear the center of the selection to black.
132 run("Clear", "slice");
133 run("Select None"); //This clears the selection from the current image so you can add the next selection.
134
135
136 open(inputSelectOutline + listSelectOutline[i]); // Open up the outline selection of neuropshere for this image.
137
138 run("Clear Outside");//These clears the outside of the selection to black.
139
140 run("Select None"); //This clears the selection from the current image.
141
142
143 //Analyze Particles: Now we analyze the particles from this image that is still open.
144
145 run("Analyze Particles...", "size=20-1000 pixel show=Outlines display clear summarize in_situ");
146
147 filenameOutputNuclei = outputNuclei + "Output" + uncorrectedNucleiList[i];// This is the new filename for the new output nuclei
148                                                                             // image you just made. Now you are going to save it.
149 onlyFilenameOutputNuclei = "Output" + uncorrectedNucleiList[i];
150 saveAs("Tiff", filenameOutputNuclei);
151 close();
152
```

```
//Now open up the original Nuclei Image with the editied Brightness and Contrast, and open up the Neuron Image with edited
//brightness and contrast.

open(inputNuclei + uncorrectedNucleiList[i]);//Nuclei Uncounted IMAGE
open(inputNeuron + uncorrectedNeuronList[i]);//Neuron
open(filenameOutputNuclei); // Nuclei Outlines you just made

//Since the original B/C Nuclei and Neuron pictures are 16 bit, and the Processed Nuclei image is 8-bit, we need to convert
//all of these to 16-bit images to merge them together.

selectWindow(onlyFilenameOutputNuclei);//Process Nuclei Image to 16-Bit
run("Invert");//Note: Need to invert colors first for overlay.
run("16-bit");

selectWindow(uncorrectedNucleiList[i]);//
run("16-bit");

 selectWindow(uncorrectedNeuronList[i]);//
run("16-bit");

//Now, we rename these open images to different names so we can run the composite macro to merge them together.

selectWindow(onlyFilenameOutputNuclei);
rename("CountedNuclei.tif");

selectWindow(uncorrectedNucleiList[i]);
rename("OldNuclei.tif");

selectWindow(uncorrectedNeuronList[i]);
rename("Neuron.tif");

//Now we merge the three image together
run("Merge Channels...", "c1=Neuron.tif c3=OldNuclei.tif c7=CountedNuclei.tif create keep");//<<(Here, change c1 to c2 to
                                                                                            //make green instead of red.)

//Before saving this composite, you need to change the composite image to an RGB image instead of an RBG stack:
selectWindow("Composite");
run("RGB Color");

//Now save the RGB composite image and close all windows.
saveAs("Tiff", outputComposites + "Composite " + i);
run("Close All");

//Now repeat but save another image but just without the CountedNuclei into another folder.

open(inputNuclei + uncorrectedNucleiList[i]);
open(inputNeuron + uncorrectedNeuronList[i]);
open(filenameOutputNuclei);

selectWindow(onlyFilenameOutputNuclei);
run("Invert");
run("16-bit");

selectWindow(uncorrectedNucleiList[i]);//
run("16-bit");

 selectWindow(uncorrectedNeuronList[i]);//
run("16-bit");

selectWindow(onlyFilenameOutputNuclei);
rename("CountedNuclei.tif");

selectWindow(uncorrectedNucleiList[i]);
rename("OldNuclei.tif");

selectWindow(uncorrectedNeuronList[i]);
rename("Neuron.tif");

//Now we merge TWO image together...
run("Merge Channels...", "c1=Neuron.tif c3=OldNuclei.tif create keep");//<<(Here, change c1 to c2 to
                                                                        //make green instead of red.)

//AND save into a different folder.
selectWindow("Composite");
run("RGB Color");
saveAs("Tiff", outputComposites2 + "Composite No Counted Cells " + i);
```

```
229
230 //Close all the Images
231 //Close the Neuron Picture WITHOUT SAVING
232 //Close the Nuclei Outline Picture WITHOUT SAVING
233 //Close the RGB composite image WITH SAVING
234 run("Close All");
235
236
237 }
238
239 setBatchMode(false);
240
241 ////////////////////////////////////////////////////////////////////////////////////////
```